Conducting polymer based materials for on-skin applications

Fu, Xiaoxu

2020

Fu, X. (2020). Conducting polymer based materials for on-skin applications. Doctoral thesis, Nanyang Technological University, Singapore.

https://hdl.handle.net/10356/146294

https://doi.org/10.32657/10356/146294

NANYANG TECHNOLOGICAL UNIVERSITY
SINGAPORE

CONDUCTING POLYMER BASED MATERIALS FOR ON-SKIN APPLICATIONS

FU XIAOXU

SCHOOL OF CIVIL AND ENVIRONMENTAL ENGINEERING

2020

Conducting polymer based materials for on-skin applications

FU XIAOXU

School of Civil and Environmental Engineering

A thesis submitted to the Nanyang Technological University

in partial fulfilment of the requirements for the degree of

Doctor of Philosophy

Statement of Originality

I hereby certify that the work embodied in this thesis is the result of original research, is free of plagiarized materials, and has not been submitted for a higher degree to any other University or Institution.

29.07.2020

Date

Fu Xiaoxu

Supervisor Declaration Statement

I have reviewed the content and presentation style of this thesis and declare it is free of plagiarism and of sufficient grammatical clarity to be examined. To the best of my knowledge, the research and writing are those of the candidate except as acknowledged in the Author Attribution Statement. I confirm that the investigations were conducted in accord with the ethics policies and integrity standards of Nanyang Technological University and that the research data are presented honestly and without prejudice.

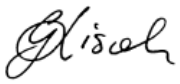

29.07.2020

Date

Grzegorz Lisak

Authorship Attribution Statement

This thesis contains material from 4 papers published in the following peer-reviewed journals in which I am listed as an author.

1. Fu, Xiaoxu; Zeng, Wenqiu; Ramírez-Pérez, Ana Cristina and Lisak, Grzegorz, 3-D and electrically conducting functional skin mapping for biomedical applications. *Chemical Communications*, 54, 980–983 (2018).

Chapters 4.1.1 and 4.1.2 contain material published in this article.

The contributions of the co-authors are as follows:

Asst/Prof Lisak provided the initial project direction and revised the manuscript drafts.

I performed most of the lab work at School of Civil and Environmental Engineering, analysed the data and prepared the manuscript drafts.

Ms Wenqiu Zeng assisted part of the lab work and collected the data.

Dr Ana Cristina Ramírez-Pérez assisted part of the lab work, collected the data, and revised the manuscript draft.

2. Talikowska, Milena[*]; Fu, Xiaoxu[*] and Lisak, Grzegorz, Application of conducting polymers to wound care and skin tissue engineering: A review. *Biosensors and Bioelectronics*, 135, 50-63 (2019) (*[*]equally contributed).*

Chapter 2.2 contains material published in this article.

Asst/Prof Lisak provided the initial project direction and revised the manuscript drafts.

Dr Milena Talikowska and I collected the data and prepared the manuscript drafts together.

3. Fu, Xiaoxu; Wang, Jun Kit; Ramírez-Pérez, Ana Cristina; Choong, Cleo and Lisak, Grzegorz, Flexible conducting polymer-based cellulose substrates for on-skin applications. *Materials Science and Engineering: C*, 108, 110392 (2020).

Chapters 4.2 and 4.3.2.1 contain material published in this article.

Asst/Prof Lisak and Asst/Prof Choong provided the initial project direction and revised the manuscript drafts.

I performed the synthesis, electrochemical characterization, and FE-SEM characterization of the materials. I also prepared the manuscript drafts together with Dr Wang Jun Kit.

Dr Wang Jun Kit performed mechanical characterization and cellular studies of the materials. He also prepared the manuscript drafts together with me.

Dr Ana Cristina Ramírez-Pérez assisted part of the lab work and data collection.

4. Fu, Xiaoxu; Cheong, Yi Heng; Ahamed, Ashiq; Zhou, Chao; Robert, Chima; Krikstolaityte, Vida; Gordon, Keith C and Lisak, Grzegorz. Diagnostics of skin features through 3D skin mapping based on electro-controlled deposition of conducting polymers onto metal-sebum modified surfaces and their possible applications in skin treatment. *Analytica Chimica Acta*, 1142, 84-98 (2021).

Chapters 4.1.2, 4.1.3, 4.3.1, and 4.3.2.2 contain material published in this article.

Asst/Prof Lisak provided the initial project direction and revised the manuscript drafts.

I performed the lab work including synthesis of the materials, optimization of the protocol, analysis of the data. I also prepared the manuscript drafts.

Mr Yi Heng Cheong assisted in operation of profilometer and collection of profilometry data.

Mr Ashiq Ahamed assisted part of the lab work and revised the manuscript drafts.

Mr Chao Zhou assisted the design of skin mapping device and 3D model.

Ms Chima Robert, Dr Vida Krikstolaityte, and Prof Keith C Gordon performed the Raman spectroscopy .

29.07.2020

Date

Fu Xiaoxu

Acknowledgement

The past four years may have not been the most fantastic but were definitely the most special four years of my life. I have so many things to say for expressing my gratitude to the individuals and groups of people for going through this journey with me.

To begin with, I would like to express my special gratitude to my supervisor Dr. Grzegorz Lisak for his patient, valuable, and constructive guidance, and suggestions during the past four years. I would never reach here without these. I did have lab experience in my undergraduate studies but it was fall 2016 when I officially started PhD studies that being the true start of my research career when I sat down and meet Greg in his office for the first time. Thank you, Prof! Dziękuję Ci!

I would like to thank Dr. Ana Cristina Ramírez-Pérez, who also helped me during the start of my research work. My thanks extend to all the collaborators who I did research with. Furthermore, I would like to thank all my friends for their support and company, without who I could never go through this journey. Of course, special thanks to my dear Pangguo.

Most of this work was conducted in Environmental Laboratory at School of Civil and Environmental Engineering and Residues and Resources Reclamation Center (R3C) at Nanyang Environment and Water Research Institute (NEWRI), NTU. I would like to express my full respect and thanks to all the technicians and staffs who helped me a lot with instruments operation. I would also like to thank NTU Research Scholarship for the financial support.

Finally, I wish to thank my family members for their most special support and encouragement throughout my study. Dad, with all the thing we've gone through together, nothing is a better gift than you being there, happy and healthy. Mom, you walked me into every stage of my school career including this one, but you missed my last graduate. There is no word that I can

say to let you know how much I want to share the joy with you. I do not believe in any god but I do believe you are watching me somewhere all the time. Thank you for being my mother!

Thank you all!

Xiaoxu, 2020.08.03 in Singapore

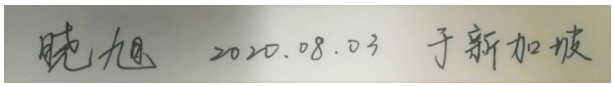

TABLE OF CONTENTS

Summary

Skin health is of a major concern especially for construction workers who are exposed to extended sun radiation and thus are more prone to develop pathological skin conditions, such as skin cancer. In this study, a portable, fast and economical skin mapping technique was established, aiming to assist on-site dermatological skin diagnostics with the option of customized treatment of pathological skin conditions. To do that, the electro-controlled deposition of conducting polymers in the presence of the insulating skin stamp was performed on various conducting surfaces. As a result of electropolymerization of conducting polymers onto sebum-conductor surfaces the 3D skin patterns relating to the skin topographies were realized. The 3D skin patterning demonstrated adequate capability for recognition and reproduction of various skin features, supporting a resolution of up to µm-level, which encompass most circumstances in dermatology diagnosis. To achieve portability, the device prototype entirely powered by dry battery was developed. To add the functionality to the developed 3D skin patterning technique, such as wound treatment, cellulose substrates were introduced to improve flexibility and breathability of the material. Cellular studies proved that the developed material is cytocompatible and safe to use in on-skin applications. Furthermore, both PET- and cellulose-based substrates were explored on electro-controlled metal loading and release. Zn^{2+} and Cu^{2+} were firstly investigated as therapeutic ions via passive or active methods. The results showed a successful loading and well-controlled release profile within an effective concentration range in ppb level. The study of various conducting polymer based materials shows a promising perspective not only in on-skin diagnosis but also in skin treatment.

List of publications

1. Fu, Xiaoxu; Zeng, Wenqiu; Ramírez-Pérez, Ana Cristina and Lisak, Grzegorz, 3-D and electrically conducting functional skin mapping for biomedical applications. *Chemical Communications*, 54, 980–983 (2018).

2. Talikowska, Milena*; Fu, Xiaoxu* and Lisak, Grzegorz, Application of conducting polymers to wound care and skin tissue engineering: A review. *Biosensors and Bioelectronics*, 135, 50-63 (2019) (* *equally contributed)*

3. Fu, Xiaoxu; Wang, Jun Kit; Ramírez-Pérez, Ana Cristina; Choong, Cleo and Lisak, Grzegorz, Flexible conducting polymer-based cellulose substrates for on-skin applications. *Materials Science and Engineering: C*, 108, 110392 (2020).

4. Fu, Xiaoxu; Cheong, Yi Heng; Ahamed, Ashiq; Zhou, Chao; Robert, Chima; Krikstolaityte, Vida; Gordon, Keith C and Lisak, Grzegorz. Diagnostics of skin features through 3D skin mapping based on electro-controlled deposition of conducting polymers onto metal-sebum modified surfaces and their possible applications in skin treatment. *Analytica Chimica Acta*, 1142, 84-98 (2021).

List of figures

Figure 38 Raman spectrum FESEM images, and EDS mapping of loaded Cu

List of tables

List of abbreviations

AFM	Atomic force microscopy
Au-PET	Gold covered polyethylene terephthalate plastic
CA	Chronoamperometry
CAC	Circulating angiogenic cell
CE	Counter electrode
CNT	Carbon nantube
CP	Conducting polymer
CS	Chitosan
CV	Cyclic voltammetry
DMEM	Dulbecco's Modified Eagle's Medium
DMI	Diffuse multispectral imaging
EDOT	3,4-ethylenedioxythiophene
EDS	Energy dispersive X-ray spectroscopy
EDTA	Ethylenediaminetetraacetic acid
EGF	Epidermal growth factor
FBS	Fetal bovine system
FDA	Fluorescein diacetate
FD-OCT	Frequency-domain optical coherence tomography
FE-SEM	Field emission scanning electron microscopy
GCP	Galvanostatic chronopotentiometry
HA	Hyaluronic acid
HaCaT	Immortalized human keratinocytes
LDI	Laser doppler imaging
MMPs	Matrix metalloproteinases

MRI	Magnetic resonance imaging
MSI	Multispectral imaging
MTs	Metallothioneins
MW	Molecular weight
OCT	Optical coherence tomography
PA	Polyacetylene
PANI	Polyaniline
PBS	Phosphate buffer saline
PDLLA	Poly(D,L-lactide)
PE	Polyethylene
PEDOT	Poly(3,4-ethylenedioxythiophene
PET	Polyethylene terephthalate
PI	Propidium iodide
PLA	Poly(lactic acid)
PPy	Polypyrrole
PSPD	Position-sensitive photo diode
PSS	Polystyrene sulfonate
PT	Polythiophene
Pt-PET	Platinum covered polyethylene terephthalate plastic
PVA	Poly(vinyl alcohol)
Py	Pyrrole
RE	Reference electrode
SDS	Sodium dodecyl sulphate
SEM	Scanning electron microscopy
SPM	Scanning probe microscopy
WE	Working electrode

CHAPTER 1 INTRODUCTION

1.1 Conducting polymers.

1.1.1 General introduction to conducting polymers.

Conducting polymers (CPs), or rather, electrically CPs are polymers that poses the ability to conduct electricity. Back to the middle of 20th century, organic polymers were exclusively considered as insulators, until the discovery of halogen doped trans-polyacetylene (PA). This new material was characterized with a remarkable ability to conduct electricity compared to unmodified trans-PA [1]. The basic molecular structure of CPs consists of π-conjugated backbone, e.g. polypyrrole (PPy) and trans-PA, where a conjugated backbone system has a region of overlapping p-orbitals, bridging the interjacent single bonds. This allows a delocalization of π electrons across all the adjacent aligned p-orbitals. The π electrons do not belong to a single bond or atom, but rather to a group of atoms. Thus, the result of conjugation in the CPs is that there are extra π bonding interactions between the adjacent π systems. This extra bonding results in an overall stabilization of the system. This increased stability due to conjugation is referred to as the delocalization energy, the resonance or conjugation energy. Delocalized π-electrons along the whole polymer chain are the blueprint of CPs, which provides basic possibility of fast electron transfer in the material [2].

Similar to inorganic semiconductors, such as silicon, conjugated conducting polymers show very low conductivities in their pristine state. There are variety of ways to increase conductivity of the polymer, e.g. by chemical doping, irradiation, and through the stimulation of external electric fields [3]. The term doping is in some way misleading since it is more common used in solid-state physics for the introduction of a foreign neutral atom into a host lattice, changing the electronic structure in that lattice. In the context of conducting polymers, doping refers to

a chemical reaction, namely oxidation or reduction that involves introduction of a foreign ion (dopant) in the close vicinity of the polymer backbone. As a result, a new electronic state is achieved, and the material becomes conductive. Both electron donating (n-type) and electron accepting (p-type) dopants, that are, reducing and oxidizing agents, have been used to introduce charges into conjugated polymers and render them conductive [2, 4]. Importantly, as a result of doping, the conductivity of conjugated polymers can be increased by many orders of magnitude, to be similar to that of some metals [2, 5]. In addition, doping, together with the formation of composites, copolymers and blends, allows for some of the limitations inherent to the pristine forms of CPs to be overcome [6]. For example, by creating a PPy/poly(D,L-lactide) (PDLLA) composite, the brittleness and mechanical rigidity of pure PPy[7, 8] can be avoided [9]. Likewise PPy can be applied as a coating onto other materials, such as poly(D,L-lactide-co-Ɛ-caprolactone) in order to produce a flexible yet electrically conductive membrane [10]. In a similar manner, while the biocompatibility of CPs such as PPy [11], PANI [12, 13] and PEDOT [14] has been well proven in animal models [11, 15], it can be further enhanced through the intentional incorporation of biomolecules [6, 16]. Chemical structures of some commonly used conducting polymers are shown in Figure 1.

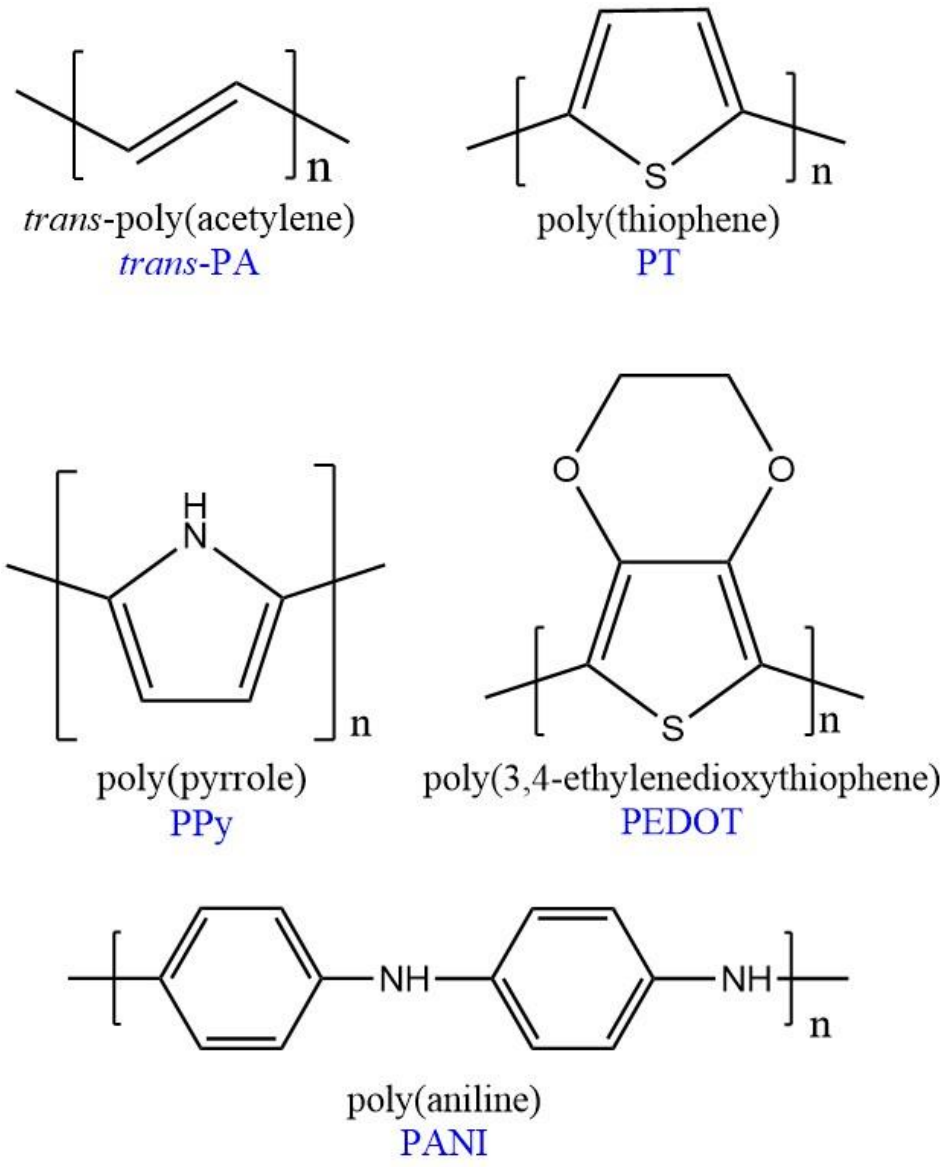

Figure 1. Chemical structures of common conducting polymers.

1.1.2. Poly(3,4-ethylenedioxythiophene).

The first mention of polythiophenes as potential conducting polymers can be found in the literature in 1967. A. G. Davies *et al.* investigated the acid catalyzed polymerization of furan, pyrrole, and thiophene heterocycles [17]. The electrical conductivity in polythiophenes was firstly observed by Tourillon and Garnier in 1982 [18]. The thiophene was electropolymerized on platinum electrodes in acetonitrile with perchlorate or tetra-fluoroborate counter ions. A remarkable conductivity of 10-100 S/cm was reported. Polythiophenes have an enormous

potential for practical applications, as oxygen substituents at the 3- and 4-positions in the thiophene moiety stabilize the doped, bipolaronic state in polythiophenes by their electron donating properties [19]. Poly(3,4-ethylenedioxythiophene) (Figure 2) is one of the most stable, processable and highly conductive of polythiophenes. The PEDOT was firstly synthesized, from 3,4-ethylenedioxythiophene (EDOT), in 1988 by Bayer AG, Leverkusen [20]. It is said to be the best conducting polymer available in terms of conductivity, processability, and stability, especially when it is made with polystyrene sulfonate (PSS) as a dopant [21]. Furthermore, PEDOT is the one of the few conducting polymers that is commercially produced in a large scale and sold for the use in various applications [22]. It also possess good enough flexibility and high enough electrical conductivity for wound electrostimulation, good environmental stability [23] and are widely applied in electronical [24-27], chemical and biological systems [28-31].

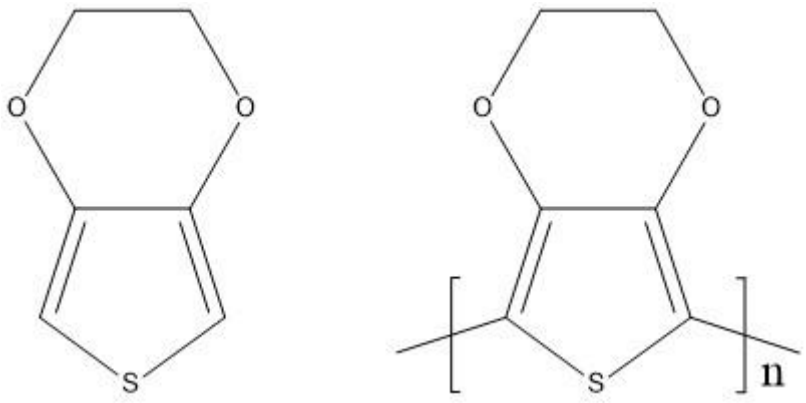

Figure 2. Chemical structures of EDOT (left) and PEDOT (right).

The electropolymerization of PEDOT follows similar polymerization route known for pyrrole, e.g. the use of iron(III) chloride as the chemical oxidant, which results in insoluble powder with a tremendously high conductivity, compared to all other known polyheterocycles [32]. For that, also several other metal ions have been used, with different success, to oxidize EDOT, including manganese, cerium(IV) and copper(II) [33, 34]. Besides oxidation in liquid phase, a

new route to highly conductive PEDOT was obtained by vapor phase polymerization (VPP), which was established at the beginning of 21st century [35-37]. Finally, electrochemical oxidation is another route to synthetize PEDOT. This method will be discussed in detail in chapters 1.1.4.

Electrochemically synthesized PEDOT is insoluble in aqueous solution, but it also may exist as polymer dispersion with poly(styrenesulfonate) (PSS) as counter ion. Such dispersion is produced on an industrial scale and has widespread applicability, e.g. PEDOT(PSS), H.C. Starck Clevios GmbH is sold under the trade name of Clevios™. A slit, bar and spin coatings, drop casting, electrospinning, and spraying are the most common deposition techniques to obtain uniform layers from PEDOT(PSS) dispersions [38, 39]. Compared with other highly conducting polymers, PEDOT(PSS) thin films have good thermal stability [32] and conductivity [40]. The mechanism of charge transport in PEDOT(PSS) is relatively still poorly understood. A comprehensive theory describing the charge transport properties especially of strongly doped conjugated amorphous polymers is still missing. Owing to its random order of charge transporting segments in these systems without having any translation symmetry, the quantum mechanical model of Bloch's eigenstates commonly invoked to explain electrical properties of crystalline semiconductors and metals are not applicable. The frequency of charge transport between adjacent sites depend on its relative energetic position, the distance and the relative orientation, as outlined by Borsenberger and Weiss, to explain charge transport in molecularly doped polymers [41]. Owning to PEDOT's properties to conduct electricity and its stability as well as possibility to functionalize and process it was investigated in this study as one of the main materials for conducting polymer development, e.g. a monomer, 3,4-ethylenedioxythiophene (EDOT) was intensively used throughout of this study for electropolymerization of poly(3,4-ethylenedioxythiophene).

1.1.3 Poly(pyrrole).

The poly(pyrrole) was firstly synthetized from its monomer, pyrrole (Figure 3), and reported by Dall'Olio *et al*. in 1961. It is one of the most extensively studied conducting polymers. The pyrrole monomer is easily oxidized, water soluble, possesses environmental stability, good redox properties, and high electrical conductivity. The PPy is the promising material for applications in batteries, supercapacitors, electrochemical biosensors, conductive textiles and fabrics, mechanical actuators, electromagnetic interference shielding, antistatic coating and drug delivery systems [42-45].

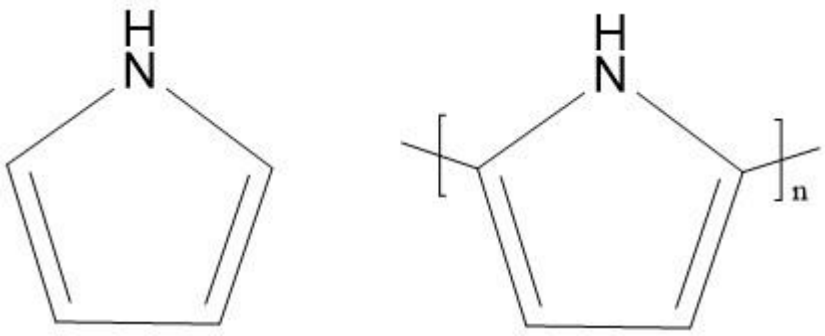

Figure 3. Chemical structures of Py (left) and PPy (right).

The polymerization of pyrrole was proposed to involve complex reactions that include oxidation, deprotonation, and crosslinking. The most widely accepted polymerization mechanism of PPy is the coupling between radical cations [22]. In this study, the synthesis of polypyrrole was done via electropolymerization process and the detailed mechanism for polymerization will be discussed in Chapter 1.1.4. PPy possess similar properties to that of PEDOT. It has, however, higher water solubility, which makes it easier to be more processable in aqueous solutions [46]. Thus, PPy was also investigated in this study for the use in electroactive cellulose substrates and skin mapping technique, as alternative to that of PEDOT.

1.1.4 Electrochemical synthesis of conducting polymers.

Electrochemical polymerization, or electropolymerization, is a commonly used method to synthetize conducting polymer films on the surface of electrodes/conductors. In electropolymerization, monomers are used that are able to be oxidized or reduced within the potential window of specific electrolyte and electrodes. In general, during electropolymerization process, the monomer is firstly oxidized, and a radical cation is then generated. Two radical cations form a dimer, which is more easily oxidized than the monomer. In this way, the dimers continuously couple with radical cations, thus forming large molecules [3, 47]. After a critical chain length is achieved, the formed oligomers start to precipitate on the electrode surface. Chain propagation includes several approaches. Oligomer species do not always have high enough reactivity for further propagation [48]. The chain propagation can proceed by coupling of dimers (to form tetramers) then forming polymers, meanwhile, the oligomers can also react with radical cations [48, 49]. Another reaction model assumes that the monomers are oxidized at the electrode but form thereafter a layer of polymer very near to the working electrode. When the layer is saturated, conducting polymers start to grow on electrode surface [48].

To perform a successful electropolymerization, two requirements are essential, namely the oxidation/reduction potential of the monomer is suitable for the electrolyte used and monomer concentration is high enough [50]. An equally important is to assure that the radical cations react with each other more quickly than that with other nucleophiles in the electrolyte. Electropolymerization of most conjugated monomers results in mainly linear polymer chains so that a conjugated system is created. Side reactions may lead to limited chain growth. The purity of monomer solution also has a significant effect on electropolymerization process [51]. When the electrode surface is relatively small (square centimeter grade), uniform films with

good adherence tend to be obtain [50]. In this study, electropolymerization were mostly performed in a typical beaker-based three-electrode electrochemical cell. Besides that, a specially designed electrochemical cell for on-skin electropolymerization was introduced in on-body skin mapping. This will be described in detail in Chapter 3.

1.2 Human skin.

1.2.1 Skin and pathological skin conditions.

Skin is the largest organ in human body. On average it comprises 15% of adult total body weight [52]. It is a very vital, often underestimated organ, as skin acts as a barrier against dehydration, abrasion, pathogens, regulates body temperature and provides information about the environment body is in contact with owning to the presence of in its structure various sensory receptors [53]. Skin consists of three major components, namely the outer epidermis (or epidermis), the underlying epidermis (or dermis) and hypodermis, which is made up of subcutaneous tissue (Figure 4) [54]. The epidermis consists of a particular kind of tissue called stratified squamous epithelium. Epithelium consists of cells that are packed together very tightly, which is very important to an organ that must cover and protect the rest of the body. The word “stratified” describes the dozens of layers of cells that are piled up to create the epidermis. In this study, I focus mainly on outer epidermis, especially the outermost part of epidermis, which are mostly dead and dry cells. Those cells are also of vital importance to the living organism because they are efficient barrier to water loss and hostile microorganism entrance to the body.

Allergens, environmental irritants, infection, hereditary factors, and stress are just a few of the factors that can trigger or exacerbate skin vulnerability. Skin conditions, or skin disorders, is a term describing various skin pathological conditions [55]. Common signs of pathological skin conditions include itching, swelling, redness, rash, flakiness, bumps or various growths [56].

Some skin conditions can be unsightly but harmless, while others may be contagious. Many skin conditions are also itchy or painful. Dermatologists specialize in treating diseases, disorders and injuries of the skin, hair, and nails. They treat common conditions such as acne and warts; chronic skin conditions such as eczema and psoriasis; and more serious diseases like skin cancer [57]. Dermatologists consider a patient's medical history and physical symptoms for skin condition diagnoses. Assessing the size, shape, location, and colour of lumps, blisters, and rashes can help medical personnel pinpoint the exact cause of skin abnormal conditions. Their imaging facilities better understanding of the skin conditions and are needed to make up for the visual limitation of human eyes, because the tiny topological structures on skin surface are hard to examine by naked eyes.

The situation becomes even more complex when a wound is present in the structure of the skin. A skin wound is defined as the disruption of the normal anatomic structure and function of the skin [58]. The diagnosis of surface condition is still high related to wound healing processes, but different treatment is certainly needed to accelerate these processes. Novel investigation related with wound healing process will also be introduced in this study and more details can be found in chapter 1.2.3.

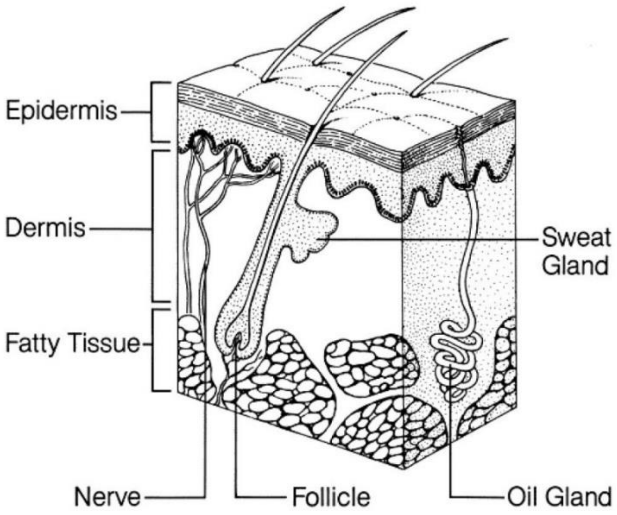

Figure 4. Simplified skin structure [59].

1.2.2 Skin wound healing.

The whole process of skin wound healing consists of four steps (i) inflammation, (ii) re-epithelization, (iii) extracellular matrix synthesis and (iv) maturation [60-62]. For most of wounds, recent advances in tissue engineering raised considerable interests in wound dressing, which has a great clinical potential in wound healing [63-67]. Wound dressing has many advantages for wound healing including large specific surface area, good flexibility, structural similarity to cellular matrix and good biocompatibility. To facilitate accelerated wound healing, the surface of the wound should generally be kept moist, rather than being exposed to air [68]. The application of a dressing over the wound not only protects against infection, but also helps to maintain a moist environment that promotes faster re-epithelization [69]. Traditional, passive wound dressings include gauze and tulle. Although these provide coverage, they can adhere to the wound bed and cause disruption and pain upon removal [70]. In contrast, modern wound dressings not only cover the wound but interact with it to actively promote healing [70]. They utilize more advanced materials in their formulations and can be classified as either interactive or bioactive. They include semi-permeable films and foams (often constructed of polyurethane), hydrogels, hydrocolloids, alginates, collagens and hydrofibers. Bioactive dressings are comprised of biomaterials with high biocompatibility, biodegradability, and a non-toxic nature; common constituents include hyaluronic acid (HA), chitosan (CS) and elastin, among others [70, 71].

Besides those factors, there are more possible modification approaches which could enhance materials wound healing ability, such as presence of copper and zinc ions in the wound environment. Copper is an essential element for wound healing owing to its ability to enhance angiogenesis [72, 73]. Angiogenesis is the physiological process through which new blood vessels form from pre-existing vessels. It helps blood vessel formation by stabilizing the

expression of hypoxia-inducible factor [74, 75]. Studies on mice indicate that copper ions releasing stimulate proangiogenic factors like transforming growth factor-β and vascular endothelial growth factor [76, 77]. Both of the factors have significant positive effect on accelerating wound healing process. Matrix metalloproteinases (MMPs) and interleukin-8 (IL-8) are the main facilitators for wound healing and skin aging, while copper plays its role by regulation of their genes [78]. Due to its important role in wound healing, copper-doped wound dressings like microfibres, membrane nanocomposite, and bioactive glass are widely investigated [79-81]. Zinc is another transitional metallic element which is highly related to wound healing process. Zinc is mainly as essential component of many enzymes, which regulate the biochemical reactions during the wound healing process [82, 83]. Zinc was found to be an essential cofactor of carbonic anhydrase, the first metalloenzyme discovered in 1940s [84]. Nowadays zinc has been found in over 300 different enzymes, including but not limited in alcohol dehydrogenase, angiotensin-converting enzyme, matrix metalloproteinases (MMPs), reverse transcriptase, DNA and RNA polymerases [85, 86]. Directly functional to wound healing, zinc is instrumental in stabilizing cellular membrane [87, 88], main component of metallothioneins (MTs) and zinc metalloenzymes [89, 90]. Metallothionein (MT) is a family of cysteine-rich, low molecular weight (MW ranging from 500 to 14000 Da) proteins. They are localized to the membrane of the Golgi apparatus. The MTs have the capacity to bind both physiological (such as zinc, copper, selenium) and biotic (such as cadmium, mercury, silver, arsenic) heavy metals through the thiol group of its cysteine residues, which represent nearly 30% of its constituent amino acid residues. In this study, a new material of paper-based conducting polymer doped with copper and zinc ions was synthesized and characterized in terms of releasing Zn^{2+} and Cu^{2+} to potentially accelerate wound healing process.

1.3 Research gaps and objectives.

Typically, the optical techniques serve as supplementary methods to dermatologist visual diagnose of various skin pathological conditions. Currently optical cameras/devices are used for that purposes, e.g. skin surface 2D imaging, however, they lack in the capability of obtaining 3D information. Some instruments such as OCT, LDI, MRI and DMI are also used for dermatological diagnosis including obtaining 3D information in specific conditions [91-94]. Moreover, those instruments are either relatively time-consuming and/or expensive. On the other hand, many skin and dermatological diseases related conditions contain much information in their third dimension, e.g. growths, scars and wounds. Thus, taking into account the practical limitations of current skin surface-based dermatological diagnostic techniques there is a clear need for a portable, cheaper and feasible method to produce 3D skin patterns. Additionally, if the 3D skin maps are electroactive it could open a new area of customized, cheap skin treatment substrates based on the skin patterns. Such materials would have direct applicability in cheap on-site skin diagnostics. For example, the skin may be vulnerable, especially when exposed to the extended sun radiation. Uncontrolled and prolonged sun ultraviolet light radiation on the skin is the most common environmental factor that increase the risk of a skin cancer [95]. In civil engineering practices, such as construction sites, the long-time daily exposure of the construction site workers to the sun is a common occurrence [96-98]. To facilitate on site health safety through health safety checks, including that of skin diagnostics through portable, fast, and economical methodology for imaging of skin pathological skin conditions is of an interest. To do that, the portable and cheap skin diagnostic technique, with the option of skin pathological skin conditions treatment, has been investigated in this work. The technique is based on electrochemical 3D skin patterning via selective growth of the conducting polymers onto the conducting surface modified with the insulating stamp correlating to the skin surface topography.

CHAPTER 2 REVIEW OF THEORY AND PREVIOUS WORK

2.1 Dermatological diagnosis of skin morphology.

As a natural barrier for the inner organs, skin often suffers from mechanical damages, skin diseases, bacterial, fungal and viral infections and develop pathological growths [99]. Thus, appropriate, and precise dermatologic diagnosis is highly needed to recognize and evaluate those abnormal skin conditions for an adequate treatment. Current practice of dermatologic diagnosis in epidermis is based on visual inspection and assistance of optical imaging devices. Various high-resolution digital cameras are currently used to obtain 2D images of patient's skin. Besides, optical coherence tomography (OCT) is used to provide 3D images of skin tissues [92], a technique which is most widely used in ophthalmology. The OCT is used in diagnosis of multiple skin conditions and skin related processes, such as psoriasis vulgaris [100], differentiating blisters [101], actinic keratoses [102] and wound healing [103]. Anke Bossen *et al.* used frequency-domain optical coherence tomography (FD-OCT) system to acquire 3D image of an internal fingerprint [104]. Internal fingerprints are used for a person identification and false fingerprint discrimination. Furthermore, a Laser Doppler Imaging (LDI) can capture moving objects [93, 105]. It is used to assess vascular lesions and provide skin related information via targeting the flow of red blood cells. In clinical treatments, the LDI is used to monitor Kaposi sarcoma [93] and evaluate skin blood perfusion after cold stimulation in patients with systemic scleroderma [106]. A Diffuse multispectral imaging (DMI) is another optical method used in skin diagnosis. The DMI uses light sources of multiple wavelength to provide 2D images of skin, e.g. evaluate treatment response of Kaposi sarcoma patients [94] and differentiate malignant from benign lesions [107]. Other common optical techniques for skin condition diagnosis include confocal microscopy, Raman spectroscopy and dermoscopy [108-110]. Besides the optical methods, other techniques such as ultrasound imaging provide

3D images, but it is more popular for its B-mode that provide 2D images of organs. In fact, it has the ability to generate images with resolution of 200-300 μm [111, 112]. It is also used to characterize skin lesions [113] and evaluate their response to treatment [114]. In addition, magnetic resonance imaging (MRI) is also used in skin diagnosis [91]. Despite many advanced techniques and devices, none of them can be carried by dermatologists on a daily basis. Moreover, the resolution of most techniques is still limited. While the OCT and the ultrasound imaging can provide 3D images of internal tissues, none of them can provide clear 3D images of skin surface. Nonetheless, the similarities and differences of 3D analytical skin patterning technique to other existing techniques are provided in Table 1. Furthermore, all of those are restricted to the diagnosis stage only while for skin treatments such as drug release and wound healing through electrostimulation are not possible.

Thus, taking into account the practical limitations of current skin surface-based dermatological diagnosis techniques there is a clear need for a portable, cheaper and feasible method to produce 3D and possibly electrically conducting skin patterns [115]. This may be offered by the application of conducting polymers, which can be easily fabricated. In 2015, Hillman *et al.* reported an intriguing application of PPy and PEDOT co-polymer films, where he enhanced latent fingerprints on stainless steel for forensic applications [116]. That was possible based on the fact that the skin leaves insulating mark on any surface that is in contact with (in form of skin extract, sebum). If that substrate is electrically conducting, the localized electropolymerization of the co-polymer in the presence of the fingerprint (conducting metal and non-conducting sebum skin pattern) resulted in the clear visualization of the fingerprint (increased contrast between the dark conducting co-polymer and unoccupied deposited sebum).

Table 1. Comparison of various skin imaging/processing techniques to 3D skin patterning.

Technique	Target skin	3D information?	Function	Similarities	Difference	References

Light sheet microscopy	Skin biopsies	Yes	Visualize in-depth skin structure, 3D tissue visualization.	Contains skin surface topological information in cross-section images; obtains 3D images of biopsies; non-invasive method.	Focus on in-depth histological structures; reconstruction via software needed when obtaining 3D image.	[117]
Optical Image system	Mainly facial skin	Yes	Objectively quantify changes in skin hemoglobin, melanin, and surface contour in 3D.	Obtains 3D images of skin surface; non-invasive method.	Focus on photodamaged skin; reconstruction via software is needed; has different accuracy level but shows real 3D topography.	[118]
OCT cm-OCT	Vascular structure beneath forearm skin	Yes	Provides high sensitivity and imaging speed for in vivo microcirculation imaging within the human skin.	Contains skin surface topological information in cross-section images; non-invasive method.	Focus on in-depth structures beneath skin;	[119]
PAT-OCT	Vascular structure beneath skin	Yes	High-resolution 3D imaging of vascular structures to depths of up to 5 mm.			[120]
Digital camera	Wounds	Yes	Color image processing of wounds.	Obtains 3D images of wound area; non-invasive method.	Has different accuracy level; reconstruction via software needed; only focus on wounds.	[121]
Laser scanner	Ulcer wounds	Yes	Obtain surface scan, estimate top area and true surface aera.	Obtains 3D images with wound surface topology information; non-invasive method.	Only focus on ulcer wounds; has different accuracy level; reconstruction via software is needed.	[122]
Confocal laser scanning microscopy	Histological structures inside the skin	Yes	Explore cutaneous microstructures via merge serial histological sections together.	Contains skin surface topological information in cross-section images; non-invasive method.	Focus on in-depth structures beneath skin; reconstruction via software is needed.	[123]
Fingerprint identification systems	Fingerprint outlines	No	Forensic applications, identification recognition.	Focus on skin surface; obtains 2D patterns in specific skin areas (fingerprints).	Only focus on fingerprints; difficult to obtain 3D images or acquire 3D information; has different accuracy level.	[68]

Well-trained dermatologists analyse the skin colour and interpret the clinical conditions of the skin based on their knowledge and experience, but diagnosis based on visual observation are subjective as colour perception depends on human visual response to light [124]. This kind of visual assessment is highly restricted to the individual judgement and experience of the dermatologists. Human eyes do not have the same sensitivity to all wavelengths, which cause a significant loss of skin information [125]. In the field of dermatology, luckily, a variety of optical techniques are used to map the skin conditions. Spectroscopy measures the light intensity as a function of wavelength, which was proved to be useful to acquire information about the skin [126]. Another series of optical techniques include the use of digital cameras. Digital cameras nowadays have ever higher resolution to record skin morphology with high precision, providing the 2D skin information. However, both spectrophotometer and digital camera have their respective limitations. Spectrophotometer lacks in spatial variation and

digital cameras lacks in spectral resolution [127]. Combinations of these two technologies were also investigated, which usually were called multispectral imaging (MSI) system [128-130]. Shi and Dimarzio [130] presented a hyperspectral imaging system applied to foot wound care and analysed data with two methods (Beer-Lambert law and two-layer optical model); however, the system was limited to the visible range and only three parameters (oxy/deoxyhaemoglobin concentration and epidermis thickness) were retrieved. Moncrie *et al*. have developed a multispectral imaging system covering visible and near-infrared light combine with an algorithm retrieving five parameters (total melanin content of the epidermis and papillary dermis, collagen and haemoglobin content, and the presence of melanin in the papillary dermis) but did not consider skin layer thickness [129]. Romuald Jolivot *et al*. developed a skin parameter map retrieval from a dedicated multispectral imaging system [127]. Those new optical techniques served as good supplementary methods to dermatologist visual diagnose. However, none of them have revealed the 3D information of skin (topography). Many skin and dermatological diseases related conditions contain much information in their third dimension such as scars and wounds.

2.2 On-skin applications of conducting polymers.

2.2.1 Application of conducting polymers in skin-related biomedical engineering.

Conducting polymers and their composites have been widely applied in various electronic devices to confer or to enhance the conductivity to the materials [31, 131]. Since the monomers are organic moieties that usually exhibit a certain degree of biotoxicity, it has initially dissuaded the potential application of conducting polymers in other research areas, such as biomedical engineering [132]. However, there have been an increasing number of studies using conducting polymers as biomaterials over the past decades owning to the fact that the materials are indeed cytocompatible in its polymeric form contrary to their monomer moieties [16, 115, 133, 134].

In fact, studies have also shown that conducting polymers can be doped by metal ions, which provide adequate conductivity as functional electrical stimulation materials for various tissue engineering applications [8, 135] as well as specific dermatological applications [136-140].

Moreover, CPs and their composites have shown intrinsic antibacterial properties. For example, Gizdavic-Nikolaidis *et al.* proved that polyaniline exhibited antibacterial properties against *E.coli, S. aureus* and *P. aeruginosa*, both the wild types and antibiotic resistant strains, as well as against other types of antibiotic resistant bacteria. The antibacterial activity was further enhanced by the use of the composites of poly(aniline-co-2-aminobenzoic acid) and poly(aniline-co-2-aminobenzoic acid) [141]. Similarly, polypyrrole/dextrin composite demonstrated antibacterial activity against *E. coli, P. aeruginosa, S. aureus* and *B. subtilis* [142]; the former three being bacterial strains that are commonly found in infected wounds [143]. The antimicrobial properties of CPs and composites could further be enhanced through the incorporation of silver nanoparticles [144-147]. Silver has traditionally been used in wound dressings to endow antibacterial properties [148], with silver nanoparticles, in particular, exhibiting more potent bactericidal effects [149]. For example, the deposition of silver nanoparticles onto PPy or PANI coated cotton fabrics further enhanced their antimicrobial activity [147]. Similarly, while microfibrillated cellulose/PPy aerogels inherently showed antimicrobial activity against *E. coli*, the incorporation of silver nanoparticles lead to significant activity also against *S. aureus* [144]. As an alternative to silver, some authors have even incorporated antibiotics into CP-based materials. For example, the antibiotic mupirocin, used for the treatment of skin infections, was incorporated by Jotiram *et al.* into PANI nanofibers, resulting in enhanced antimicrobial activity [150]. In fact, another key advantage of CPs use in wound dressings and tissue scaffolds is that they provide the opportunity for the controlled release of pharmacological and biological moieties.

Furthermore, CPs conduct electricity, thus can be used to electro stimulate skin or wound. The electrical stimulation (ES) in relation to wound care refers to the application of an external electrical stimuli to the tissue adjacent to, or directly within, a wound [151]. The intent is to exert greater control over cellular differentiation and proliferation, thereby accelerating the wound healing process [152]. The mechanism behind its functionality is that, in human skin, the epidermis normally maintains a transepithelial potential, analogous to an 'endogenous battery' [153]; any compromise to its structural integrity leads to a short circuit, resulting in a current vector at the perimeter of the wound which acts to guide cell migration towards the wound center, thus enhancing wound healing. It also controls the orientation and frequency of cell division [152]. It was found that by applying an external and appropriate electric field to the wound area, the rate of wound healing can be further accelerated [151, 154]. In fact a recent review provided strong support for the use of electrical stimulation to facilitate improved wound healing of chronic wounds [155]. The incorporation of CPs into wound dressings and tissue scaffolds provides the opportunity for ES to be more uniformly and routinely delivered to the injured tissue. In addition, some researchers have noted that CPs used alone, even without the application of an external electrical stimuli, resulted in accelerated wound healing [145].

Finally, the ability of CPs to be doped with specific moieties gives rise to the possibility of controlled release of drugs at the site of the wound. Ionic additives could be doped or loaded via reversible oxidation and reduction of film in the presence of ions in the solution or to perform electropolymerization in the presence of the ion solution. Differently, cations cannot be directed incorporated via oxidation along with monomers. They can be loaded on conducting polymer films by reducing the film and replace the previous doped cations [156, 157]. Control of delivery is achieved through the use of an externally applied electrical field. For example, Nguyen *et al.* examined the use of a PEDOT nanotubes patch for transdermal drug delivery in an *ex vivo* porcine skin model. The authors observed that controlled delivery

could be achieved via both short potential bursts and long term applied potential. They concluded that the transdermal patch offers a promising drug delivery method, particularly for drugs such as insulin [158]. Other authors have also examined the use of CPs to facilitate transdermal drug delivery [159-163]. Justin *et al.* demonstrated the controlled release of the anti-inflammatory and analgesic drug ibuprofen sodium salt from PPy films. Active, on-demand release was achieved via the application of an external potential. The authors also noted a lesser degree of passive release of the drug in the absence of an electrical stimuli [164]. Overall, CPs present an opportunity for facilitating controlled drug release, which in the case of wound dressings and skin tissue scaffolds, can be targeted specifically to the wound site.

2.2.2 Application of conducting polymers in wound healing.

The principle of wound healing is widely studied and investigated because it is not only related to dermatology but also could cause more serious issues such as infection. Thus, not limited to research publications, many books about wound healing have been published since last century [165-168]. The healing of wounds is a complex process that involves the activation and synchronization of intracellular, intercellular, and extracellular elements, including coagulatory and inflammatory events, fibrous tissue accretion, deposition of collagen, epithelialization, wound contraction, tissue granulation and remodelling. The research introduced in this thesis is more related to the functional dressing which have the potential to accelerate wound healing process in general via release of therapeutic moieties. O'Loughlin *et al.* investigated the use of type 1 collagen scaffolds for the topical delivery of autologous circulating angiogenic (CACs) cells (precursors to endothelial progenitor cells), to full thickness cutaneous ulcers [169]. It was revealed that the CACs could also be pre-stimulated through the addition of matricellular protein osteopontin (OPN), a glycoprotein involved in immune function, neovascularization, and facilitation of cell migration and survival [170].

Ehashi *et al.* compared subcutaneously implanted scaffolds for their host body reactions in order to assess their wound healing capacities [171]. The scaffolds consisted of collagen coated porous (Ø32 μm and Ø157 μm) polyethylene (CCPE), bio-inert poly (2-methacryloyloxyethyl phosphorylcholine-co-n-butyl methacrylate) (PMB) coated polyethylene, and uncoated porous polyethylene (UPPE). Jin *et al.* investigated a novel scaffold comprised of electrospun core-shell gelatin/poly(l-lactic acid)-co-poly-(ε-caprolactone) nanofibers, which encapsulated a photosensitive polymer poly (3-hexylthiophene) (P3HT) and epidermal growth factor (EGF) at its core [172].

Also, the CPs have been incorporated into wound dressings to provide enhanced antibacterial activity, to facilitate cell growth and to enable the provision of electrical stimulation or controlled drug release through the application of an external electric field [173]. A number of studies have combined CPs with polyurethane, a modern wound dressing material that are used for interactive dressings [71, 174]. The researchers sought to design an ideal dressing that maintains a moist wound environment, exhibits good mechanical properties under both dry and hydrated conditions, possesses potent antimicrobial activity, antioxidant activity and stimulates fibroblast growth and proliferation. Again, commonly used polyurethane was employed as the backbone, while siloxane was incorporated to supply enhanced mechanical stability. Aniline tetramer was used to provide the other desired aspects of the wound dressing. In general, PANI and oligoaniline derivates have been shown to exhibit inherent antioxidant activity; this was confirmed in the following study by measuring the dressing's scavenging capacity against the free radical 1,1-diphenyl-2-picrylhydrazyl (DPPH). Antibacterial and antifungal properties were demonstrated against *E. coli*, *P. aeruginosa* and *C. albicans*. Furthermore, cytocompatibility was demonstrated using murine L-929 fibroblasts. Accelerated cell growth and proliferation associated with the dressing itself, without the employment of electrical stimulation, was recorded by the authors, when compared to a control membrane that did not

contain the conducting aniline tetramer component [145]. This dressing provided many advantages and warranted further *in vivo* testing. Subsequent work was carried out on similar membranes using full thickness skin wound models in Wistar rats. Incisions of 1.5 cm^2 were inflicted and monitored for up to 20 days. Inclusion of the aniline tetramer in the membrane was associated with greater re-epithelialization, collagen deposition and vascularization of the wound area. In fact, on day 20, the aniline tetramer-containing membrane was associated with complete wound closure in the animal model (compared to 90% closure with the non-electroactive dressing and 76% in the control group that used cotton gauze to cover the wound) [175].

Other authors also utilized PANI to create electrospun nanofibrous membranes for use in wound care. The advantages of electrospun nanofibrous dressings in general are that they promote hemostasis, provide high absorption of wound exudate due to their high surface area to volume ratio, allow for atmospheric oxygen permeation, maintain control of an appropriately moist environment due to their semi-permeability, protect against bacterial infection due to their small pore size and provide 3D conformability to the wound contour [71]. Moutsatsou *et al.* created nanofibrous membranes comprised of PANI and chitosan [176]. Chitosan is a biocompatible, biodegradable and antimicrobial natural polymer and a commonly used ingredient for bioactive dressings [71]. The resultant PANI/CS membranes were assessed for cytotoxicity and effect on cell proliferation using human dermal fibroblasts and human osteoblasts (hOST-T85 cell line). It was found that even with higher ratios of PANI to chitosan (for example, 3:5), cell attachment and proliferation was supported. This highlights the potential for use of PANI/CS nanofibrous membranes for wound dressing applications [176]. Others to investigate electrospun nanofibrous membranes, included Karim *et al.* and Gizdavic-Nikolaidis *et al.* and Karim *et al.*, created membranes based on PANI with o-amino benzenesulfonic acid copolymer (PANI-co-PABSA) and poly (vinyl alcohol) (PVA)/chitosan

oligosaccharide (COS) biopolymers. These membranes were tested in a full thickness skin defect model in Sprague Dawley rats, together with the application of the commercially available topical ointment Fucidin®. Wounds of diameter 8mm were inflicted and monitored for up to 15 days; those treated with the PANI-co-PABSA/PVA/COS membranes plus Fucidin® demonstrated a statistically significant reduction in wound area compared to the control [177]. Gizdavic-Nikolaidis *et al.* created nanofibrous mats comprised of HCl-doped poly(aniline-co-3-aminobenzoic acid) (3ABAPANI) and poly(lactic acid) (PLA) via electrospinning. The growth of African Green Monkey COS-1 fibroblasts was supported at various ratios of 3ABAPANI to PLA, ranging from 5:95 to 45:55. Furthermore the nanofibrous mats were found to demonstrate antimicrobial properties against *S. aureus.* The authors highlight their potential use in wound dressings and tissue engineering scaffolds, particularly where the application of ES is desired [178].

The PPy was also incorporated into wound dressing materials. Da Silva Jr. *et al*. deposited PPy and carbon nanotubes (CNTs) onto polyurethane sponge, citing its possible application as a 'smart' dressing. Polyurethane is again a common wound dressing material. Carbon nanotubes have been previously examined as a potential material for use in biomedical applications such as tissue engineering [179, 180]. However, at high concentrations, they have been shown to exhibit cytotoxicity [181]. To address this issue the authors stated that when adhered to polyurethane and coated in PPy, direct contact of CNTs with skin is minimized, therefore the potential cytotoxicity of the overall material was significantly reduced. Cytotoxicity was not directly assessed in this study; however the enhanced antimicrobial activity of the PPy/CNT/PU composite was demonstrated against *S.aureus, K.pneumoniae* and *E.coli*. Further work is required to explore the possible use of this composite for 'smart' wound dressings [182]. Chowdhury *et al.* likewise utilized PPy to generate a novel potential wound dressing material. They produced composite films of regenerated cellulose coated with PPy and silver

nanoparticles, loaded with ionic liquid, for use as wound healing patches. Cellulose is a biocompatible and biodegradable natural polymer, whilst, as described previously, silver nanoparticles exhibit bactericidal activity. Ionic liquid loading further enhanced this effect. The antimicrobial activity of the composite was confirmed against *S.aureus* and *S.infantis* [146].

Besides, hydrogels and aerogels as wound dressings since they possess the advantage of high water content (70-90%) and thus maintains a moist environment, important for wound healing [70]. Additional advantages include that they can be easily applied and removed without inflicting damage to the wound bed and they can elicit a soothing and cooling effect to the wound area. Some of their disadvantages however include the fact that excessive accumulation of wound exudate can lead to tissue maceration, whilst overall they exhibit low mechanical strength [70]. They can also be used to manufacture aerogels by replacing the liquid component with gas (usually air). The resultant aerogels are characterized by very high porosity and low density and can likewise be used as wound dressings [144]. PANI-based hydrogels are one of the biggest groups for this type of wound dressings. PANI were usually incorporated or decorated with other polymers or materials including chitosan, gelatin and carbon nanotubes [183, 184]. Hydrogels have also been created incorporating PPy. Similar to those PANI-based hydrogels, those PPy-containing composites take advantages of both PPy and their principle compounds such as gelatin or cellulose [144, 185]. Silver nanoparticles were also blended in some trials to provide an antibacterial nature [144, 186]. Overall, both hydrogels and aerogels incorporating CPs were used to provide enhanced skin tissue healing capabilities.

CHAPTER 3 EXPERIMENTAL METHODS AND TECHNIQUES

3.1 Reagents and materials.

Polystyrene sulfonate (PSS), 3,4-ethylenedioxythiophene (EDOT), sodium dodecyl sulphate (SDS), ethanol (98%), pyrrole (Py; 98%), potassium chloride (KCl), copper chloride dihydrate ($CuCl_2 \cdot 2H_2O$), zinc chloride ($ZnCl_2$), Dulbecco's Modified Eagle's Medium (DMEM)-high glucose, sodium bicarbonate ($NaHCO_3$; 99.7%), fluorescein diacetate (FDA; cell viability stain) and propidium iodide (PI; 94.0%), glycerol trioleate and silicone oil were obtained from Sigma-Aldrich (Merck KGaA, USA) and directly used as obtained without any further purification. Sputter coater targets of gold (99.999%) and platinum (99.95%) were purchased from Ted Pella, Singapore. Quantitative cellulose filter paper (Grade 390, Sartorius, Singapore) was obtained from Sartorius Inc, Singapore. Food-grade pork with skin (Bulan pork skin, Indonesia) and olive oil (Borges) were used for simulating the natural skin fractures through application of a pig skin model and replacement of natural sebum, respectively. Gelatin was purchased from Wako Pure Chemical Industries, Ltd. Fetal Bovine Serum (FBS) was obtained from Research Instruments Pte. Ltd. - GE HycloneTM. Antibiotic-antimycotic (ABAM), 0.25% trypsin-ethylenediaminetetraacetic acid (EDTA) solution and PrestoBlue® cell viability reagent was purchased from Life Technologies. Immortalized human keratinocytes (HaCaT cells) were obtained from Division of Genetics of Skin Carcinogenesis, Germany Cancer Research Centre.

In this thesis, various substrates were used for fabricating materials for on-skin applications, they included cellulose filter papers, weighing papers (Grade 390, Sartorius, Singapore), glass plates, and polyethylene terephthalate (PET) films. The PET films (0.26 mm thick) were cut from computer screen protector films (27.4 × 20.6 cm^2, Emotal, China). The later one had dustproof covers on both sides, which were peeled off before coating with metal to maintain the substrate clean. Membrane filter (ME 25 ST, Schleicher & Schuell, Germany), weighing

paper (4 × 4 cm^2, Fisher Scientific, USA) and glass plates (2.5 × 5 cm^2) were directly used as obtained before coating. Films were cut into different size upon specific utilization. All of them were insulators, thus, to make them electrically conducting, coating of a thin film of metals was required. In this study, gold covered PET plastic (Au-PET), platinum covered polyethylene terephthalate plastic (Pt-PET), gold covered cellulose paper (Au-paper), platinum covered cellulose paper (Pt-paper) films were all prepared by a sputtering of the metal using a sputter coater (JFC-1600, JEOL, Japan), applying 40 mA current for 300 s that resulted in 50-60 nm thick metal films.

3.2 Electrochemical techniques.

All the electrochemical measurements reported in this thesis including electropolymerization and electrochemical characterizations were conducted using a CHI 700E series electrochemical Analyzer (Shanghai Chenshan, China) and a Gamry interface 1000 potentiostat (Gamry, USA).

3.2.1 Chronopotentiometry and chronoamperometry.

Galvanostatic chronopotentiometry (GCP) is an electrochemical technique in which a controlled current, usually a constant current (or currents at multiple stages) is applied between two electrodes; the potential of one electrode is monitored as a function of time with respect to a reference electrode. The solution is usually, but not necessarily, unstirred and contains an excess of a supporting electrolyte so that diffusion is the principal mechanism of mass transport [187]. The GCP was extensively used for electropolymerization of PEDOT and Py in this thesis.

Chronoamperometry (CA) is an electrochemical technique in which the potential of the working electrode is stepped and the resulting current from faradaic processes occurring at the electrode (caused by the potential step) is monitored as a function of time. While the potential is applied, current passing through the working electrode is monitored as a function of time

with respect to a reference electrode. The CA was also extensively used for electropolymerization of PEDOT in this thesis.

3.2.2 Cyclic voltammetry (CV).

CV is an electrochemical technique in which the potential is controlled and swept at a constant sweeping rate, back and forth between two particular border potentials. The current is monitored and recorded as a piecewise linear function of time (also as a piecewise linear function of potential) with respect to a reference electrode. The CV is a powerful technique commonly employed to investigate the reduction and oxidation processes of molecular species and electron transfer-initiated chemical reactions [188]. In this thesis, CV was applied as a basic electrochemical characterization technique of the synthesized materials, including skin maps and cellulose substrates. Besides, CV was also used as an electropolymerization technique to electrosynthesize different polymers. The CVs were used to calculate of area-based specific capacitance of the investigated substrates. The equation used to calculate the specific capacitance is shown below:

$$\boldsymbol{C = \frac{\int jvdv}{2\mu\Delta V}}$$

Where:

C, specific capacitance, F/cm^2.

j, current density in CV test, A/cm^2.

v, potential in CV test, V.

μ, scan rate, V/s.

ΔV, potential window of discharge, 1.3 V here.

3.2.3 Electrochemical setup.

In all the electrochemical measurements, a standard three-electrode electrochemical cell was used. The potential was applied to the working electrode (WE), which was controlled against the reference electrode (RE). The current was measured/applied between the working electrode and the counter electrode (CE). The scheme of three electrode electrochemical cell is shown in Figure 5. In the electrochemical setup, target synthesized materials were used as working electrodes while a platinum mesh (2 × 7 cm) served as a counter electrode and an Ag/AgCl (3M KCl) served as a reference electrode, respectively. All the electrochemical activities were carried out in ambient temperature (22 ± 2 ºC). Additionally, novel electrochemical cell was used for on-body skin patterning, which will be described in chapters 4.1.1. Notably, the designed portable skin mapping device was working in a two-electrode system where only working electrode and counter electrode were applied (1.5 V dry battery powered system). Specific arrangements of the electrochemical cell, electrodes and substrates used throughout this thesis will be discussed separately in subsequent chapters.

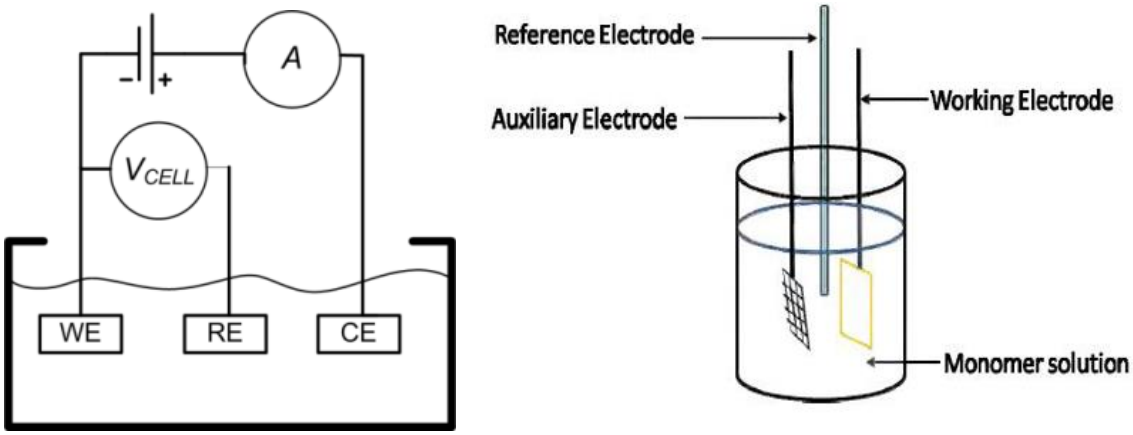

Figure 5. Schemes of three-electrode electrochemical cell.

3.3 Cellular studies of electroactive cellulose substrates for on-skin treatment.

The cytocompatibility and the cell-material interactions with the electroactive cellulose substrates were assessed using HaCaT cells according to the previously established methods

[189]. Briefly, HaCaT cells were cultured and expanded using DMEM-high glucose medium supplemented with 10% FBS, 1.6 g/L $NaHCO_3$ and 1× ABAM. The cells were cultured at 37 ºC and 5% CO_2 environment with saturated humidity. The medium was changed every other day and sub-cultured upon reaching 80% confluency using 0.5% Trypsin-EDTA solution. Prior to cell seeding, the various electroactive cellulose-based substrates (1.5 × 2.0 cm) were coated with 200 µL of 5 mg/mL gelatine via air-drying process. Subsequently, the samples were sterilized by soaking in 70% ethanol for 30 min followed by washing with 1× phosphate buffered saline (PBS) solution (137 mM NaCl, 2.7 mM KCl, 10 mM Na_2HPO4, 1.8 mM KH_2PO_4) and DMEM-high glucose medium. Cells from passages 4-6 were then seeded onto the samples with an initial cell seeding density of 3 × 104 cells/cm^2. Subsequently, the cell-material interactions were assessed over 7 days under three different pH conditions (pH 6.5, 7.5 and 8.5). On various time points, the number of cells attached and proliferated on the different samples was quantified using PrestoBlue® cell viability reagent. Briefly, the cell-seeded samples were washed with 1× PBS followed by incubation with 10% PrestoBlue® solution for 30 min at 37 ºC and 5% CO_2 environment with saturated humidity. At the end of the incubation, the reagent medium was transferred to 96-well plate and the fluorescence intensity was measured at 560 nm excitation (ex) and 590 nm emission (em) using a SpectraMax M2 microplate reader (SpectraMax® Gemini, Molecular Devices, USA). The number of cells on the different samples was calculated using a standard curve that correlates the fluorescence intensity with the known number of cells. On day 7, the viability and the distribution of the cells on the different samples were evaluated by staining the cells with 5 mg/mL of FDA and 2 mg/mL of PI in serum-free cell culture medium for 5 min in dark.[190] At the end of the incubation, the staining solution was removed followed by washing with 1× PBS. Subsequently, the samples were imaged using Zeiss Axio Observer.Z1 inverted fluorescence microscope (Carl Zeiss, Germany), where FDA with a green fluorescence

(ex488/em517) was used to assess the live cells and PI with a red fluorescence (ex561/em618) was used to assess the dead cells.

3.4 Ion loading and release of the materials for on-skin treatment.

Both cellulose-based and PET-based materials in this study have been tested with loading and release of therapeutic metal ions. For cellulose-based substrates, ions loading was carried out simultaneously during conducting polymer synthesis, where the metal ions (Cu^{2+} and Zn^{2+}) were present in the polymerization solution. Briefly, the platinum-coated cellulose substrates were used for the electropolymerization of conducting polymers (PEDOT and PPy, both doped with SDS). Electropolymerization process was conducted in a typical three-electrode electrochemical cell. In general, platinum mesh (2 × 7 cm) served as counter electrode, silver/silver chloride with saturated potassium chloride served as a reference electrode and platinum-coated cellulose substrate served as working electrode. Chronopotentiometry (CP) was used for the electropolymerization process at the parameter of 0.2 mA/cm^2 and 1000 sec. Four different groups of electropolymerization solutions were used to fabricate different types of electroactive cellulose-based substrates, as listed in Table 3. At the end of the electropolymerization process, the electroactive cellulose-based substrates were pre-cleaned by rinsing with distilled water on both sides for 5 sec. Subsequently, the samples were washed thoroughly by soaking the samples in fresh distilled water with light shaking for 5 s. The washing step was repeated for 5 times to fully remove the residual monomers and unbound metal ions.

These substrates were tested in passive release of Cu^{2+} and Zn^{2+} ions and the ion release were quantified by inductively coupled plasma mass spectrometry (ICP-MS; Thermo Fisher, USA). Briefly, to observed passive ion release, the electroactive cellulose-based substrates (2 × 3 cm) were immersed in 5 mL of bicarbonate-buffered solutions at three different pH conditions (i.e. pH 6.5, 7.5 and 8.5) and kept at room temperature for 48 h. After that, 5 mL of the respective buffered solution was transferred into the ICP-MS injector tube where the amount of copper and zinc that was released into the buffered solution was quantified and compared based on the average values of three replicates (n = 3). Particularly, none-electropolymerized samples were used as negative controls (i.e. pyrrole (Py) and 3,4-ethylenedioxythiophene (EDOT)) to eliminate the physical interactions of the metal ions with the platinum coating. Also, the platinum-coated cellulose substrates were purely immersed in the electropolymerization solutions, such as Py(SDS) or EDOT(SDS) solution in the presence or absence of Cu^{2+} and Zn^{2+} ions without the applied potential or current. Subsequently, the samples were removed and washed with distilled water prior to the ions release study following the same procedures as ion-loaded electroactive cellulose substrates [133].

Furthermore, PET-based materials were also tested for their metal loading ability and electro-controlled release. In this material, metallic copper (Cu^0) was deposited on the conducting polymer substrates. Standardized 1 × 1 cm^2 PEDOT(PSS) deposited films were electrochemically prepared in EDOT(PSS) solution by applying 0.2 mA/cm2 under CP for 300 s. The metallic copper was electrodeposited onto PET-Au/ PEDOT(PSS) films via reduction of Cu^{2+} to Cu^0 from 0.1 M $CuCl_2$ aqueous solutions, by applying 0 V and –1 V vs Ag/AgCl (3M KCl) under CA, respectively. Metal reduction duration ranged from 10 to 150 s to identify the optimal metal deposition quantities. A field emission scanning electron microscope (FESEM) (JSM-7600F, JEOL, Japan) equipped with energy dispersive X-ray spectroscope (EDS) was used to confirm successful metal deposition and observe the surface morphology.

Raman spectra analysis was also performed using alpha 300R confocal Raman microscope (WiTec, Ulm Germany) for the same purpose. Before and after the metal reduction, the films were rinsed with deionized water for 5 times. The rinsing after the electroreduction was done vigorously to remove the excess of free ions and reduce the amount of nonspecifically adsorbed ions onto the film. Once dried in air, the films were connected to the three-electrode electrochemical cell to study the release of Cu^{2+} with or without electrostimulation. The ion release was conducted in 0.1 M KCl during 1800 s. Initially, with no current applied for 400 s, then respective constant current (GCP) was applied until 1800 s was reached. A 1 mL solution was taken out every 200 s to investigate released concentration of Cu^{2+}. The same ICP-MS (iCAP Q, Thermo Scientific, USA) was used to analyze the concentration of released ions. At the same time, 1 mL 0.1 M KCl solution was added to the test solution in order to keep the electrolyte volume unchanged. Diluting coefficient was considered when analyzing the final released metal concentrations.

3.5 Material mechanical testing.

The mechanical properties of the cellulose-based materials were determined by measuring the tensile modulus following previously established method [191]. Briefly, the rectangular bars of dimensions of 4 × 1 cm were used for the tensile testing. Prior to the tensile testing, the various samples were soaked in bicarbonate-buffered solutions at three different pH conditions (pH 6.5, 7.5 and 8.5) overnight at room temperature. Subsequently, the sample was blotted dry and loaded to an Instron mechanical tester Model 5567 (Instron Corp., USA). Tensile test was performed by pulling the sample at a constant rate of 0.5 mm/min using a load cell of 10 kN until the sample rupture. The tensile modulus of the sample was obtained based on the initial gradient of the stress-strain curves and the physical properties of the samples were compared based on average values of eight replicates (n = 8).

3.6 Microscopic and spectroscopic characterization of the developed materials.

3.6.1 Field Emission Scanning Electron Microscopy (FE-SEM).

FE-SEM is microscope that works with electrons instead of light. These electrons are liberated by a field emission source. The detector catches the secondary electrons and an image of the sample surface is constructed by comparing the intensity of these secondary electrons to the scanning primary electron beam. The FE-SEM produces clearer, less electrostatically distorted images which is 3 to 6 times better than conventional SEM [192, 193]. Besides, FE-SEM is usually equipped with an energy dispersive X-ray spectroscopy (EDS), which could help with elements discrimination both in contents and distribution [192]. In this study, the surface morphology of the obtained 3D electrically conducting skin patterns, the evaluation of the modification during the optimization process, and micro-structure of synthesized polymer films were investigated using a FE-SEM (JSM-7600F, JEOL, USA).

3.6.2 Energy dispersive X-Ray Spectroscopy (EDS).

EDS is a chemical elementary microanalysis technique used in conjunction with SEM or FE-SEM. In this work, EDS analysis was performed in combination with the introduced FE-SEM. The EDS technique detects x-rays emitted from a sample during its bombardment by an electron beam to characterize the elemental composition of the analyzed volume [192, 193]. Features or phases as small as 1 µm or less can be analyzed. In this thesis, EDS was used to confirm the presence of CPs, metal doping, and sebum deposition by investigating elemental composition of various materials.

3.6.3 Atomic Force Microscopy (AFM).

AFM is one of scanning probe microscopes (SPM). An AFM uses a cantilever with a very sharp tip to scan over a sample surface. As the tip approaches the surface, the close-range, attractive force between the surface and the tip cause the cantilever to deflect towards the surface. By reflecting an incident beam off the flat top of the cantilever, any cantilever deflection will cause slight changes in the direction of the reflected beam. A position-sensitive photo diode (PSPD) can be used to track these changes. Thus, if an AFM tip passes over a raised surface feature, the resulting cantilever deflection is recorded by the PSPD [70]. To image the topography, an AFM scans the cantilever over a region of interest. The raised and lowered features on the sample surface influence the deflection of the cantilever, which is monitored by the PSPD. By using a feedback loop to control the height of the tip above the surface thus maintaining constant laser position the AFM can generate an accurate topographic map of the surface features [194, 195]. One of the most valuable property of AFM is that it is able to provide 3-dimensional pictures, which is essential for characterization of surface topography of the obtained 3D electrically conducting skin patterns. In this work, the topography of obtained 3D electrically conducting skin patterns was studied by an atomic force microscope (AFM) (XE-Series, Park, Korea).

3.6.4 Stylus profilometry.

In a profiler, a probe moves along the sample surface, monitoring the force feedback against the probe. The vertical heights of samples are recorded as it scans the area. Thousands or even millions of feedbacks of vertical positions are then used to reconstruct the investigated area. Stylus profilometer has direct contact with the sample when running, which is similar to AFM. It has lower resolution but higher coverage area than AFM. Its high handleability and excellent repeatability make it a perfect tool for analyzing thin films [196]. In this work, a KLA Tencor-L6 stylus profilometer was used to characterize 3D nature of the developed skin maps.

3.6.5 Raman spectroscopy.

Named after an Indian physicist, Chandrasekhara Venkata Raman, Raman spectroscopy is a fast technique to identify moieties based on their unique structural fingerprints. When light is scattered from a molecule, most photons are elastically scattered (with the same frequency and wavelength as the incident light) while a small part of photons (approximately 1 in 10^7) are inelastically scattered usually with a lower frequency. This is called Raman scattering or Raman effect. Raman scattering can occur with a change in vibrational, rotational, or electronic energy of a molecule, and thus the technique of Raman spectroscopy for identifying molecule/crystal structure was founded based this theory [197]. In this work, Raman spectra measurements were performed using an alpha 300R confocal Raman microscope (WiTec, Ulm Germany) equipped with a 532 nm excitation laser. Spectral acquisition was performed as spot measurements across the surface over a spectral region of –52 to 3789 cm^{-1} using a 50× air objective (NA = 0.8) and 5 mW laser power. Each spectrum consisted of 4 second times 30 accumulations.

For a clearer description of the experiments and studies included in this thesis, a table of summary of experiments was shown below (**Table 2**).

Table 2. Summary of experiments conducted in the thesis.

No	Experiments	Featured materials	Methods
1	On-body skin mapping development	Au-PET substrates, custom layered electrochemical cell.	On-site electropolymerization.
2	Off-body skin mapping development	Au-PET substrates.	Pressure-controlled sampling, beaker-based electropolymerization.
3	Prototype development of skin mapping device	Dry battery, 3D-printed prototype.	Design on Solidworks, realization via 3D printing.
4	Cellulose substrates preparation	Cellulose paper.	Beaker-based electropolymerization.
5	Characterization of cellulose substrates	Developed cellulose substrates.	Electrochemical, mechanical, microscopical methods.
6	Cellular studies of cellulose substrates	HaCaT cells, developed cellulose substrates.	*In vitro* cellular studies, evaluating the cell adhesion and the proliferation of HaCaT cells over 7 days of cell culture.
7	Skin mapping trial using simulated pig wounds	Unfrozened-pig skin.	Pig skin was cut into simulated wounds models, followed by off-body skin mapping technique.
8	Bimetallic ions loading and release tests of cellulose substrates	Zn^{2+} and Cu^{2+} mixed monomer solutions.	Electropolymerization with presence of ions, passive release of ions.
9	Copper loading and electro-controlled release tests of PET-based materials	Au-PET with PEDOT(PSS) coverage.	Electrodeposition of copper metal, electro-controlled oxidative release.

CHAPTER 4 DEVELOPMENT AND PERFORMANCE OF CONDUCTING POLYMER-BASED MATERIALS

4.1 Controlled deposition of conducting polymer films: skin mapping.

A clear need for a portable and fast 3D skin mapping to specific skin surfaces, mainly for dermatological diagnosis, monitoring and treatment has resulted in the development of the portable and fast technique to map various skin features. Overall, the technique consists of two modes, namely on-body skin mapping and off-body skin mapping, which was designed to be applicable for sampling different skin features. The general scheme of 3D electrically conducting skin patterns preparation is shown in Figure 6.

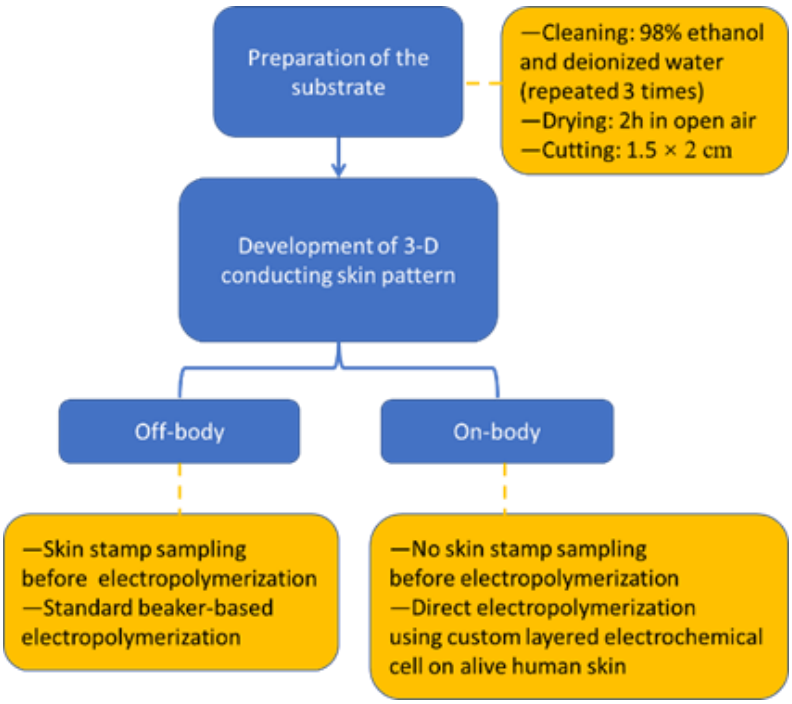

Figure 6. Procedure of on- and off-body 3D skin mapping techniques.

4.1.1 On-body skin mapping.

In on-body skin mapping the sampling and patterning process were realized on live human skin. The PEDOT(PSS) electropolymerization was performed directly on a human skin. A custom layered electrochemical cell was developed specially for this application in this work, to the best of my knowledge, for the very first time. It consisted of one piece of gold substrate (working electrode), a platinum mesh (counter electrode) and one Ag/AgCl (3M KCl) reference electrode. To avoid short-circuiting and to allow electropolymerization solution retention around the electrochemical cell, the electrodes were separated with the layers of paper spacer (cellulose filter paper, grade 390, Sartorius, Singapore). The paper contained absorbed electropolymerization solution (aqueous EDOT and PSS solution) that was further on used to electro-deposited PEDOT(PSS) at the gold surface in spaces where the electrode was not in direct contact with the skin. The electrochemical cell was then placed on an untreated, live human subject skin where clean gold surface was in direct contact with the live skin. The reference electrode was used to press the electrochemical cell onto the skin. Detailed scheme presenting the custom layered electrochemical cell is shown in Figure 7. Electropolymerization solution was applied on the whole custom layered electrochemical cell by pipetting the solution on top of the cell. The flowing downwards electropolymerization solution filled in the narrow gaps between skin and PET-Au layer (working electrode). The gaps were generated because the surface of skin is uneven (with pronounced topological features, e.g. wrinkles), allowing electropolymerization solution to accumulate in the crevasses where the surface of the electrode was not directly touching the electrode. Once the anodic current was applied, conducting polymers electropolymerized in that gaps (as there was available electropolymerization solution and the surface of the electrode was not blocked by direct contact with the skin). On the other hand, the conducting polymer was unable to electropolymerize in places where there was direct contact between the electrode and the skin.

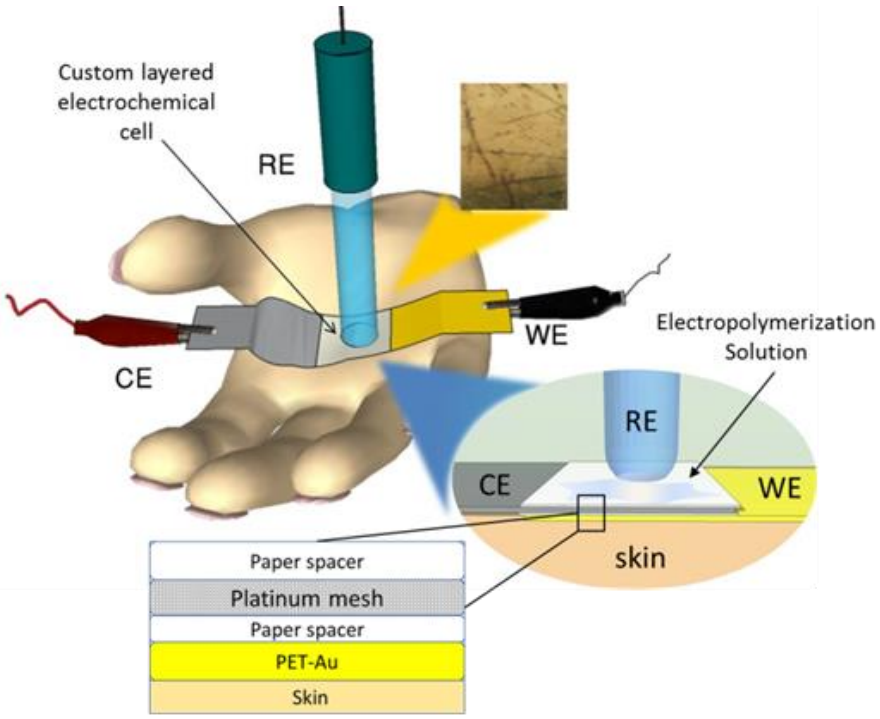

Figure 7. Scheme of on-body, direct electropolymerization on live human skin featuring high-resolution camera picture of developed 3D and electrically conducting skin pattern.

4.1.2 Off-body skin mapping.

Off-body skin mapping was the main method investigated in this thesis with well-optimized performance of the developed skin maps. A depiction of the proposed off-body skin mapping technique is illustrated in Figure 8. The fabrication protocol of 3D skin patterns consisted of two steps, namely skin stamp sampling and 3D skin patterning. Skin stamp sampling (Figure 8a) was realized as the skin leaves a mark in the shape of its pattern after the contact with the conducting substrate surface, e.g. PET or paper covered with metal such as Pt or Au. A skin surface is not homogeneous but consists of wrinkles, lines, pores and various pathological features [198]. Thus, it has topological structures, which correspond to its pattern outlines. When skin surface was pressed against the homogeneous substrate, IRs were deposited on skin surface in a shape that imprinting skin surface topological structure and forming a mirror stamp of the skin pattern outlines. Then the 3D skin patterning was realized via electro-controlled

deposition of conducting polymers on an electrically conducting surface (Figure 8b). Conducting polymers were hypothetically only deposited on bare metal surface while the electropolymerization was prevented within IRs-deposited substrate areas. Conducting polymers grew vertically, which reflects the topological structure of the objective skin parts. After the electropolymerization, the positive mirror IRs stamp was replaced by a negative mirror 3D conducting polymer pattern, a 3D skin map, with high visibility and stability. Electropolymerization of conducting polymers onto a conducting substrate is a well-established process [199, 200]. The amount of conducting polymers and the doping level can be precisely controlled by changing applied current or potential [201], which makes it particularly suitable for precise skin mapping. Conventional skin mapping usually refers to measurement or monitoring of biophysical properties of skin including surface pH, surface temperature, barrier function against water loss, stratum corneum hydration and erythema index [202, 203]. These can be easily realized by noninvasive instruments, namely Tewameter, Corneumeter, pH-meter, Mexameter, surface thermometer, and Sebumeter [202]. In comparison, the new developed skin mapping technique focuses on recognition and reproduction of various skin surface morphologies and topologies. They focused more on algorithm development and the use of artificial skin features evaluation, and the resolution is still limited by the intrinsic property of an ultrasound probe [204]. Therefore, the new-developed skin mapping technique is believed to provide an advantageous role in dermatological diagnosis of the skin.

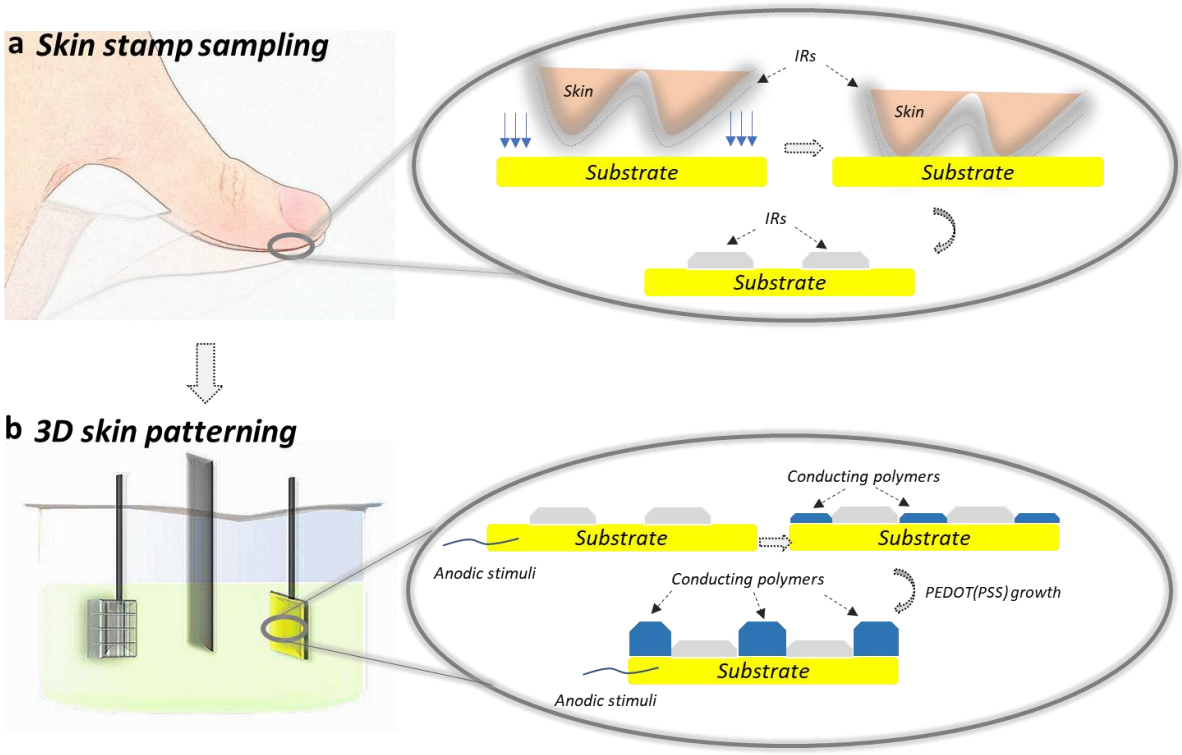

Figure 8. Scheme of proposed skin mapping: (a) skin stamp sampling and (b) 3D skin patterning.

4.1.2.1 Electrochemical characterizations of the on- and off-body skin patterns.

Electrochemical characterization of all on- and off-body 3D and conducting skin patterns was performed and compared to the standard PEDOT(PSS) without any modification (Figure 9). All the films exhibited a capacitive behavior, a very typical for PEDOT(PSS) films. Although, the surface area available for electropolymerization of the off-body 3D and electrically conducting skin pattern was smaller than for PEDOT(PSS) on the unmodified surface, developed substrates were characterized with nearly the same specific capacitance, 3.0×10^{-3} F/cm^2 (off-body 3D and electrically conducting skin pattern) and 2.9×10^{-3} F/cm^2 (unmodified PEDOT(PSS)). The film specific capacitance depends on the surface area available for the polymerization, time of the polymerization and resulting thickness of the film. In off-body skin patterning the area available for the electropolymerization was smaller than in unmodified

PEDOT(PSS), thus applying the same polymerization time, it resulted in thicker films. In on-body skin pattering the thickness of conducting polymer was limited (as explained before) and it resulted with thinner conducting polymer than that of pure PEDOT(PSS) and subsequently with lower specific capacitance (1.9×10^{-3} F/cm^2).

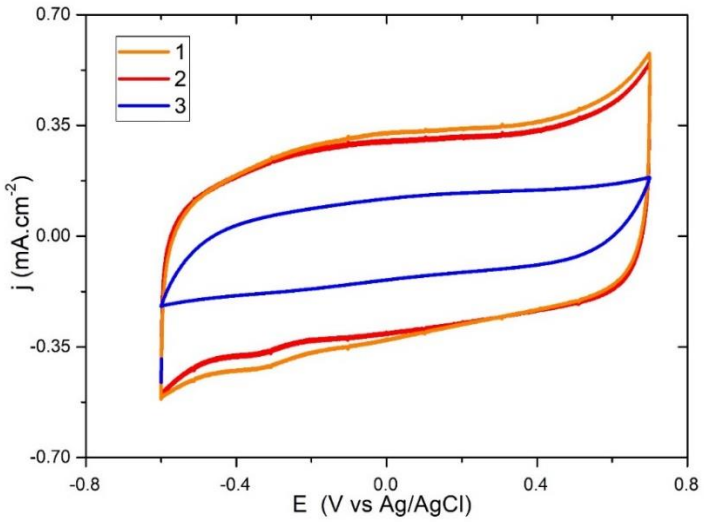

Figure 9. CVs of off-body handprint (1), pure PEDOT(PSS) (2) and on-body hand print (3): obtained in 0.1 M KCl by scanning the potential between -0.6 and 0.7 V *vs* Ag/AgCl (scan rate: 0.1 V/s). Only 5th (last) scan is presented.

The electropolymerization potential transient curves of developed off- and on-body 3D and conducting skin patters are shown in Figure 10. The potential *vs* time curves were compared to the ones obtained for the standard PEDOT(PSS) electropolymerization. The standard and off-body skin mapping the pure PEDOT(PSS) electropolymerization were found very similar (instant potential peak maximum approx. 0.9 V with gradual potential decrease). Thus, the electropolymerization of sebum-modified gold surface was found not to be affected by the presence of sebum. The on-body polymerization resulted in nearly double potential of that for standard PEDOT(PSS) electropolymerization. This, however, can be explained by the

relatively complex measurement setup and low availability of the solution in the paper matrix (thus, high resistance). The potential-time curve was also relatively unstable owning to the small uncontrolled movements of the hand during the polymerization. Both CVs and polymerization curves showed an unstable process that on-body skin mapping provided. This could be attributed to the setup itself, as discussed above, the complexity and high resistance of paper matrix. The other reason comes from the natural instability of live human skin surface with vibration from blood flow and pulse. On the contrary, off-body mode does not have any of those disadvantages mentioned. It performs stably on EDOT(PSS) polymerization, and results in adequate thickness of PEDOT(PSS) films. The off-body skin patterning avoids direct contact between monomer solution and live human skin, which could be a potential toxicity concern for further application. Considering those reasons, off-body mode was further investigated towards more optimization use of the material in the 3D skin patterning.

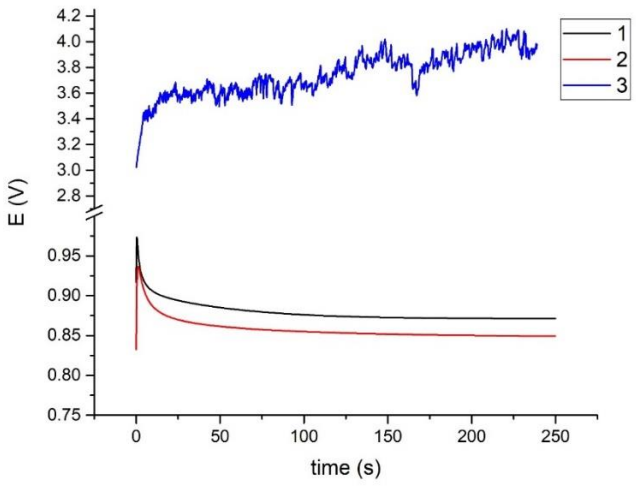

Figure 10. Potential-time curves registered during electropolymerization of off-body handprint (1), pure PEDOT(PSS) (2) and on-body handprint (3).

4.1.2.2 Evaluation of the developed skin maps.

Figure 11 presents some examples of developed 3D skin patterns using PET-Au substrate. The pristine 0.26-mm-thick PET substrate has excellent flexibility, which is an essential property for mapping different skin topographies. The flexibility of PET, PET-Au, IRs-deposited substrate, and 3D skin pattern on PET-Au are shown in Figures 11 a-d. The metal coating and subsequent deposition of conducting polymers had a negligible effect on the flexibility of PET substrate. The flexibility of the sampling substrate allowed the material fit better onto the skin surface during the sampling of skin stamp, especially for uneven skin areas such as gaps between fingers or elbow surface. Moreover, the gold is flexible in nanometer-layer thickness, which assures metal continuity when bending [205]. Finally, the conducting polymers in micrometer-layer thickness were proven to have good flexibility for usage in flexible batteries and sensors [206, 207]. The possibility of the development of 3D skin mapping on various skin topographies, including fingerprints, scars, palm hand, skin on the hand, and joint wrinkles were also shown in Figure 11. The developed skin patterns of fingerprint (Figure 11d), back of a hand (Figure 11g) and palm hand (Figure 11h) stamps show high resolution, which was found to be sufficient to define skin topography. In contrast, the 3D skin pattern developed from scar (Figure 11e) and joint wrinkle (Figure 11f) stamps presented the main skin outlines while the minor structures were diffused. That is because the main structure in scars and wrinkle are too obtrusive against the minor lines/structures. As the substrate was put on a flat surface when sampling, the minor lines/structures became less distinct compared with the main scar or wrinkle structure. The fingerprints possess abundant textural features and clear minor ridges that reveal enormous details of the skin mapping quality; thus, in order to obtain detailed information and standardize the evaluation of the 3D skin patterning, fingerprints were selected as the representative skin topography.

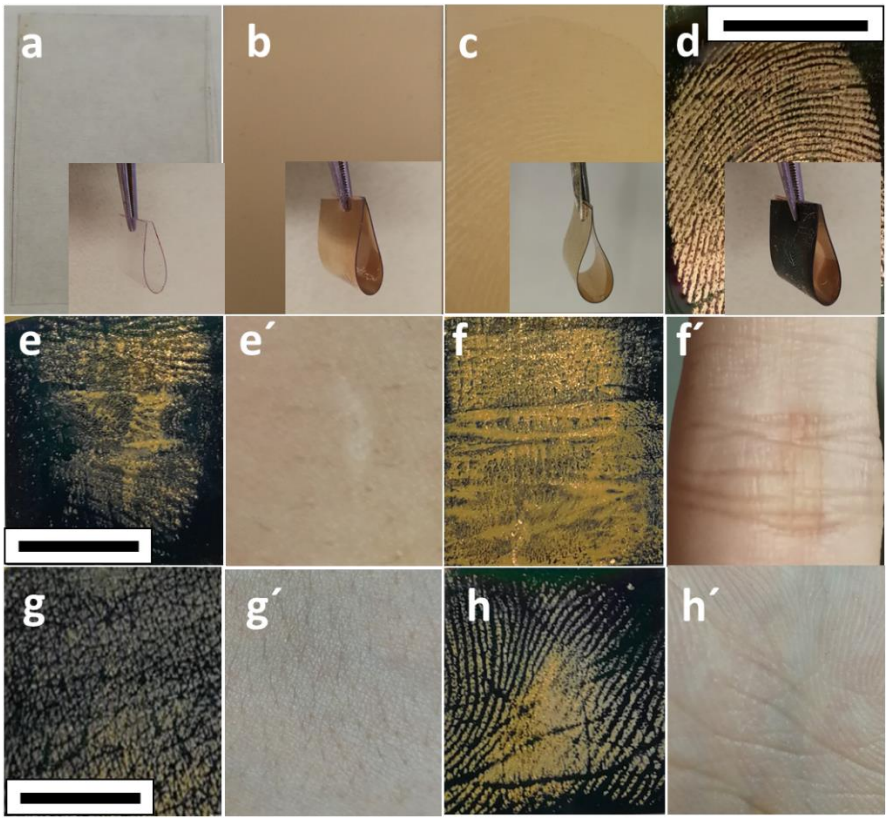

Figure 11. (a-d) High resolution camera pictures of: (a) Pristine PET substrate, (b) Au-PET, (c) Au-PET with IRs stamp, (d) developed skin map (fingerprint); and Developed skin patterns from off-body skin mapping of (e) scar, (f) joint wrinkle, (g) back of the hand, (h) palm of the hand and their corresponding camera pictures (e´, f´, g´, h´). Scale bar: 1 cm

Furthermore, images with even higher resolution were taken and shown in Figure 12. Notably, for comparison pure gold surface (Figure 12a) and electropolymerized PEDOT(PSS) on such gold surface (Figure 12d) were shown. Figure 12b and 12e present a local part of IRs deposits (skin stamps) on the pure gold surface, while Figure 12c and 12f presents their corresponding developed skin patterns, respectively. The IRs modified gold inhibited the electropolymerization (bright skin lines) while the rest was occupied by the electropolymerized 3D conducting polymer (dark area) corresponding to the sampled skin features. It is clear that conducting polymer-based patterns have better color contrast than IRs-based patterns, the fact

which was utilized by Hillman *et al.* for forensic purposes [208]. Figure 12g, 12h and 12i show the developed skin patterns of a mole, a hand scar and forehead print, respectively.

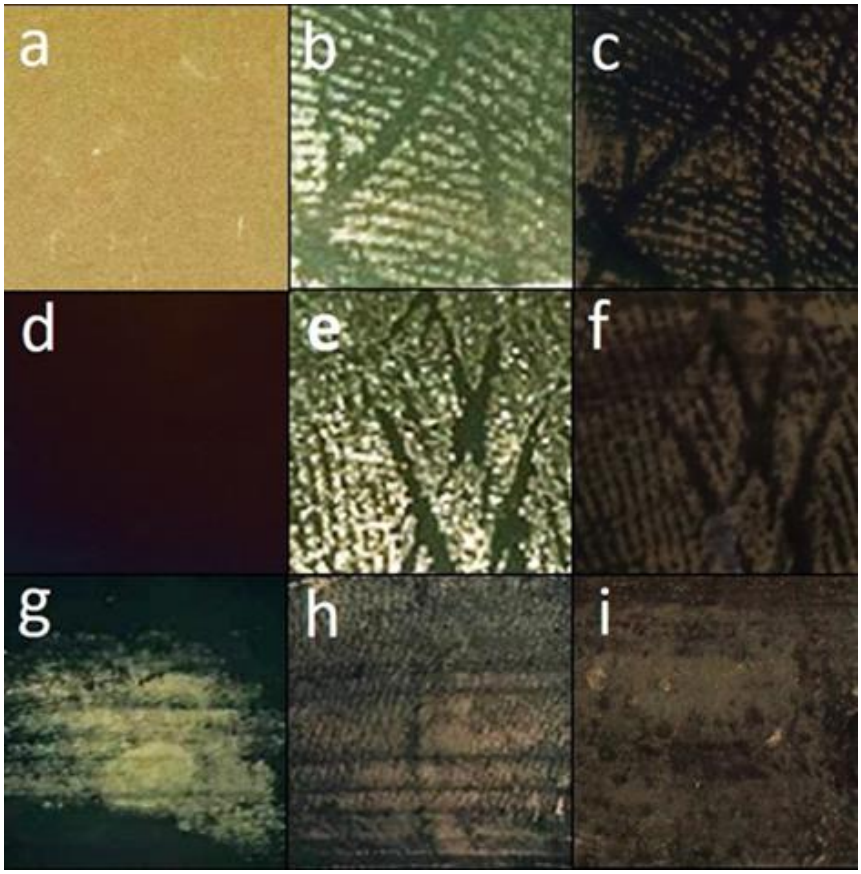

Figure 12. High-resolution camera images of local patterns from off-body skin mapping: Pure gold substrate (a), sebum-gold skin pattern stamp (b and e), developed skin patterns (c and f), pure PEDOT(PSS) electropolymerized on plastic-gold substrate (d), developed mole print (g), developed hand scar print (h) and developed local forehead print (i).

An energy dispersive X-ray spectroscopy (EDS) was also used to confirm the presence or absence of the conducting polymer in the developed 3D electrically conducting skin patterns by investigating elemental composition of sebum/IRs and conducting polymer modified regions of 3D skin patterns. The PEDOT(PSS) contain relatively high concentration of sulfur, thus the signal from sulfur was taken as indication of presence or absence of conducting polymer in the investigated regions of the 3D electrically conducting skin patterns. Signal from

sulfur was registered only in the regions where conducting polymer was electrosynthesized, while space where sebum was stamped onto the PET-Au surface were left without electropolymerized PEDOT(PSS). This confirms 3D nature and successful selective modification of the surface corresponding to the topography of the skin. That was confirmed also by AFM of the off-body 3D electrically conducting skin patterns. The EDS spectra and corresponding region FE-SEM images (inset) are shown in Figure 13.

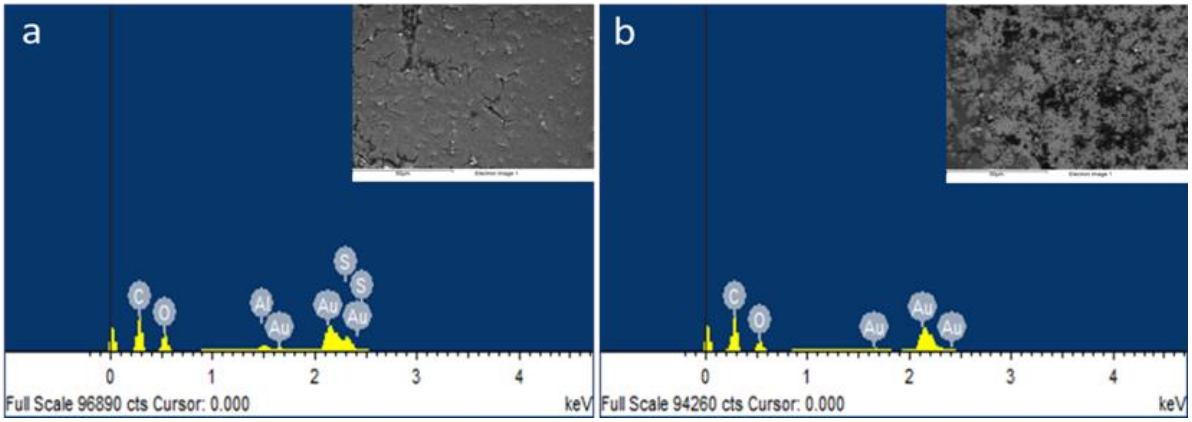

Figure 13. EDS elementary analysis of a conducting polymer (a) and sebum (b) modified regions of off-body 3D electrically conducting skin patterns.

4.1.2.3 Resolution and 3D structure of developed skin maps.

The 3D structure of the developed skin patterns was studied using FESEM, AFM, and a stylus profilometer equipped with an optical microscope. The morphology and topography of skin patterns before and after electropolymerization are shown in Figure 14, which consist of high-resolution camera (a and b), FE-SEM (c and d) and AFM (e and f) images. High-resolution camera pictures revealed that the stamp of the skin pattern is very well pronounced (Figure 14a), which in turn inhibits the electropolymerization of conducting polymer on sebum modified surface, leaving behind mirror picture of the skin pattern (Figure 14b) with conducting polymer growth only on unmodified gold surface. Higher resolution of the skin patterns obtained with FE-SEM before and after electropolymerization revealed that the skin

pattern stamp (Figure 14c) was not uninform in context of leftover sebum stamp. The skin stamp consisted of a thinner line with droplet-like thicker sebum that in turn resulted in residual conducting polymer electropolymerization in thinner sebum-modified regions of the skin stamp (Figure 14d). Although there was uneven distribution of sebum, on a macroscopic level of skin features that was enough to produce clear 3D electrically conducting skin patterns. Moreover, it was found that sebum from different individuals wary, which has direct influence on the quality of the developed 3D electrically conducting skin patterns. Visible by naked eye, sebum left significant deposit of skin bio extract at the surface of pure gold surface (Figure 14e). When the conducting polymer was electropolymerized on the gold substrate that was carrying skin pattern stamp the conducting polymer grew on gold surface leaving sebum modified area mostly unaffected (Figure 14f). Thus, sebum modification and subsequent development of conducting polymer truly produced 3D structures corresponding to skin topographic features.

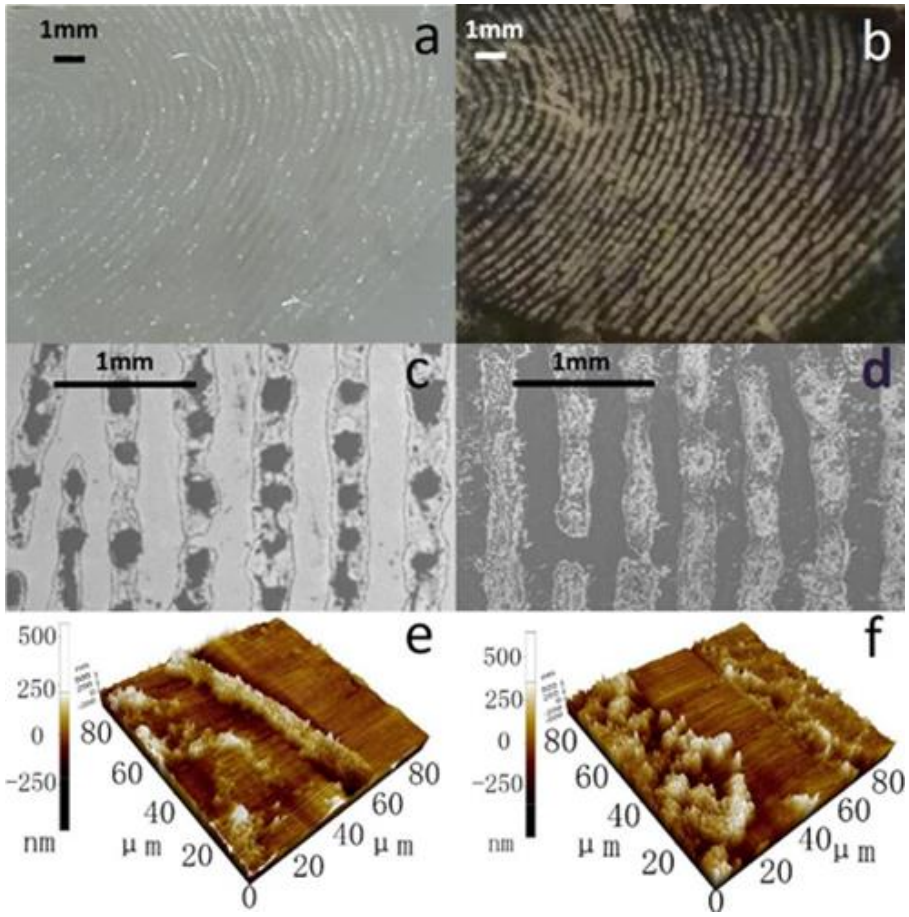

Figure 14. Images of skin patterns on gold surface before (a, c and e) and after electropolymerization (b, d and f), taken with: High-resolution camera (a and b), FE-SEM (c and d) and AFM (e and f).

Figure 15a presents the optical microscope image of a 3D fingerprint pattern with correlated 2D thickness profile obtained via profilometry. Under the optical microscope, the 3D skin fingerprint pattern consisted of alternating dark and bright stripes (Figure 15a). The bright stripes correspond to IRs deposited at the sampling surface while dark stripes corresponded to the developed conducting polymer. In a well-developed 3D conducting skin pattern as shown in Figure 15, a clear separation between dark and bright stripes were observed, which reflected as high-resolution patterning in macro-level visualization. The 3D profilometry map (Figure 15b) proved the thickness difference between dark and bright stripes. The height difference between dark and bright stripes ranges from 0.2 µm to 2 µm. The skin minor structure surface

within the stripes was revealed as intrinsically not even or homogeneous posing a certain degree of roughness. The roughness reflected as impurities within dark and bright stripes in Figure 15a, which is also consistent with the Raman spectra (Figure 16), indicating both bright and dark stripes contained PEDOT(PSS) deposition of certain degree. Specifically, the acquired Raman spectra (results no shown here) provided unique PEDOT(PSS) signatures at approximately 571, 991 cm^{-1} (C – O deformation), 1262 cm^{-1} (Cα – Cα' stretching and C-H bending), 1364 cm^{-1} (thiophene ring Cβ – Cβ' stretching, 1437, 1497, 1561 (symmetric and asymmetric C = C stretching), 2863 (O – H stretching) [209]. The presence of these signatures outside and within the print is indicative of the presence of PEDOT(PSS) throughout the film.

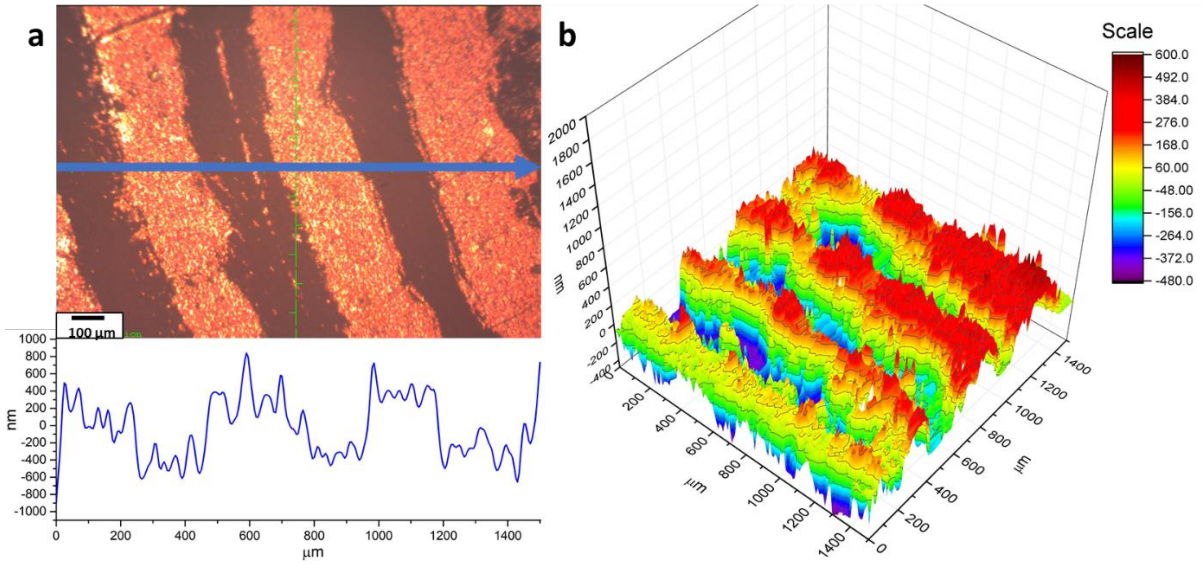

Figure 15. (a) Optical microscope image of developed 3D fingerprint pattern and 2D profile of thickness (blue arrow); (b) 3D skin map (1.5 × 1.5 mm^2) obtained by profilometry.

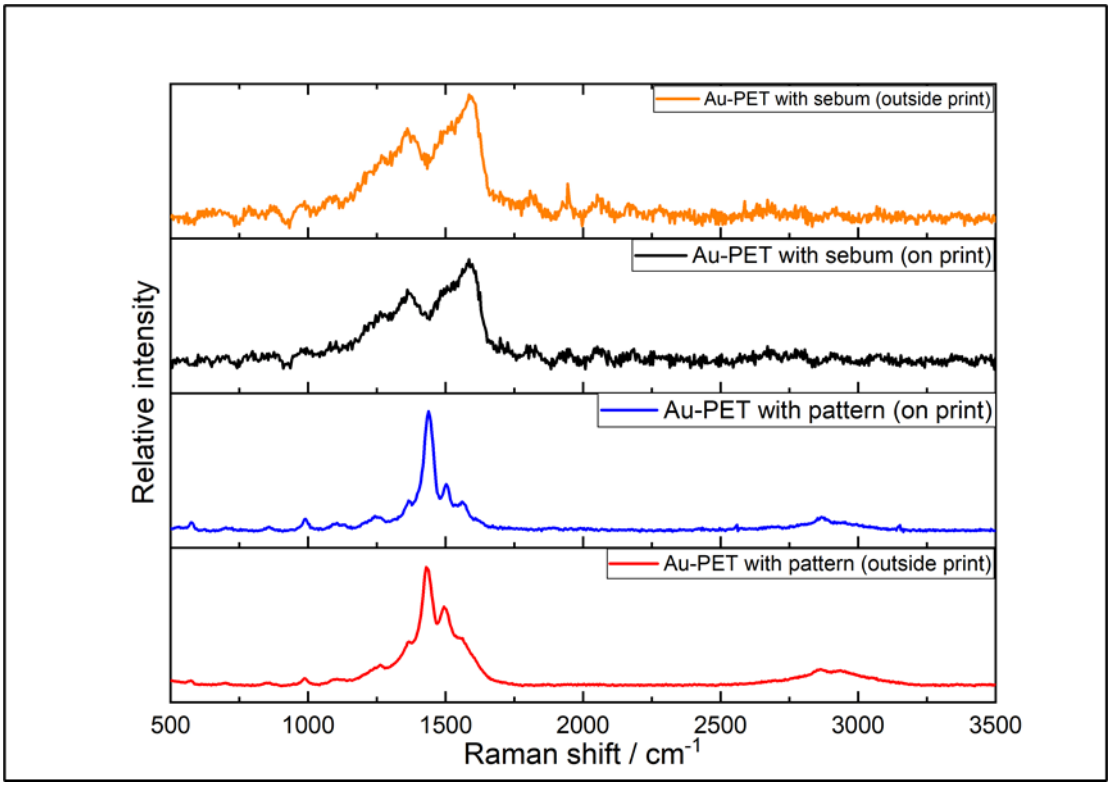

Figure 16. Raman spectrum of Au-PET with sebum (outside and on print), and Au-PET with pattern (outside and on print).

4.1.2.4 Optimization of the 3D skin mapping.

4.1.2.4.1 Electropolymerization of 3D skin patterns.

Development of 3D skin patterns was performed by application of the electrochemical polymerization of the conducting polymer in the presence of the skin stamp. Typically, 0.1% (by volume) EDOT concentration was used during electropolymerization of PEDOT. In the study however, owing to the application of relatively high surface of the working electrode 1.5 × 2 cm the best conditions of electropolymerization were found to be when 0.3% (by volume) of EDOT in electropolymerization solution was used. Additionally, when current density of 0.2 mA/cm^2 was applied to the working electrode the optimal duration of the electropolymerization was found to be 450 s (Figure 17). Further experiments were performed following the optimized conditions for EDOT concentration in the polymerization solution and

the duration of the electropolymerization. Various methods of electropolymerization were tested, namely CP, CA and CV. Firstly, CP was applied for electropolymerization of PEDOT(PSS) with a typical constant current density of 0.2 mA/cm^2. As shown in Figure 16, a sample was synthesized in 2000 s. The amount of PEDOT(PSS) synthesized depends on the overall electric charge passing through the working electrode within electropolymerization time [210]. Thus, the electropolymerization process was paused every 50 s and basic electrochemical characterization on such sample was performed. A clear trend was observed that the pattern gradually turned to visible from the initially blurry IRs stamp. In terms of visual observation, the resolution improved from the beginning of the electropolymerization to 500 s, while films obtained after 1500 s to 2000 s were characterized with the decreased resolution as the PEDOT(PSS) initially grew vertically on IRs-free area until vertical growth reached a limiting thickness, when the PEDOT(PSS) stops further growing or starts detaching. The PEDOT(PSS) film has the conductivity up to 10^{-2} S/cm though, it is not comparable to Au metal, which has the conductivity of 10^4 S/cm at 20 ^{o}C [211]. Therefore, after a certain time of vertical growth, PEDOT(PSS) started depositing on sides to the IRs-deposited area, deteriorating the pattern quality. In addition, IRs deposition could not be ideally executed. For example, sebum consists of many compositions including water, fatty acids, wax esters, and salts [212, 213]. This natural inhomogeneity prohibits ideal deposition and furtherly results in unexpected PEDOT(PSS) deposition in the prolonged electropolymerization process. Fortunately, from 500 s to 1000 s, the quality of developed skin pattern had a much smaller change on a visual observation basis and was deemed applicable for skin maps development.

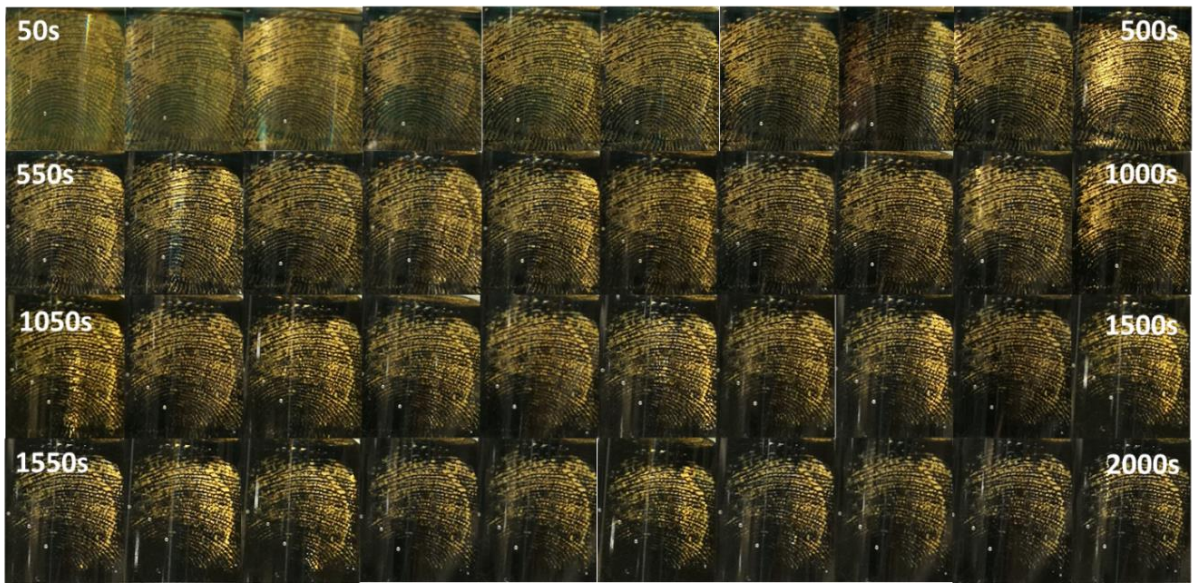

Figure 17. Digital images of the developed 3D fingerprint skin pattern, taken every 50 s interval, during 2000 s electropolymerization of conducting polymer in the presence of the skin stamp at the Au-PET substrate.

In order to quantitatively evaluate the PEDOT(PSS) deposition amount during the patterning process, skin patterns with different polymerization durations were synthesized and specific capacitance of the obtained skin patterns was calculated (Figure 18). CVs of the developed skin map with increasing durations showed the typical capacitance behavior of PEDOT(PSS) and constant growth of films current densities [115]. Due to various applications, PEDOT(PSS) films or thin layers are well-designed with a fairly wide thickness range from tens of nanometers to hundreds of micrometers [214-216]. This is consistent with the results, which makes the developed skin mapping technique technically supported. Figure 19 showed a single sample's CVs and capacitance behaviors along the polymerization process from beginning to 1100s. It can be seen that within the polymerization duration the PEDOT(PSS) was depositing at a stable rate, with supporting from capacitance-time linear fit (R^2 = 0.9865).

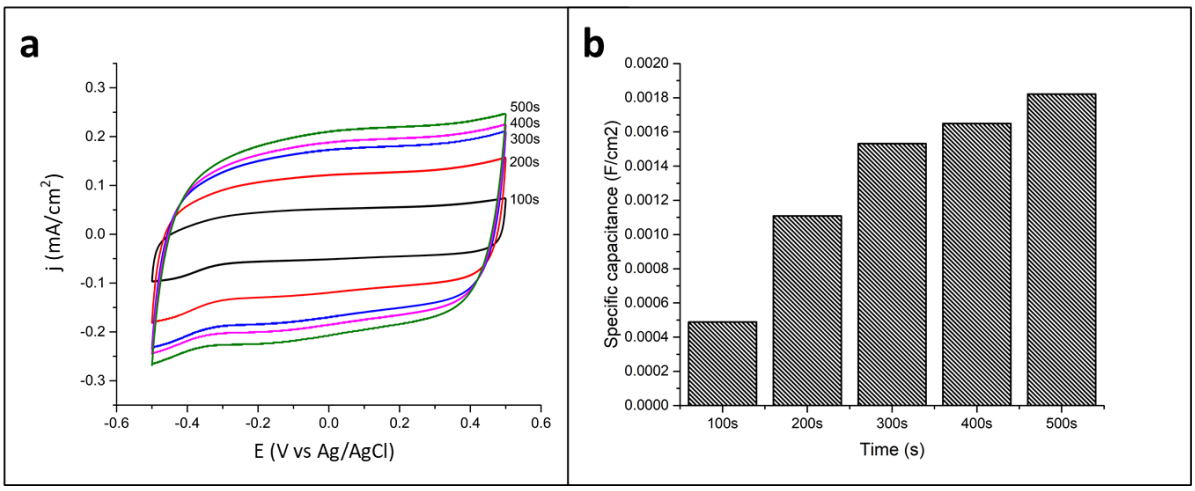

Figure 18. Cyclic voltammetry graph of developed skin patterns with different polymerization durations (a) and corresponding specific capacitance (b).

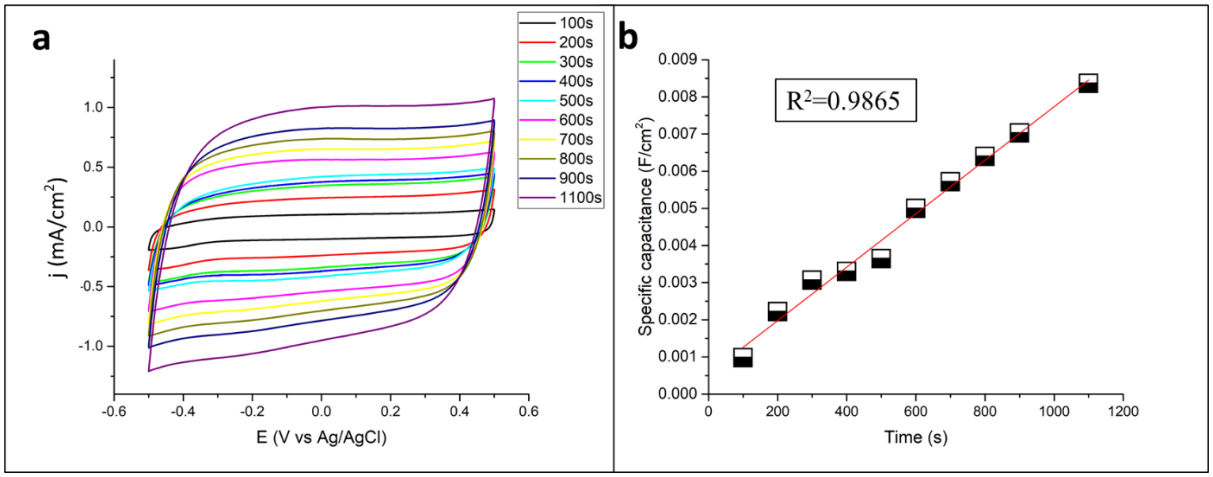

Figure 19. Electrochemical properties of 3D fingerprint skin patterns developed after different electropolymerization time: (a) cyclic voltammograms and (b) calculated specific capacitance.

Besides GCP, CV and CA were tested and evaluated as electropolymerization methods for development of 3D skin patterns (Figure 20). It was found that skin patterns achieved comparative quality to the GCP mode with appropriate optimization to respective parameters. However, successful development of the skin patterns using CA makes it promising to transfer this technique into portable economical device, many of which only provide a constant potential, such as a battery [217].

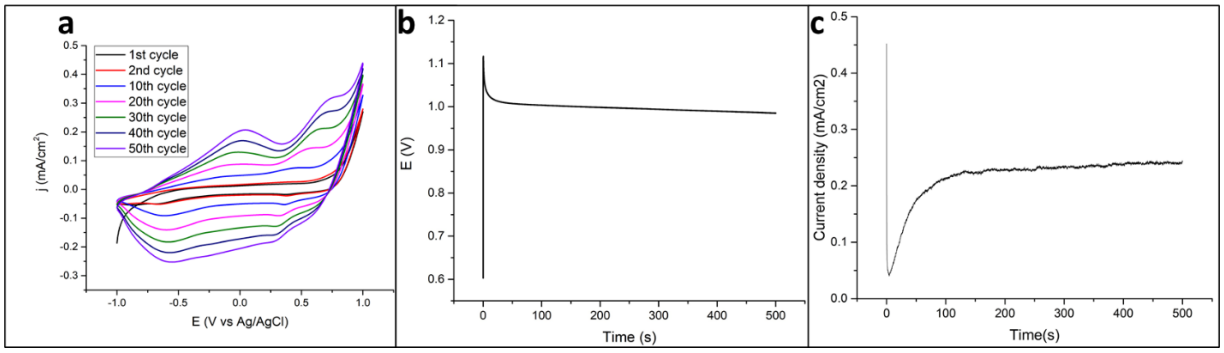

Figure 20. Electropolymerization curves under different electrochemical modes. (a) Cyclic voltammetry; (b) Chronopotentiometry; (c) Chronoamperometry.

4.1.2.4.2 IRs deposition during the skin stamp sampling.

IRs deposition at the sampling substrate is a crucial part of the successful skin mapping. The IRs deposition copies the accurate footprint of the skin pattern, thus ideally mirrors the surface outlines of an objective skin pattern. Its function is to hinder conducting polymer electrosynthesis on the exact deposited area, so that the 3D structure of the skin pattern grows predominantly in IRs unoccupied areas of the substrate, providing a matching template to the skin topography. As discussed, deposition inhomogeneity of IRs on the sampling substrate is inevitable. Additionally, nature of the insulating substances and deposition pressure have significant influence on the quality of the skin stamp deposition. Deposition pressures were the first parameter that were investigated. A piece of clean tissue paper was put on the balance with a clean substrate sample on (ready for skin stamp sampling). After the balance was brought to zero, the skin (finger) was pressed on the substrate sample until it reaches the target weight values. The pressure of the skin-substrate contact was calculated from the mass obtained during the pressing the skin against the substrate that was placed onto the electronic balance (Mettler Toledo, Singapore). For each pressure, two different substrates were used, Au-PET and Pt-PET. Deposition pressures of 6533 to 16333 N/m^2 were found optimal. Pressures below 6533 N/m^2 resulted in incomplete deposition of sebum, while pressures over 16333 N/m^2 caused smudging of the sebum onto the sampling substrate. Two sequences of different deposition pressure skin

mapping samples are shown in Figure 21, where one is using Au-PET and the other is using Pt-PET substrate. The reason why the optimal pressure was provided in a scope instead of a precise number is that the resolution of developed patterns was a multivariable function while many factors such as sebum nature varies among different skin parts and from person-to-person.

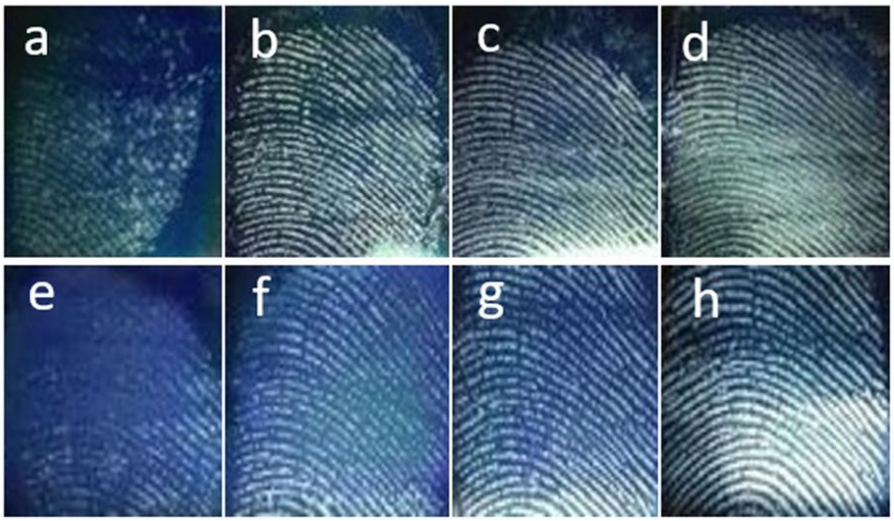

Figure 21. High-resolution camera pictures of skin patterns developed on PET-Au (top row) and PET-Pt substrates (bottom row) after various pressure applied between sampling substrate and the skin during the skin stamp pattern sampling, namely: 218 N/cm^2 (a and e), 436 N/cm^2 (b and f), 871 N/cm^2 (c and g) and 1316 N/cm^2 (d and h).

Furthermore, Figure 22 presents 3D skin patterns developed from a silicone oil- and a natural sebum-based skin stamp sampling. In both cases, the skin stamp sampling was done under the same and optimal skin mapping parameters, namely skin stamp depositing pressure between 6533 to 16333 N/m^2, PEDOT(PSS) used as a conducting polymer to develop 3D skin patterns. The 3D fingerprint skin patterns obtained using silicone oil (Figure 22a) and natural sebum (Figure 22d) during the stamp sampling displayed clear outlines for every ridge of the fingerprint. However, the skin map using natural sebum had significantly higher color disparity between skin's ridges and valleys. As shown in Figure 22b and 22e, in the 3D skin pattern from natural sebum, fingerprint ridges were evenly deposited onto the sampling substrate, which in

turn resulted in the sharp 3D structure of the skin pattern. On the other hand, silicone oil deposition tends to shrink into irregular lumps or thin lines. The residues kept macroscopic image visible and recognizable but with a significant microscopic quality decreased. From the profile thickness obtained using 2D profilometry (Figure 22c and 22f), there was no recurring height difference owning to the 3D nature of the skin pattern (Figure 14 and 15). This phenomenon can be attributed to the difference in viscosity and wetting behavior of both substances on the metal surface. The viscosity of human sebum at 25 ºC ranges from 900 to 1000 mP [218, 219] while the silicone oil has a viscosity around 100 mP [220]. Moreover, sebum has a lower surface tension and, thus, maintains higher stability in volume/surface residence on the metal substrate than silicone oil [221]. Therefore, silicone oil or other insulating substances with similar properties may still be applicable for skin stamp sampling if the resolution requirement of the 3D skin pattern is relatively mediocre, e.g. recognition of the skin features. However, if higher resolution is required, the natural sebum used for skin stamp sampling must be applied.

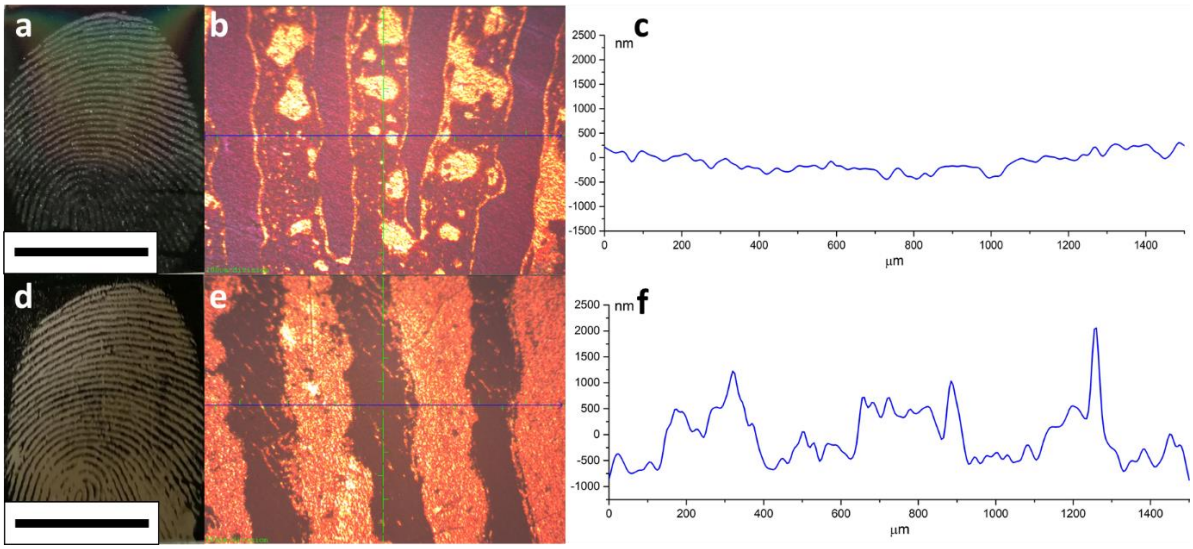

Figure 22. Digital camera (a and d) and microscope (b and e) images, and their corresponding 2D thickness profiles (c and f) of 3D skin patterns developed from a silicone oil (a, b, c) and a natural sebum (d, e, f) based skin stamp samplings. (scale bar: 1 cm)

4.1.2.4.3 Skin pre-treatment for universal skin stamp sampling.

Skin stamps were taken from untreated human subject skin. The possible removal of the sebum by 98% ethanol or skin washing with household detergent with subsequent application of oil were studied as a method of the universal collection of the skin pattern stamp from rather unpredicted conditions of human skin and variations of person-to-person sebum compositions. Using PET-Au substrate, sebum removal and subsequent application of masking substance (common cooking oil) for universal skin stamp pattern sampling were investigated. High-resolution camera pictures of sebum removal by 98% ethanol and common detergent followed by application of masking substance (common cooking oil) for universal skin stamp pattern sampling is shown in Figure 23. The application of 98% of ethanol did not remove the sebum from human skin, leaving distorted sebum lines. On the other hand, application of the detergent removed sebum from the human skin. Subsequent application of oil on the skin for the recovery

of sebum-like lines was unsuccessful as deposited oil created droplets in form of discontinued sebum lines. In this respect, although removal of sebum was performed successfully by application of detergent, the attempt to apply oil as standardized sebum-like substance for skin pattern sampling was found unsuccessful. Further optimization of sebum-like substance is needed.

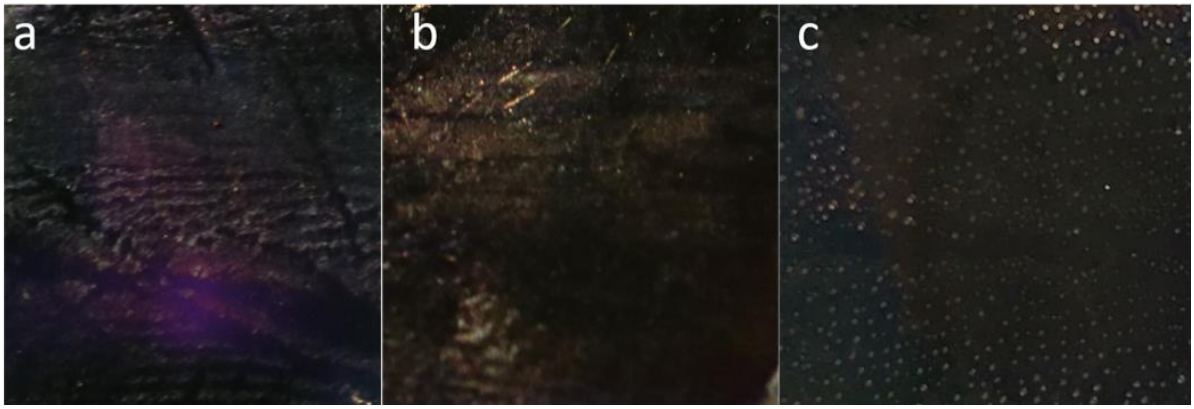

Figure 23. High-resolution camera pictures of sebum removal by 98% ethanol (a) and common detergent (b) and subsequent application of masking substance for universal skin stamp pattern sampling, common cooking oil (c).

4.1.2.4.4 The choice of substrates for 3D skin mapping.

The flexibility of developed skin patterns highly depends on the supporting substrate flexibility. The PET, weighing paper, membrane filter and glass were studied as supporting substrates (Figure 24), while gold and platinum sputtered at these substrates were studied as electroactive layers used for sampling of the skin stamps. In respect of the surface homogeneity or stability under electrochemical conditions, platinum displayed equivalent performance as gold. Thus, unless specified, the results shown in this thesis are shown for gold plastic substrate (Au-PET). The weighing paper offered higher flexibility but was found to fold during development of the 3D skin patterns owning to its low thickness. Folding during electropolymerization process also caused a decrease in the quality of the developed 3D skin patterns. This however could be

solved by manufacturing of holding cell so that the folding of the paper is avoided and paper could be used for 3D skin pattering. The membrane filter offered a moderate flexibility that was comparable with PET film, but the 3D information of the skin print was disused owning to its relatively high surface roughness. The glass performed well in 2D patterning and 3D structure synthesis of the skin features. However, it raised practical difficulty concerning sampling and patterning owing to its brittle and inflexible nature. Nevertheless, a glass substrate provided a highly homogeneous and even surface that stabilized the skin patterning process for 3D skin features. Therefore, glass can be regarded as the supporting substrate for specific circumstances where high flexibility is not a strict requirement.

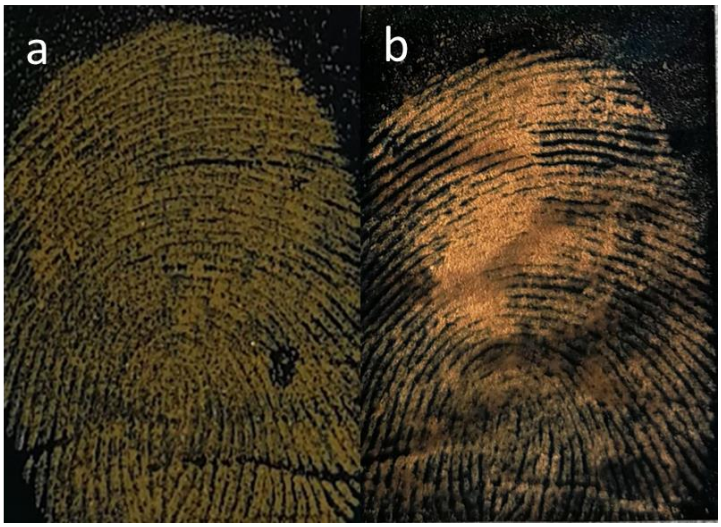

Figure 24. Digital camera images of developed skin mapping patterns of different substrates: Glass-Au (a), Membrane-Au (b).

4.1.3 Prototype of portable and fast skin mapping device.

With the optimized laboratory-based system a device prototype was designed, engineered and 3D-printed (Figure 25). The device was powered by a 1.5V AAA dry battery and was able to produce skin maps as comparable quality as using the beaker-based cell using a potentiostat. The battery-powered system allowed easy portability of this rather small and inexpensive device. The device consisted of three main parts: (α) stamp sampling platform; (β) skin

patterning cell; and (γ) power supply chamber/battery box. The actual, 3D printed device can be seen in Figure 26. The stamp sampling platform (α) was a detachable element consisted of skin stamp sampling platform (2×7 cm^2) equipped with two springs, which control the strength applied to the skin surface during the skin stamp sampling, resulting in the surface pressure applied on the skin in the range of 6500 to 15000 N/m^2. The skin patterning cell (β) consisted of electropolymerization chamber equipped with two electrodes connectors, namely (i) in-build platinum film (2×3 cm^2) and (ii) the connector for placing the fabricated (PET-Au) substrate with skin stamp deposited. To develop the 3D skin pattern, a 30 mL of 0.023 M EDOT and 0.1 M PSS was used as electrolyte. The 3D skin patterns were developed by applying constant potential between the two electrodes for 500 s. The applied potential was delivered using an AAA alkaline battery (Gold Peak) with 1.5 V output voltage (γ). To my best knowledge, this is the very first time that battery was used to electrosynthesize conducting polymer, instead of using potentiostat. The realization of this portable protocol makes the cell possible to be taken on site, e.g. to the construction site, to perform (within 5 min total measurement time) a quick in-situ diagnosis of pathological skin conditions of construction workers.

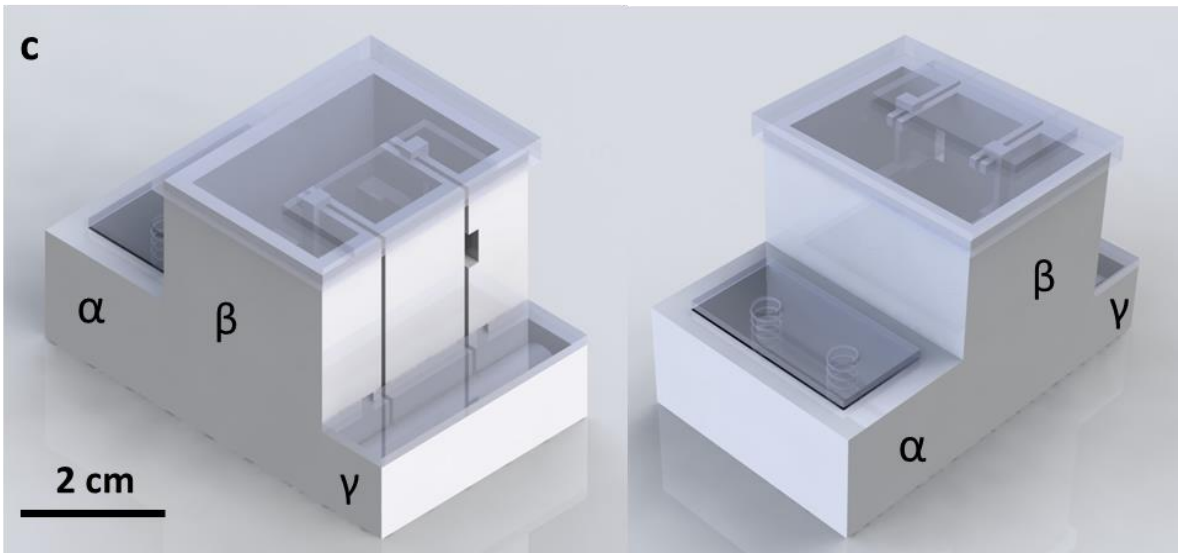

Figure 25. Prototype of the portable 3D skin mapping device.

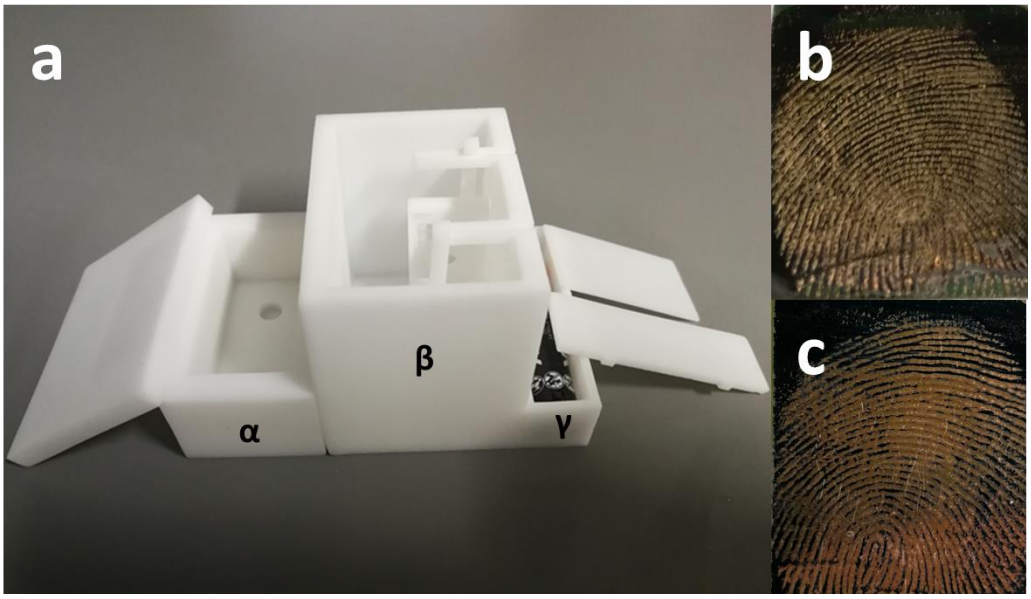

Figure 26. Image of the porotype of the portable and fast 3D skin mapping device (a); developed skin pattern using the device powered by battery (b); developed skin pattern using potentiostat following ordinary procedure (c).

4.2 Development of conducting polymers coating based substrates for wound dressing applications.

PET-Au substrates showed excellent performance when used as skin mapping substrates owning to their homogeneous surfaces which provide the basic platform for differentiating delicate morphologies in micron scale. However, with the intention to use the material for wound treatment such as patch or wound dressing, higher breathability, and flexibility than that of PET is required. None of the investigated materials (PET films, weighing paper, glass, membrane) possess these required essential properties. Thus, cellulose papers which have higher porosity and better flexibility was explored for the use in development of functional wound dressing material to be possibly integrated with 3D skin patterning and subsequent skin treatment.

4.2.1 Preparation and optimization of the electroactive and functional cellulose substrates.

Briefly, the cellulose paper was cut into 4×2 cm rectangular pieces followed by coating with a thin layer of platinum using a sputter coater for 300 s at 40 mA. The platinum-coated cellulose substrate was then used for the electropolymerization of conducting polymers. Electropolymerization process was conducted in a typical three-electrode electrochemical cell where cellulose substrates serve as working electrode. GCP was used for the electropolymerization process at 0.2 mA/cm^2 for 1000 s. Four different groups of electropolymerization solutions were used to fabricate different types of electroactive cellulose-based papers, as listed in Table 3. All the electropolymerization solutions were aqueous based. At the end of the electropolymerization process, the electroactive cellulose-based papers were pre-cleaned by rinsing with distilled water on both sides for 5 s. Subsequently, the samples were washed thoroughly by soaking the samples in fresh distilled water with light shaking for 5 s. The washing step was repeated for 5 times to fully remove the residual monomers and unbound metal ions.

Table 3. Electropolymerization settings of different electroactive cellulose-based substrates.

	PPy	Cu/Zn-PPy	PEDOT	Cu/Zn-PEDOT
Py	0.3%	0.3%	—	—
EDOT	—	—	0.3%	0.3%
SDS	0.1	0.1	0.1	0.1
Cu^{2+}	—	0.05	—	0.05
Zn^{2+}	—	0.05	—	0.05

Notes: Percentages in the table are expressed in volume, while concentrations of Cu^{2+} and Zn^{2+} are expressed in M.

4.2.1.1 Electrochemical characterization.

Electrochemical characterization of the developed films was performed using cyclic voltammetry (CV) (Figure 27). The measurements were performed in bicarbonate-buffered

solutions in typical three electrode system at three different pH conditions (6.5, 7.5 and 8.5). The potential was cycled between −0.5 and 0.5 V vs Ag/AgCl with a scan rate of 0.1 V/s (five cycles in total were performed, only the fifth cycle was used for graphical preparation). Along with the substrate surface area, CVs were used to calculate of area-based specific capacitance.

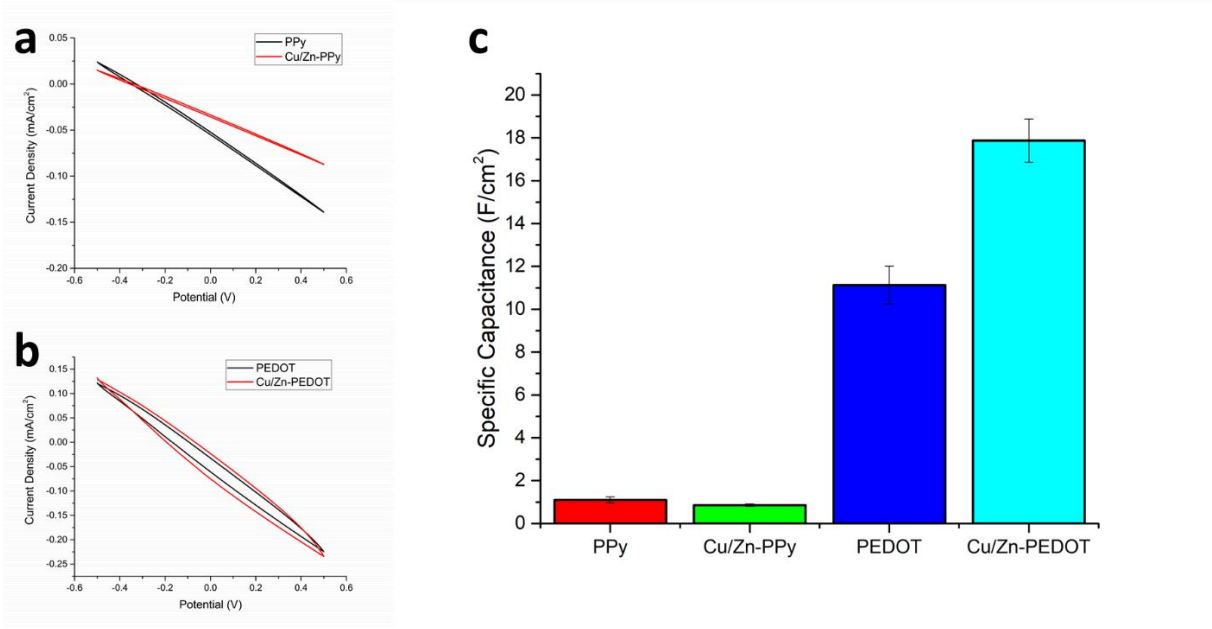

Figure 27. Representative cyclic voltammetry graphs of electroactive cellulose substrates after cellar studies at pH 7.5 condition (a) PPy and Cu/Zn-PPy, (b) PEDOT and Cu/Zn-PEDOT, and (c) Specific capacitance.

The cyclic voltammograms of representative samples investigated in three different pH are shown in Figure 27. All different electroactive cellulose substrates exhibited an effective voltammograms, confirming the success in conferring electroactivity to the inert cellulose substrate which in general was aimed to promote the better cellular activities. Between the PPy- and PEDOT-based samples, PEDOT(SDS) exhibited a larger curve enclosed area as compared to PPy(SDS), and thus demonstrating the higher charge storage (capacitance) of PEDOT(SDS). In general, the current density of the PPy(SDS) ranged from -0.2 to 0.3 mA/cm^2. On the other hand, a significantly higher current density range was observed for PEDOT(SDS) from -0.6 to

0.8 mA/cm^2, similar to those reported by others [133, 222]. Hence, the presence of Cu^{2+} and Zn^{2+} ions further improved the capacitance of the electroactive cellulose substrates. Among the various pH conditions, no significant differences were observed in the CV profiles of the various electroactive cellulose substrates. Regardless of the pH conditions used, all the PEDOT-based cellulose substrates exhibited significantly higher capacitance as compared to PPy-based cellulose substrates. In addition, a similar trend was observed for the various electroactive cellulose substrates before and after the cellular studies. Hence, the pH conditions and cellular works did not deteriorate the electrochemical properties of the electroactive cellulose substrates. Overall, electroactive cellulose substrates were successfully fabricated via electropolymerization process to confer electroactivity to the inert cellulose substrate. In addition, the presence of Cu^{2+} and Zn^{2+} ions successfully increased the capacitance of the electroactive cellulose substrates, particularly for PEDOT-based electroactive cellulose substrates with higher electrical performance as compared to PPy [23, 26]. Hence, PEDOT-based electroactive cellulose substrates could be promising dressing materials for wound healing applications.

4.2.1.2 Mechanical properties of the developed substrates.

The physical properties and the material stability of the wound dressings are highly important to eliminate entrapment of the dressing remnants and minimizing tissue trauma while removing the dressings [223]. Hence, the effects of platinum deposition and electropolymerization of conductive polymers onto the strength and structural properties of the electroactive cellulose substrates were investigated by tensile testing. As seen from Figure 28a, all different substrates exhibited good mechanical properties with a stiffness reaching around 60 MPa for the pristine cellulose substrate. When the cellulose substrates were sputtered with platinum (i.e. Platinum-coated), an overall improvement in the mechanical properties were observed. In general, cellulose exhibits good chemical and physical stability. Hence, the sputtering process did not

deteriorate the physical properties of the cellulose material, yet the presence of the platinum coating interlocked the cellulose fibers that increased the friction of the cellulose fibers. As a result, it prevented the slippage between the adjacent fibers of the cellulose, which in turn enhanced the stiffness of the cellulose substrates [224]. Subsequently, the platinum-coated cellulose substrates were electropolymerized with either PPy or PEDOT in the presence or absence of metal ions. Between the PPy- and PEDOT-based electroactive cellulose substrates, PEDOT-based electroactive cellulose substrates exhibited significantly higher modulus as compared to PPy-based electroactive cellulose substrates. In fact, an overall reduction in the mechanical properties was observed for the PPy-based electroactive cellulose substrates as compared to the platinum-coated samples, but not for the PEDOT-based electroactive cellulose substrates. The decrease in the mechanical properties of the PPy-based electroactive cellulose substrates could possibly due to the PPy(SDS) is more prone to aerial oxidation with lower environmental stability as compared to PEDOT(SDS) [225-227]. Hence, PEDOT(SDS) with higher environmental stability could be a better choice of electroactive cellulose substrates, particularly for long term application by providing a more consistent and stable conductivity performance throughout the course of the usage. Nevertheless, all the different samples exhibited the similar mechanical profile, regardless of the pH conditions used (Figure 28b and c). Overall, the samples exhibited good pH stability particularly for PEDOT-based cellulose substrates, and thus showing the potential as smart dressing for wound treatments even though the pH changes during the course of wound healing.

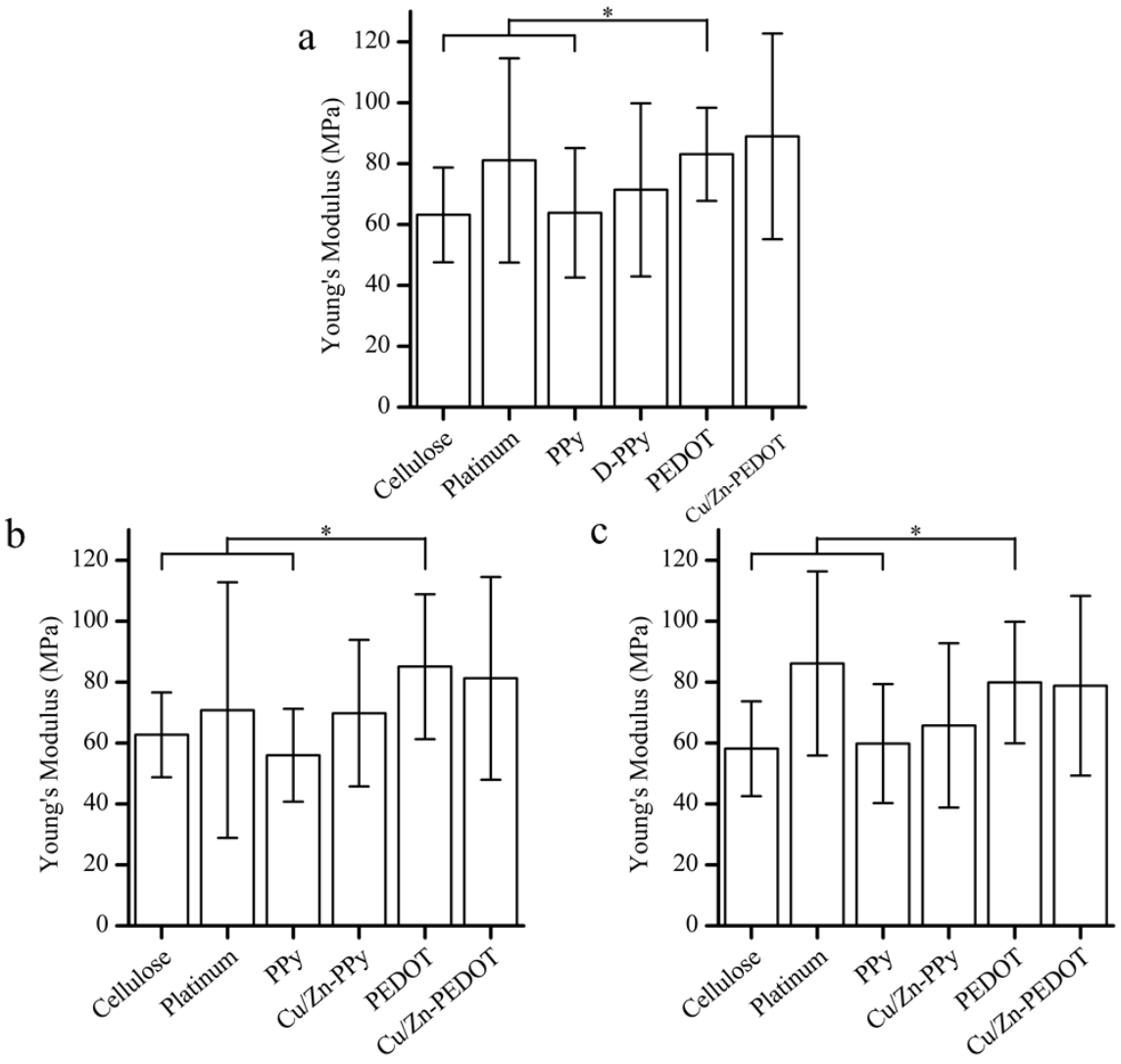

Figure 28. Mechanical properties/Young's Modulus of the various cellulose-based substrates at (a) pH 7.5, (b) pH 6.5, and (c) pH 8.5 environments. *$p < 0.05$.

4.2.1.3 Surface morphology and topology of the developed substrates

The morphology and the coverage of the PPy and PEDOT on the cellulose substrates were further imaged by FESEM. As seen from Figure 29, a rough morphology was observed for all the various electroactive cellulose substrates. After the electropolymerization process, the conductive polymers were evenly deposited throughout the individual cellulose fibres without affecting the overall roughness of the sample. Notably, the porosity was decreased due to the deposition of conducting polymers, no matter PPy or PEDOT, which could furtherly explain

the electrochemical behaviour discussed in Chapter 4.2.1.1. In fact, additional nano-roughness topography was formed on the individual cellulose fibres after the electropolymerization process created by the conductive polymers. In general, surface roughness is one of the important physical factors in regulating cellular behaviour on the material [228, 229]. Studies have shown that both micro- and nano-scale surface roughness have successfully enhanced the cell adhesion and growth, in which the roughness in the range of 5-200 nm provided a better anchorage of cells to the substrate [191, 230]. Hence, the presence of both micro- and nano-roughness features on the various electroactive cellulose substrates can provide the appropriate topography for the cell adhesion, proliferation, and migration, hence making them suitable substrates for the fabrication of smart wound dressings to promote wound healing process [231].

The elemental composition of the various electroactive cellulose substrates was also assessed by EDS analysis. As seen from Figure 30, the fundamental elements of the PPy and PEDOT, such as oxygen, carbon, hydrogen, and sulphur, as well as the presence of platinum-coating were detected. In particular, sulfur, which is the characteristic element of the SDS present in the two conducting polymers, was being detected that confirmed the successful polymerization of PPy and PEDOT, respectively. Overall, PPy- and PEDOT-based electroactive cellulose substrates were successfully fabricated by electropolymerization process onto the cellulose substrate.

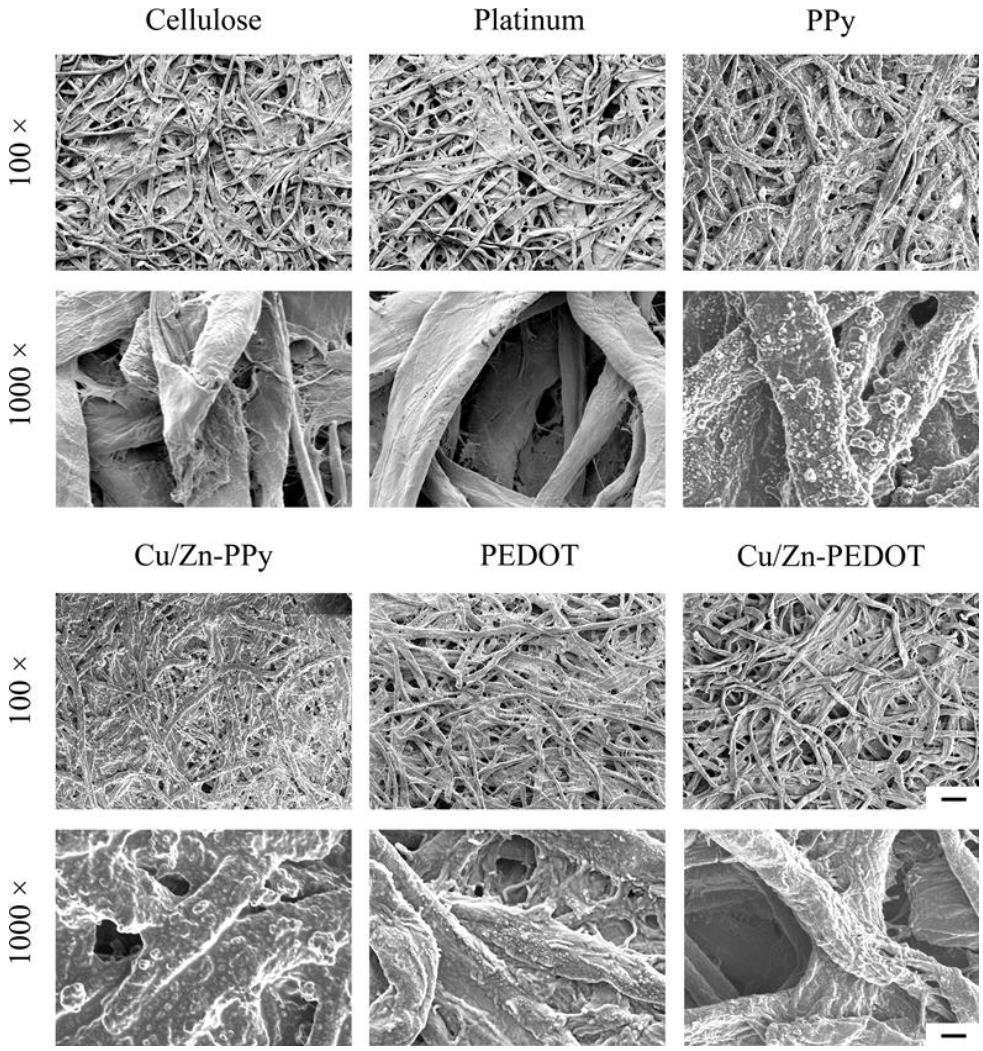

Figure 29. FE-SEM images of the various cellulose-based substrates. Scale bar: 100 μm (100 ×), 10 μm (1000 ×).

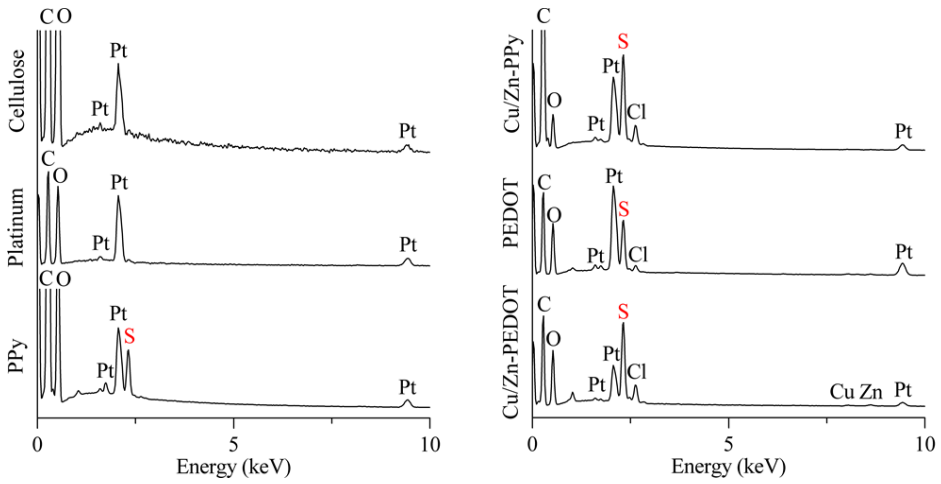

Figure 30. EDS elemental analysis of the various cellulose-based substrates.

4.2.2 *In vitro* cellular studies using developed cellulose-based substrates.

The cytocompatibility and cell-material interactions of various electroactive cellulose substrates were assessed using HaCaT cells according to the previously established methods [189, 190]. The cytocompatibility and cell-material interactions of the various electroactive cellulose substrates were assessed by evaluating the cell adhesion and the proliferation of HaCaT cells over 7 days of cell culture. As seen from Figure 31a, all the various electroactive cellulose substrates supported the cell attachment, which is an indication of the cytocompatibility of the various substrates. However, a poor initial cell attachment was observed for the PPy-based electroactive cellulose substrates, which is significantly ($p < 0.05$) lower as compared to PEDOT-based electroactive cellulose substrates. Although both the PPy- and PEDOT-based electroactive cellulose substrates exhibited additional nano-scale roughness, no significant improvement in the initial cell attachment was observed as compared to the pristine cellulose substrates. Hence, the surface chemistry of the substrate played a more important role in affecting the cellular behaviour. As PPy has a lower chemical and environmental stability as compared to PEDOT, hence it is postulated that the PPy-based substrates have potentially higher levels of leachable materials that may have induced an undesirable biological effect (i.e. contact-related cytotoxicity) with lower initial cell attachment observed [132, 135].

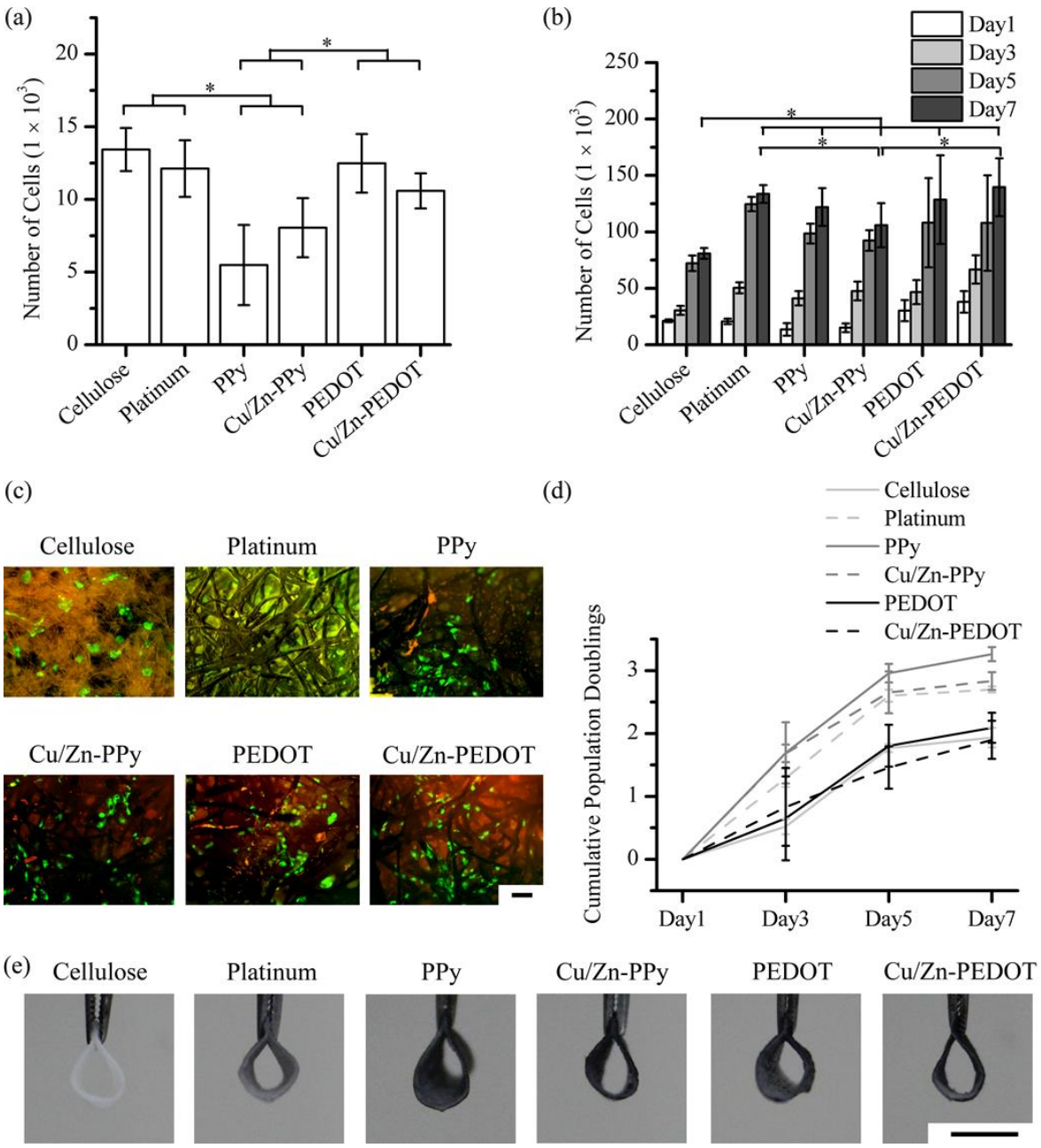

Figure 31. Cell-material interactions of HaCaT cells on the various cellulose-based substrates under pH 7.5 environment showing (a) initial cell attachment, (b) cell proliferation over 7 days, (c) representative images of HaCaT cells stained with FDA and PI on day 7, (d) cumulative population doublings, and (e) representative macroscopic images of the various cellulose-based substrates. Scale bar: 100 μm (d), 500 μm (e); Green fluorescence: viable cells, Red fluorescence: dead cells. *$p < 0.05$.

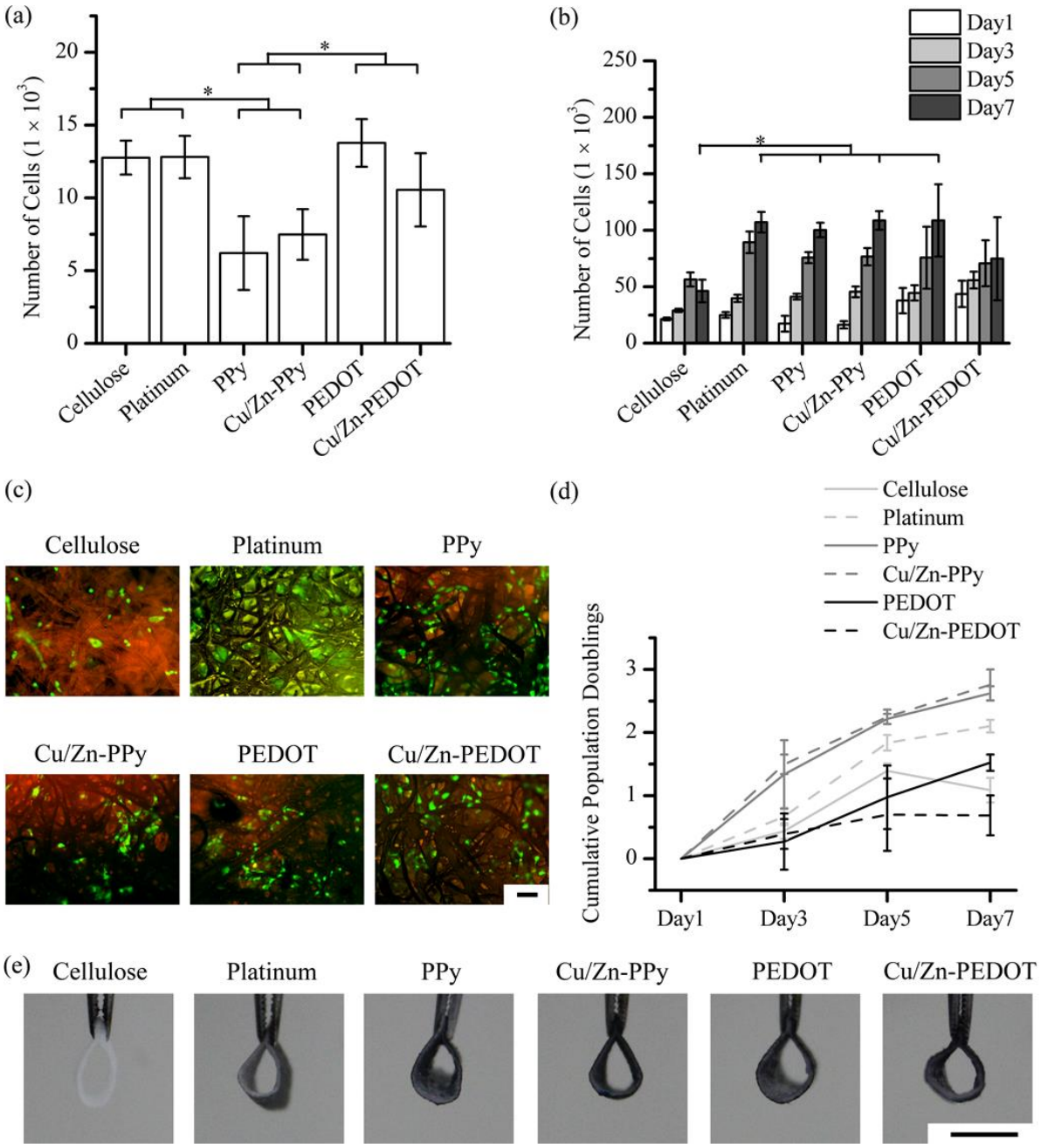

Figure 32. Cell-material interactions of HaCaT cells on the various cellulose-based substrates at pH 6.5 environment showing (a) initial cell attachment, (b) cell proliferation over 7 days, (c) representative images of HaCaT cells stained with FDA and PI on day 7, (d) cumulative population doublings, and (e) representative macroscopic images of the various cellulose-based substrates. Scale bar: 100 µm (d), 500 µm (e); Green fluorescence: viable cells, Red fluorescence: dead cells. *$p < 0.05$.

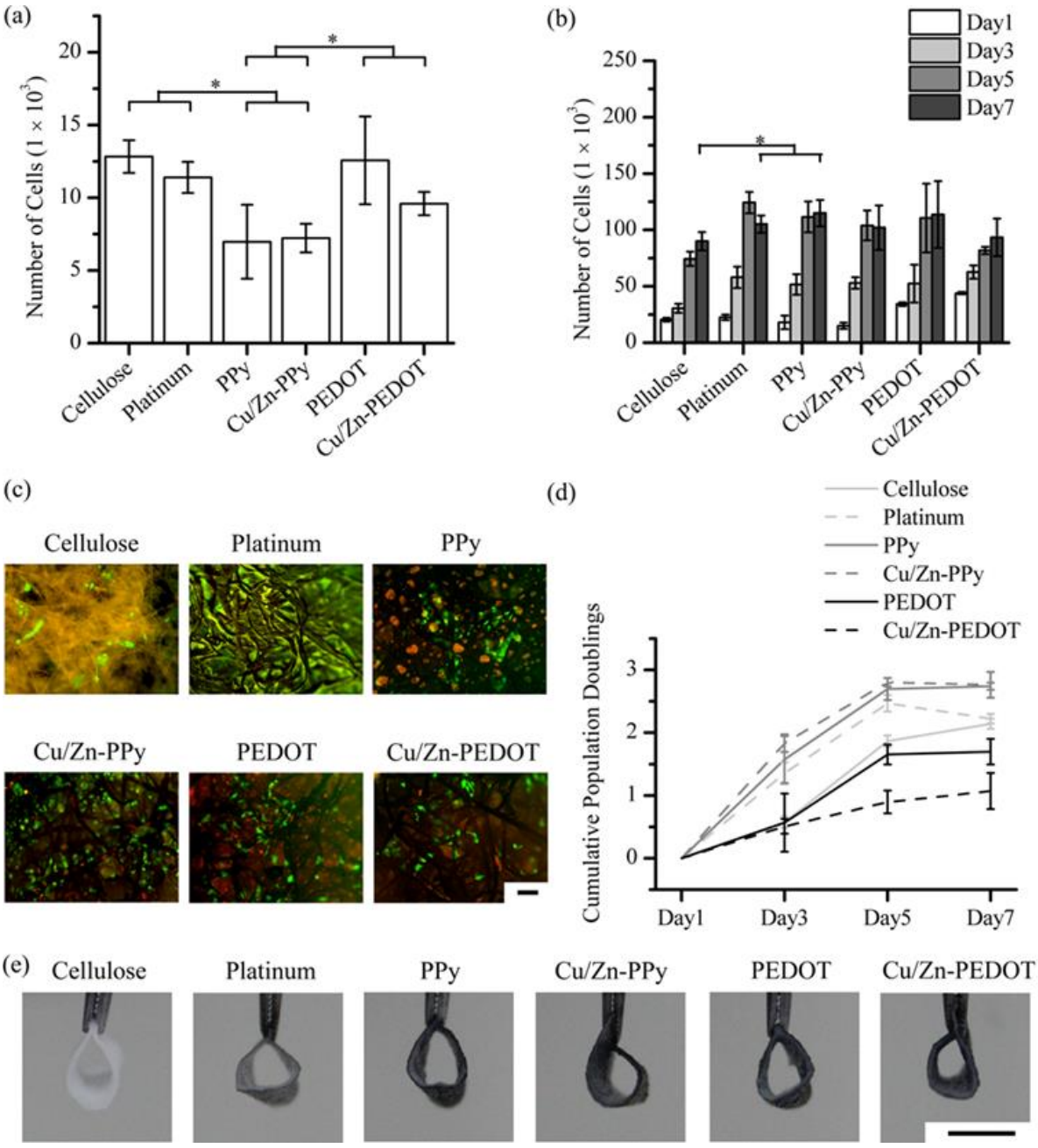

Figure 33. Cell-material interactions of HaCaT cells on the various cellulose-based substratess at pH 8.5 environment showing (a) initial cell attachment, (b) cell proliferation over 7 days, (c) representative images of HaCaT cells stained with FDA and PI on day 7, (d) cumulative population doublings, and (e) representative macroscopic images of the various cellulose-based substrates. Scale bar: 100 µm (d), 500 µm (e); Green fluorescence: viable cells, Red fluorescence: dead cells. *$p < 0.05$.

Nevertheless, HaCaT cells cultured on the various samples exhibited positive cell-material interactions with increasing number of cells observed over the 7 days of culture (Figure 31b), which further confirming the cytocompatibility of the different electroactive cellulose substrates. In fact, all the different electroactive cellulose substrates exhibited significantly ($p < 0.05$) higher number of cells as compared to pristine cellulose substrates at day 7. Similarly, observations from fluorescence staining of viable cells were in agreement with the cell proliferation results (Figure 31c), with pristine cellulose substrates had the least number of cells attached at day 7. Hence, the cellular results demonstrated the advantage of the presence of conductive polymers (i.e. electroactivity alone) in further promoting the cell-material interactions of cellulose, similar to those reported by others [175, 183, 232-234]. Although PPy-based cellulose substrate had lower initial cell attachment as compared to PEDOT-based cellulose substrates, HaCaT cells cultured on PPy-based cellulose papers exhibited slightly higher cell proliferation rate as compared to PEDOT-based cellulose substrates with the differences in the number of cells diminished over time (Figure 31d). At day 7, no significant difference was observed in the number of cells among the various electroactive papers. In general, the conductive polymers are capable of supporting cell adhesion and growth is also mediated by the static interactions of the conductive polymers with the surrounding soluble proteins, which in turn regulate the subsequent cellular behaviour. Over 7 days of culture, the subsequent cell growth could be attribute to the possible absorption of various proteins from the DMEM culture medium, hence stabilizing the papers and supported the subsequent cell growth. In addition, all the different electroactive cellulose substrates exhibited good handleability even after 7 days of culture (Figure 31e), and thus showing the great potential of the electroactive cellulose papers as smart wound dressings. On the other hand, an overall reduction in the total number of cells was observed for the samples cultured in the acidic or alkaline condition (Figures 32 and 33), which could possibly be due to the harsh environment

that limited the cellular activities. In general, the cellular metabolic activity is highly affected by the pH of the environment. In humans, the normal serum pH generally falls within 7.35 to 7.45, while a pH of less than 6.8 or above 7.8 will cause cell damage. Hence, an overall reduction in the cellular activities was observed for all the different types of cellulose-based substrates, regardless of the fabrication stages. Nevertheless, the different electroactive cellulose papers supported the attachment and growth of HaCaT cells with good physical properties retained even after 7 days of culture, regardless of the pH environments. Hence, the results showed the potential of the electroactive cellulose papers to be used as temporary or detachable smart dressings that can be easily removed or peeled off the wound without leaving any substrate remnants at the wound site, particularly for PEDOT-based cellulose papers with better initial cell attachment.

The successful fabricated cellulose papers showed excellent flexibility and handleability. The conductive polymers, including polypyrrole (PPy) and poly(3,4-ethylenedioxythiophene) (PEDOT) were electropolymerized onto the platinum-coated cellulose substrates in the presence of sodium dodecyl sulphate, which resulted in even conducting polymer coating throughout the cellulose substrates. In addition, both submicro and nanoroughness topographies were observed on the various electroactive cellulose-based papers that can provide better anchorage for cell attachment. Overall, it was found that PEDOT-cellulose substrates exhibited good mechanical properties and promoted better cell-material interactions using HaCaT cells, and thus could potentially be used in skin-related artificial electronics or skin treatment devices. In addition, PEDOT-cellulose substrates exhibited higher capacitance with higher doping of Cu^{2+} and Zn^{2+} ions into the conducting polymer matrix. Ions doping and releasing study also showed the potential of PEDOT cellulose substrates as a metal ions delivery system that could further enhance the cell proliferation and enhance integration of skin based implants. Comprehensive study and discussion towards ions doping and release will be

introduced in Chapter 4.3. Nevertheless, the results showed that the PEDOT-cellulose substrates have promising potential to be used in skin related applications, such as 3D skin patterning if their application would be directed not only for skin features diagnostics but also skin treatment.

4.3 Diagnostics and therapeutic treatment to local wounds using 3D skin patterning.

The PEDOT-based materials have a better performance in terms of cytocompatibility with HaCaT cells than PPy-based materials. Thus, PEDOT-based materials were selected for the applications in wound diagnostics and treatment. For that both paper and PET conducting polymer based substrates were investigated.

4.3.1 Wound diagnostics with skin mapping.

Skin mapping for diagnosis of different skin features was developed on the premises that the targeted skin regions were without disrupted integrity of the skin, such as scars, small lumps, rashes, or blisters. Here, application of skin mapping technique towards diagnostics of the open wounds, including abrasions, lacerations, punctures, as well as those chronicle wounds was explored. The pig skin is commonly used as a model to simulate human skin conditions [235-237]. Thus, it was used here for the simulated invasive skin wounds in order to investigate the suitability of the 3D skin mapping technology in real wound diagnostics. Pig skin samples were cut in form of simulated wounds of various depths (2, 4, 6, 8 and 10 mm), while the width of the simulated wounds ranged from 0.5 to 1 mm. Standard off-body skin mapping technique was applied as developed in Chapter 4.1.2. Briefly, Au-PET substrates were used following the same sampling and patterning procedure on simulated pig skin instead of alive human skin. Electropolymerization duration was fixed at 300 s for this patterning. As shown in Figure 34,

despite successful mapping of all the simulated wounds, depths of the wounds showed insignificant influence on the mapping quality, contrary to the topography of the skin. Unlike a human palm handprint or fingerprint, the simulated wounds prints did not have minor ridges or outlines, similarly as human scar prints. Developed skin maps tend to have higher resolution when the wounds have sharp edges corroborating the theory discussed in chapter 4.1. The deformation from pressing may to some extent change the shape of minor structures, with ridges being more affected than valleys. The convex scars can be regarded as large ridges and non-resistant to pressure. Concave wounds, especially those with sharp edges, to the contrary, are less likely to undergo compressive deformation. Besides, the developed skin mapping technique was successfully tested via simulated various types of wounds including punctures, lacerations, abrasions, and incisions (Figure 35). The development procedure was the same as applied on simulated wounds of various depths. All deeper wounds produce scars and it takes prolonged time for them to reach their final appearance[238], thus as a noninvasive method, the skin mapping technique could record or monitor the chronic wound healing process without causing any secondary damages. It can also be used to study sutures usage since skin suture marks are created once a suture is left longer than a week [238]. On the other hand, it can also be applied when monitoring or investigating scar formation and appearance out of cosmetic consideration.

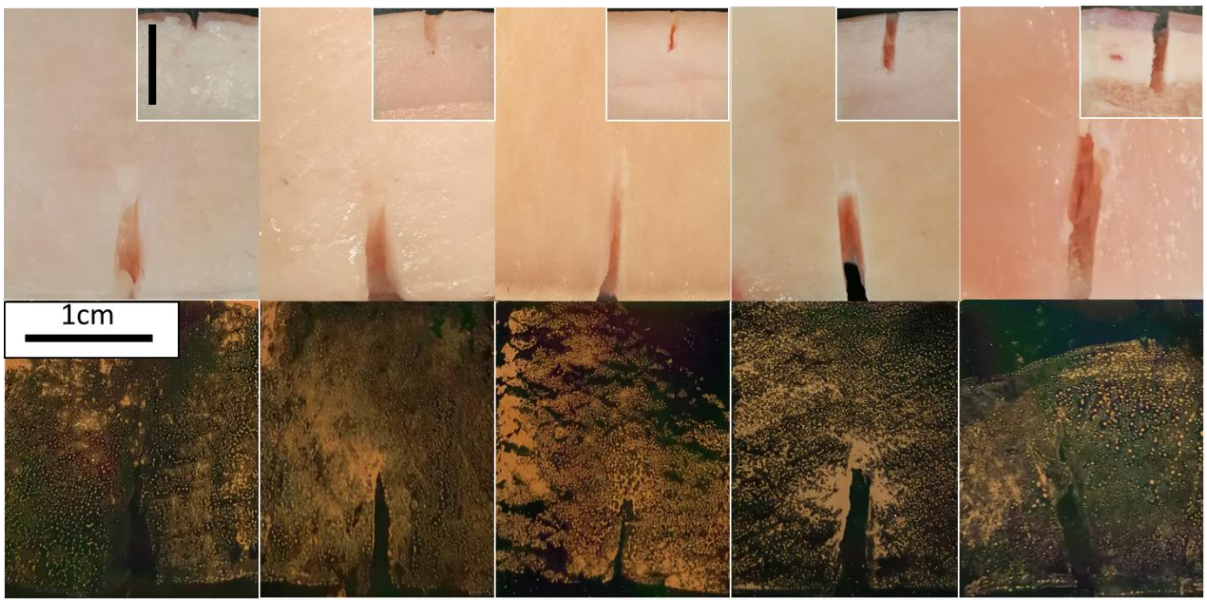

Figure 34. Digital images of simulated wounds using pig skin as model wound matrix (upper row) with various depth (scale bar: 1cm; inset side views from left to right, 2 mm, 4 mm, 6 mm, 8 mm, 10 mm) and corresponded developed 3D skin patterns (lower row).

Figure 35. Digital images of simulated various shape wounds using pig skin as a model wound matrix and accordingly their developed 3D skin patterns.

The important factor of the accuracy of 3D information and the possibility to address wounds in a geometrical manner is subjected to the controlled growth of conducting polymer corresponding to the features of the skin. Thus, pig skin simulated wounds were also used to

investigate the growth of conducting polymer thickness corresponding to the wound depth. A narrow sharp simulated laceration was created and used for skin patterning with different electropolymerization duration (100-2000 s). The profilometry of the developed wound print showed PEDOT(PSS) thickness in relation to conducting polymer unoccupied sebum (Figure 36a and b). Overall, the surface of PEDOT(PSS) film demonstrated excellent evenness despite the influence of many tiny ridges. The 3D scanning profilometry also illustrated this phenomenon (Figure 36c). Occasional irregularities were present, which were attributed to random impurities rather than irregular growth of the conducting polymer. The profilometry was used to determine the thickness of the conducting polymer after various electropolymerization times. The heights of the developed skin print from consecutive electropolymerization are presented in Figure 36d. In general, the thickness of the conducting polymer increased with the duration of the polymerization, however in the range from 1500 to 2000 s the growth of the conducting polymer was hindered. To summarize, skin mapping quality, especially the homogeneity on the PEDOT(PSS) surface becomes higher when the pattern outlines turn to simple simulated wound-like structures from more complex fingerprints. This favorable performance corroborates its practicability when used for recording or monitoring chronical wounds, as well as scar repairing processes. Yet, it should be noted that wound healing is a complicated process including hemostasis, inflammation, proliferation, maturation, and remodeling [239, 240]. The skin mapping technique may not be directly used in hemostasis or proliferation phases when there is bleeding or exudation unless appropriate pretreatment being conducted. Excessive blood and exudation highly influence the sampling accuracy. In comparison, similar concern does not exist when investigating close scar in cosmetology.

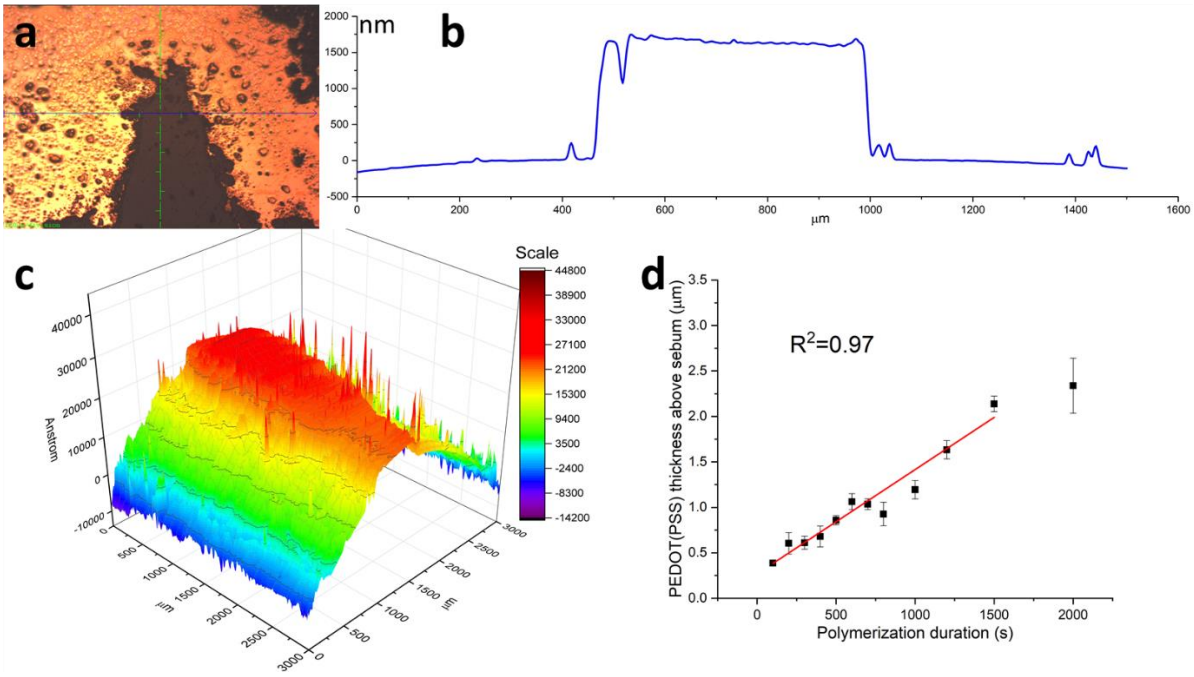

Figure 36. (a) Microscope image for 2D profilometry of developed 3D skin print of simulated wound; black arrow relates to scanning line. (b) Corresponding profilometry profile. (c) 3D profilometry of developed 3D skin print of simulated wound. (d) Conducting polymer thickness in relations to various electropolymerization times.

4.3.2 Electro-controlled metal loading and release using cellulose and PET conducting polymer-based substrates.

Metal loading onto different substrates were done via passive or active processes. Passive process did not involve chemical reactions during the loading, which means metals were loaded in ionic state mainly via sorption onto cellulose substrate and being part of the solution during the electrodeposition of the conducting polymer. Thus resulting film was loaded with metals in both substrate and CP-based film (bulk material metal loading). Differently, active loading involved chemical reaction, here referring to electrochemical reduction of metal ion to its metallic state. The PET-based substrates were loaded with Cu^0 by performing electro reduction of Cu^{2+} from the solution. Thus resulting film was loaded with metal only on the surface of the

conducting polymer film. Furthermore, the release processes could also be categorized into passive and active. Release of Cu^{2+} and Zn^{2+} ions from cellulose substrates was performed by in a passive (no electric stimulation applied) environment, while release of Cu^{2+} ions from PET-based substrates was performed by actively stimulating the conducting polymer films with oxidative currents.

4.3.2.1 Bimetal ions loading and passive release.

The loading of Cu^{2+} and Zn^{2+} ions was conducted simultaneously during electropolymerization process with ions present in electropolymerization solutions (refer to Table 1 in chapter 3.4). After that, the electroactive cellulose substrates were firstly conducted with ion release test to confirm the existence of copper and zinc in doped materials. The release of Cu^{2+} and Zn^{2+} ions from samples was quantified by inductively coupled plasma mass spectrometry (ICP-MS; Thermo Fisher, USA). Briefly, a (2 × 3 cm) samples were immersed in 5 mL of bicarbonate-buffered solutions at three different pH conditions (i.e. 6.5, 7.5 and 8.5) and incubated at room temperature for 48 h. At the end of the incubation, 5 mL of the respective buffered solution was transferred into the injector tube where the amount of Cu^{2+} and Zn^{2+} ions that was released into the buffered solution was quantified and compared based on the average value of three replicates (n = 3). In this particular study, non-electropolymerized samples were used as negative controls, i.e. pyrrole (Py) and 3,4-ethylenedioxythiophene (EDOT), to eliminate the physical interactions of the metal ions with the platinum coating. Briefly, the platinum-coated cellulose substrates were purely immersed into the electropolymerization solutions, such as Py(SDS) and EDOT(SDS) solution either in the presence or absence of Cu^{2+} and Zn^{2+} ions without the applied potential or current. Subsequently, the samples were removed and washed with distilled water prior to the ions release study.

As seen from Figure 37, both Cu^{2+} and Zn^{2+} ions were being detected in Cu/Zn-doped electroactive cellulose substrates. However, the amounts of Cu^{2+} and Zn^{2+} ions released from the PPy-based cellulose substrates were similar to that of the controls (i.e. Cu/Zn-Py and Cu/Zn-EDOT). Hence, it is postulated that the metal ions were merely absorbed onto the PPy-based cellulose substrates. On the other hand, significantly higher amounts of Cu^{2+} and Zn^{2+} ions were being detected in PEDOT-based cellulose substrates as compared to PPy-based cellulose substrates. In addition, the amounts of ions were significantly higher to that of the controls, which is an indication that the metal ions were successfully doped into the PEDOT-based electroactive cellulose substrates. Nevertheless, similar trends were observed with significantly higher amounts of metal ions being released by the PEDOT-based electroactive cellulose substrates, regardless of the pH (Figure 37). Hence, the results revealed that PEDOT-based electroactive cellulose substrates with higher storage capacities resulted in the better doping of Cu^{2+} and Zn^{2+} ions. However, the amounts of Cu^{2+} and Zn^{2+} ions being released from the samples were relatively low. Hence, a pure immersion of the samples in different pH buffer could hardly induce the release of the metal ions. As a result, no significant difference was observed in the cell proliferation between the undoped and Cu/Zn-doped samples. Nevertheless, both Cu^{2+} and Zn^{2+} ions were successfully doped into PEDOT-based cellulose substrates. In addition, the cellular results showed the cytocompatibility of the various electroactive cellulose substrates, particularly for the Cu/Zn-doped samples. Hence, the release of Cu^{2+} and Zn^{2+} ions could potentially be induced by the application of electrical stimulation in the future to further promote the cellular activities as well as the effective wound healing process.

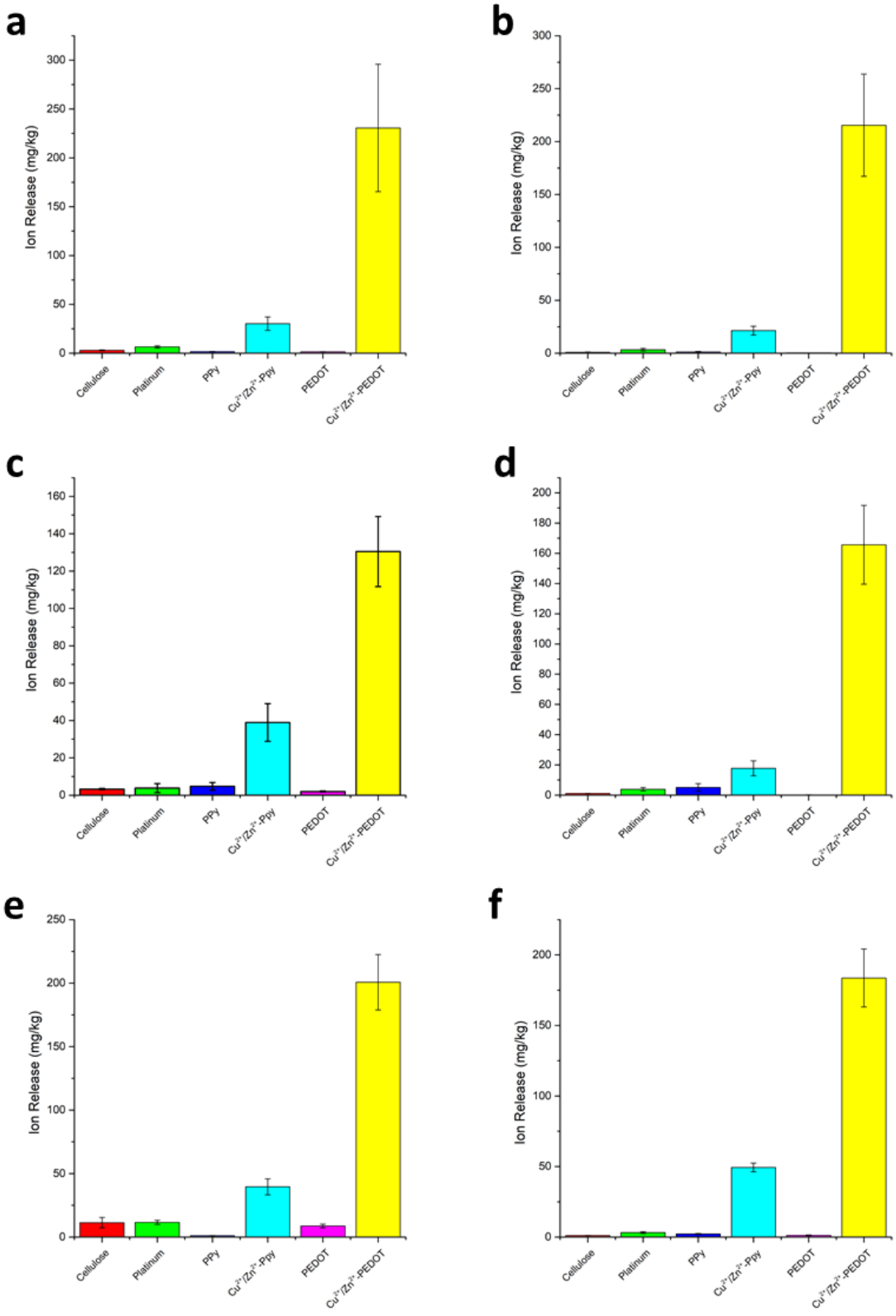

Figure 37. Ions release of electroactive cellulose substrates for (a) Cu at pH 7.5, (b) Zn at pH 7.5, (c) Cu at pH 6.5, (d) Zn at pH 6.5, (e) Cu at pH 8.5 (f) Zn at pH 8.5

4.3.2.2 Copper loading and electro-controlled release

The copper was loaded via electro reduction of Cu^{2+} to Cu^0 onto the Au-PET/PEDOT(PSS) substrates and such substrates were tested for their electro-controlled release of copper to the solution (Figure 38). The acquired Raman spectra showed unique PEDOT(PSS) signatures at approximately 571, 991 cm^{-1} (C – O deformation), 1262 cm^{-1} (Cα – Cα' stretching and C-H bending), 1364 cm^{-1} (thiophene ring Cβ – Cβ' stretching, 1437, 1497, 1561 (symmetric and asymmetric C = C stretching), 2863 (O – H stretching) [209]. As might be expected with Cu being involved in the polymer, there are band shifts and intensity changes; the upper spectrum shows the Raman signature from inside a flake- this has effectively Cu with no signature from the PEDOT(PSS). The presence of these signatures outside and within the print is indicative of the presence of PEDOT(PSS) throughout the film (Figure 38a). The copper release from the metallic copper particles were conducted under CP with four different current densities, namely, 25, 50, 75 and 100 $\mu A/cm^2$ (Figure 38c). For comparison, a passive release without applying any current was also conducted. The Cu^{2+} release curves under both 25 and 50 $\mu A/cm^2$ current densities were characterized with linear correlation (R^2= 0.99). The Cu^{2+} release curve under 100 $\mu A/cm^2$ current density reached its equilibrium after 1000 s release time, while the Cu^{2+} release curve under 75 $\mu A/cm^2$ current density reached near equilibrium state at the 1800 s, equal to approx. 700 ppb Cu (measured by means of ICP-MS). The Cu^{2+} release curves under both 75 $\mu A/cm^2$ and 100 $\mu A/cm^2$ current densities showed linear correlation (R^2, 0.99 and 0.97) with respect to the release time period (from 400 to 1200 s and from 400 to 1000 s, respectively). Notably, the passive release of Cu^{2+} was also observed, resulting in 200 ppb copper release after 1800 s. The release rates were calculated and shown in Figure 38d. The copper(II) release rate, ranging from 0.24 to 0.93 ppb/(s·cm^2), could be controlled at least within the tested current density 25 $\mu A/cm^2$ to 100 $\mu m/cm^2$. Accurate controlled release could be realized based on a

required wound healing dose. The Cu concentration in healthy human blood plasma ranges from 700 ppb to 1400 ppb [241]. The loading and release ability of the developed PEDOT(PSS) films is just within this range. Of course, the blood Cu consists of various Cu-containing proteins and other molecules besides free Cu^{2+} [242, 243]. Specifically, for example, matrix metalloproteinases (MMPs) are of major groups of proteins involved in wound healing process [244, 245]. Low concentrations of Cu^{2+} from 19.2 ppb to 192 ppb stimulate the activity of MMPs while higher concentrations from 64 ppb to 6400 ppb stimulate the expression of MMPs in fibroblast [78]. The release capability of the material is able to change the concentration from 0 up to at least 600 ppb, which is enough to modify the local Cu^{2+} concentration if applied on skin. Release under electro-controlled conditions with considerable accuracy is preferred for any form of Cu deficiency. Thus, this is a promising material for wound healing besides diagnostic skin mapping.

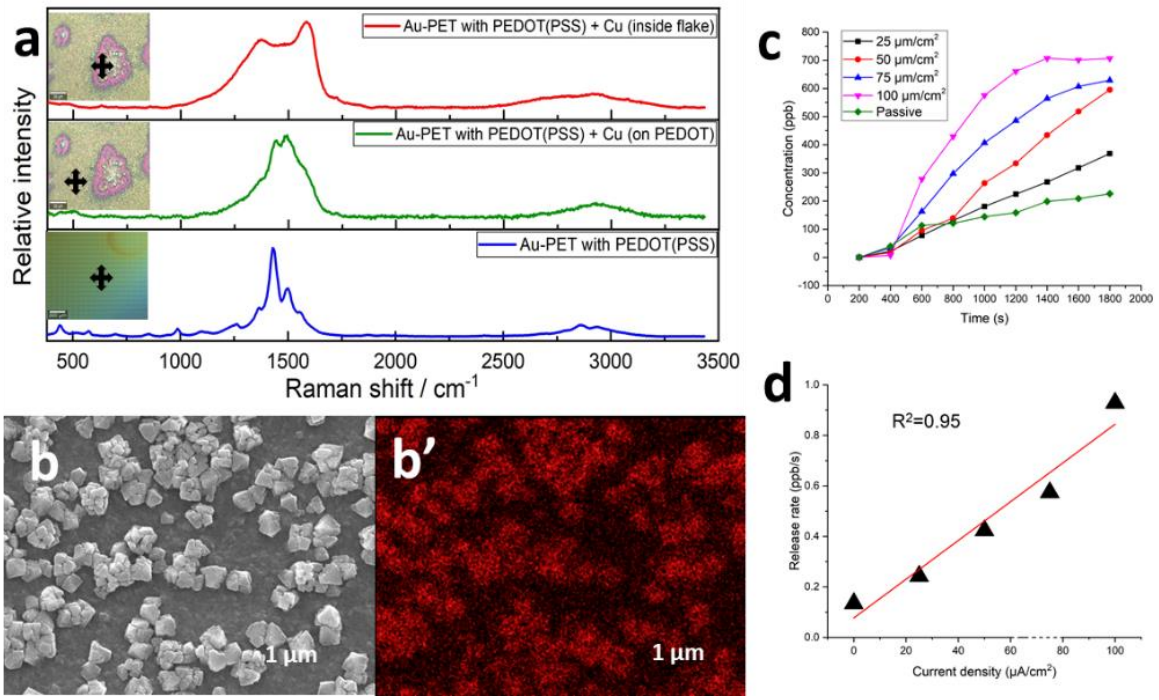

Figure 38. (a) Raman spectrum of PEDOT(PSS) coated Au-PET with/without Cu loading. The target on the left-hand side photograph shows the point where the spectrum was collected, (b)

(b') FESEM image and corresponding EDS map of Cu element, (c) Cu^{2+} release curves under various current densities, (d) a scatter diagram of Cu releasing rate under various current densities.

CHAPTER 5 CONCLUSIONS AND FUTURE PROSPECTS

5.1 Conclusions.

Based on electro-controlled growth of conducting polymers and surface chemistry of sebum-metal interactions, a portable and fast 3D skin mapping technique was developed, allowing for decentralized on-site skin mapping. The device consisted of two parts, namely skin stamp sampling and 3D skin patterning. Two skin mapping techniques were proposed, namely on- and off-body. Owning to the possible toxicity of the monomers that form the conducting polymer into 3D skin patterns, the off-body mode was found to be more feasible as it did not require direct contact between the monomer and the human skin. With the optimized protocol, it was shown that the upgraded skin mapping technique demonstrated adequate capability for recognition and reproduction of various skin features. It supported a resolution of up to µm-level, which encompass most circumstances in dermatology diagnosis. Besides, this technique showed broad tolerance to most of the practical parameters including polymerization durations, monomer choices, depositing IRs, depositing pressure and supporting substrates. The technique indicates potential to serve in a portable device with minimal operational requirements, serving as more economical option to currently offered medical diagnostic apparatus. The portable skin mapping device was powered by an ordinary dry battery (1.5 V). This eliminates the need for the analysis to be done in the environment of the laboratory/doctor's office and allow to be taken to places with no direct power supply. The device could be found optimal for taking it on-site, such as construction sites, to monitor the work health of workers that are in higher risk of developing pathological skin conditions.

To add the functionality of wound healing to the developed skin patterning technique cellulose substrates were introduced to improve flexibility and breathability of the material, as compared to the previously used PET-based substrates. The PEDOT(SDS) on cellulose substrates showed

superior performance in electrochemical properties, mechanical properties, cytocompatibility and passive ions release as compared to PPy(SDS) films. Moreover, the copper/zinc-doped (Cu/Zn-doped) electroactive cellulose substrates exhibited good mechanical and structural properties as well as good cytocompatibility by supporting the attachment and proliferation of immortalized human keratinocytes (HaCaT cells). Successful introduction of cellulose substrates provides new possibility, aside of skin features diagnostics, for on-site treatment towards pathological skin conditions.

Additionally, therapeutic ions loading and release was studied where the electroactive cellulose and PET substrates were tested with metal loading and passive/active metal release. It was found that both passive and active metal release provided adequate concentration of the metal in the solution (as studied potential wound area) to support healing of the wounds if that functionality would have been implemented in 3D skin pattern based wound dressing material.

5.2 Future prospects.

In the course of this study, portable, fast, and cheap technique to map skin was developed. The next step would be to apply this technique in clinical trials to evaluate mapping the pathological skin conditions in various patients. Such trials should be performed outside of the laboratory environment, e.g. medical ward or various occupational sites. Based on the results obtained during the clinical trial, the improvement of the prototype of the skin patterning device would be executed.

The wound healing abilities of the developed substrates in conjunction with skin patterning technique would have to be validated and clinical trials. Additionally, antibacterial activity could be introduced to the 3D skin prints thus avoiding the possibility of the secondary infection during the wound healing process, especially for chronical wounds [246, 247]. For that, silver nanoparticles (AgNPs) have been reported to have excellent antibacterial property

[248-251] and based on fact that they synthesis is relatively mature [252, 253] their incorporation into the 3D skin patterns should be rather straightforward.

Finally, the 3D skin pattering ought to be further studied in the on-body skin mapping. Currently considered monomers, for on-body skin mapping were EDOT, pyrrole and aniline. They however possess certain degree of toxicity [254-256]. Thus, study on the potentially hazardous nature of the monomer to human skin and/or open wounds at the used monomer concentrations is necessary. It may be hypothesized at this point that if the electropolymerization condition were proved to be safe with those monomers or monomer solutions (regulated with the concentration of the monomer applied), on-body skin mapping could be explored for further studies including optimization, device prototyping as well as clinical trials. Alternatively, conducting polymers or biopolymers, which have already proved with good biocompatibility and no toxicity could be introduced into the controlled polymer deposition and 3D skin mapping.

References

[1] H. Shirakawa, E.J. Louis, A.G. Macdiarmid, C.K. Chiang, A.J. Heeger, Synthesis of Electrically Conducting Organic Polymers - Halogen Derivatives of Polyacetylene, (Ch)X, Journal of the Chemical Society-Chemical Communications (16) (1977) 578-580.
[2] A.G. Macdiarmid, R.J. Mammone, R.B. Kaner, S.J. Porter, The Concept of Doping of Conducting Polymers - the Role of Reduction Potentials, Philosophical Transactions of the Royal Society a-Mathematical Physical and Engineering Sciences 314(1528) (1985) 3-15.
[3] T.A. Skotheim, J.R. Reynolds, Handbook of Conducting Polymers: Conjugated Polymers Processing and Applications, 2007.
[4] G. Nagele, G.E. Nauer, H. Kuzmany, J. Kurti, Kinetics of Electrochemical N-Doping of Polyacetylene Investigated by Impedance and Galvanostatic Pulse Measurements, Synthetic Metals 21(3) (1987) 293-299.
[5] T.-H. Le, Y. Kim, H. Yoon, Electrical and Electrochemical Properties of Conducting Polymers, Polymers 9(4) (2017).
[6] A.D. Bendrea, L. Cianga, I. Cianga, Review paper: progress in the field of conducting polymers for tissue engineering applications, J Biomater Appl 26(1) (2011) 3-84.
[7] Z.-B. Huang, G.-F. Yin, X.-M. Liao, J.-W. Gu, Conducting polypyrrole in tissue engineering applications, Frontiers of Materials Science 8(1) (2014) 39-45.
[8] B. Guo, P.X. Ma, Conducting Polymers for Tissue Engineering, Biomacromolecules 19(6) (2018) 1764-1782.
[9] G. Shi, M. Rouabhia, Z. Wang, L.H. Dao, Z. Zhang, A novel electrically conductive and biodegradable composite made of polypyrrole nanoparticles and polylactide, Biomaterials 25(13) (2004) 2477-2488.
[10] Z. Zhang, M. Rouabhia, Z. Wang, C. Roberge, G. Shi, P. Roche, J. Li, L.H. Dao, Electrically conductive biodegradable polymer composite for nerve regeneration: electricity-stimulated neurite outgrowth and axon regeneration, Artif Organs 31(1) (2007) 13-22.
[11] X. Wang, X. Gu, C. Yuan, S. Chen, P. Zhang, T. Zhang, J. Yao, F. Chen, G. Chen, Evaluation of biocompatibility of polypyrrole in vitro and in vivo, J Biomed Mater Res A 68(3) (2004) 411-22.
[12] P. Humpolicek, V. Kasparkova, J. Pachernik, J. Stejskal, P. Bober, Z. Capakova, K.A. Radaszkiewicz, I. Junkar, M. Lehocky, The biocompatibility of polyaniline and polypyrrole: A comparative study of their cytotoxicity, embryotoxicity and impurity profile, Mater Sci Eng C Mater Biol Appl 91 (2018) 303-310.
[13] M. Mattioli-Belmonte, G. Giavaresi, G. Biagini, L. Virgili, M. Giacomini, M. Fini, F. Giantomassi, D. Natali, P. Torricelli, R. Giardino, Tailoring biomaterial compatibility: in vivo tissue response versus in vitro cell behavior, Int J Artif Organs 26(12) (2003) 1077-85.
[14] L.J. del Valle, D. Aradilla, R. Oliver, F. Sepulcre, A. Gamez, E. Armelin, C. Alemán, F. Estrany, Cellular adhesion and proliferation on poly(3,4-ethylenedioxythiophene): Benefits in the electroactivity of the conducting polymer, European Polymer Journal 43(6) (2007) 2342-2349.
[15] S. Kamalesh, P. Tan, J. Wang, T. Lee, E.T. Kang, C.H. Wang, Biocompatibility of electroactive polymers in tissues, J Biomed Mater Res 52(3) (2000) 467-78.
[16] N.K. Guimard, N. Gomez, C.E. Schmidt, Conducting polymers in biomedical engineering, Progress in Polymer Science 32(8-9) (2007) 876-921.
[17] M. Armour, A.G. Davies, J. Upadhyay, A. Wassermann, Colored electrically conducting polymers from furan, pyrrole, and thiophene, Journal of Polymer Science Part A-1: Polymer Chemistry 5(7) (1967) 1527-1538.
[18] G. Tourillon, F. Garnier, New electrochemically generated organic conducting polymers, Journal of Electroanalytical Chemistry 135(1) (1982) 173-178.
[19] A. Elschner, PEDOT : principles and applications of an intrinsically conductive polymer, (2011).
[20] P.H. Chien, Y. Jee, C. Huang, R. Dervisoglu, I. Hung, Z. Gan, K. Huang, Y.Y. Hu, On the origin of high ionic conductivity in Na-doped SrSiO3, Chem Sci 7(6) (2016) 3667-3675.

[21] M. Marzocchi, I. Gualandi, M. Calienni, I. Zironi, E. Scavetta, G. Castellani, B. Fraboni, Physical and Electrochemical Properties of PEDOT:PSS as a Tool for Controlling Cell Growth, ACS Applied Materials & Interfaces 7(32) (2015) 17993-18003.
[22] T.A. Skotheim, E. Elsenbaumer, J.R. Reynolds, Handbook of Conducting Polymers, 2nd edition, 1999, pp. 37-37.
[23] D. Mawad, C. Mansfield, A. Lauto, F. Perbellini, G.W. Nelson, J. Tonkin, S.O. Bello, D.J. Carrad, A.P. Micolich, M.M. Mahat, J. Furman, D. Payne, A.R. Lyon, J.J. Gooding, S.E. Harding, C.M. Terracciano, M.M. Stevens, A conducting polymer with enhanced electronic stability applied in cardiac models, Science Advances 2 (2016) 1-13.
[24] G. Inzelt, M. Pineri, J.W. Schultze, M.A. Vorotyntsev, Electron and proton conducting polymers: recent developments and prospects, Electrochimica Acta 45(15-16) (2000) 2403-2421.
[25] J. Janata, M. Josowicz, Conducting polymers in electronic chemical sensors, Nature Materials 2(1) (2003) 19-24.
[26] R. Ramya, R. Sivasubramanian, M.V. Sangaranarayanan, Conducting polymers-based electrochemical supercapacitors-Progress and prospects, Electrochimica Acta 101 (2013) 109-129.
[27] C. Ridgway, J. Chambers, E. Portero-Larragueta, O. Prosser, Detection of mite infestation in wheat by electronic nose with transient flow sampling, Journal of the Science of Food and Agriculture 79(15) (1999) 2067-2074.
[28] T.K. Das, S. Prusty, Review on Conducting Polymers and Their Applications, Polymer-Plastics Technology and Engineering 51(14) (2012) 1487-1500.
[29] U. Lange, N.V. Roznyatouskaya, V.M. Mirsky, Conducting polymers in chemical sensors and arrays, Analytica Chimica Acta 614(1) (2008) 1-26.
[30] T. Rebis, M. Sobkowiak, G. Milczarek, Electrocatalytic oxidation and detection of hydrazine at conducting polymer/lignosulfonate composite modified electrodes, Journal of Electroanalytical Chemistry 780 (2016) 257-263.
[31] J. Young Oh, S. Rondeau-Gagné, Y.-C. Chiu, A. Chortos, F. Lissel, G.-J. Nathan Wang, B.C. Schroeder, T. Kurosawa, J. Lopez, T. Katsumata, J. Xu, C. Zhu, X. Gu, W.-G. Bae, Y. Kim, L. Jin, J. Won Chung, J. B-H Tok, Z. Bao, Intrinsically stretchable and healable semiconducting polymer for organic transistors, Nature Publishing Group 539(7629) (2016) 411-415.
[32] G. Heywang, F. Jonas, Poly(alkylenedioxythiophene)s - New, very stable conducting polymers, Advanced Materials 4(2) (1992) 116-118.
[33] R. Corradi, S.P. Armes, Chemical synthesis of poly(3,4-ethylenedioxythiophene), Synthetic Metals 84(1-3) (1997) 453-454.
[34] S.G. Im, D. Kusters, W. Choi, S.H. Baxamusa, M.C.M. van de Sanden, K.K. Gleason, Conformal coverage of poly(3,4-ethylenedioxythiophene) films with tunable nanoporosity via oxidative chemical vapor deposition, ACS Nano 2(9) (2008) 1959-1967.
[35] L. Groenendaal, F. Jonas, D. Freitag, H. Pielartzik, J.R. Reynolds, Poly(3,4-ethylenedioxythiophene) and its derivatives: past, present, and future, Advanced Materials 12(7) (2000) 481-494.
[36] F. Jonas, L. Schrader, Conductive modifications of polymers with polypyrroles and polythiophenes, Synthetic Metals 41(3) (1991) 831-836.
[37] G. Sonmez, P. Schottland, J.R. Reynolds, PEDOT/PAMPS: An electrically conductive polymer composite with electrochromic and cation exchange properties, Synthetic Metals 155(1) (2005) 130-137.
[38] D. Hohnholz, A.G. MacDiarmid, Line patterning of conducting polymers: New horizons for inexpensive, disposable electronic devices, Synthetic Metals 121(1-3) (2001) 1327-1328.
[39] F.C. Krebs, Fabrication and processing of polymer solar cells: A review of printing and coating techniques, 2009, pp. 394-412.
[40] I.S. Kolesov, H. M??nstedt, Stabilit??t antielektrostatischer beschichtungen auf der basis von polyethylendioxithiophenen, Materialwissenschaft und Werkstofftechnik 34(6) (2003) 542-548.

[41] J.P. Drummond, S.J. Clarson, J.S. Zetts, F.K. Hopkins, S.J. Caracci, Enhanced electro-optic poling in guest-host systems using conductive polymer-based cladding layers, Applied Physics Letters 74(3) (1999) 368-370.
[42] R. Ansari, Polypyrrole Conducting Electroactive Polymers: Synthesis and Stability Studies, E-Journal of Chemistry 3(4) (2006) 186-201.
[43] D.D. Ateh, H.A. Navsaria, P. Vadgama, Polypyrrole-based conducting polymers and interactions with biological tissues, Journal of The Royal Society Interface 3(11) (2006) 741-752.
[44] K. Maksymiuk, Chemical reactivity of polypyrrole and its relevance to polypyrrole based electrochemical sensors, 2006, pp. 1537-1551.
[45] I. Villarreal, E. Morales, T.F. Otero, J.L. Acosta, Electropolymerization kinetics of pyrrole in aqueous solution on graphite felt electrodes, Synthetic Metals 123(3) (2001) 487-492.
[46] G.B. Street, S.E. Lindsey, A.I. Nazzal, K.J. Wynne, The Structure and Mechanical Properties of Polypyrrole, Molecular Crystals and Liquid Crystals 118(1) (2011) 137-148.
[47] G.G. Wallace, CONDUCTIVE ELECTROACTIVE POLYMERS Intelligent Polymer Systems 3rd, 2009.
[48] J. Heinze, B.A. Frontana-Uribe, S. Ludwigs, Electrochemistry of conducting polymers-persistent models and new concepts, Chemical Reviews 110(8) (2010) 4724-4771.
[49] M. Fleischmann, D. Pletcher, Organic electrochemistry, Royal Institute of Chemistry, Reviews 2(2) (1969) 87-87.
[50] M.A. Vorotyntsev, V.A. Zinovyeva, D.V. Konev, Mechanisms of Electropolymerization and Redox Activity: Fundamental Aspects, 2010, pp. 27-50.
[51] G. Sabouraud, S. Sadki, N. Brodie, The mechanisms of pyrrole electropolymerization, Chemical Society Reviews 29(5) (2000) 283-293.
[52] K. Vig, A. Chaudhari, S. Tripathi, S. Dixit, R. Sahu, S. Pillai, V.A. Dennis, S.R. Singh, Advances in Skin Regeneration Using Tissue Engineering, Int J Mol Sci 18(4) (2017).
[53] C. Harvey, Wound healing, Orthop Nurs 24(2) (2005) 143-57; quiz 158-9.
[54] P. Zarrintaj, A.S. Moghaddam, S. Manouchehri, Z. Atoufi, A. Amiri, M.A. Amirkhani, M.A. Nilforoushzadeh, M.R. Saeb, M.R. Hamblin, M. Mozafari, Can regenerative medicine and nanotechnology combine to heal wounds? The search for the ideal wound dressing, Nanomedicine (Lond) 12(19) (2017) 2403-2422.
[55] Skin Conditions: Symptoms, Treatments, Diagnosis - Health.
[56] J.E. Grant, B.L. Odlaug, S.R. Chamberlain, N.J. Keuthen, C. Lochner, D.J. Stein, Skin picking disorder, 2012, pp. 1143-1149.
[57] Skin: Facts, Diseases & Conditions.
[58] G.S. Lazarus, D.M. Cooper, D.R. Knighton, D.J. Margolis, R.E. Pecoraro, G. Rodeheaver, M.C. Robson, Definitions and guidelines for assessment of wounds and evaluation of healing, Arch Dermatol 130(4) (1994) 489-93.
[59] A Labeled Diagram Of A Skin Skin Diagram Black And White Structure Of The Skin Diagram Labeled - Anatomy Human Charts.
[60] J.F. Wang, M.E. Olson, C.R. Reno, W. Kulyk, J.B. Wright, D.a. Hart, Molecular and cell biology of skin wound healing in a pig model, Connective tissue research 41(3) (2000) 195-211.
[61] L. Ma, C. Gao, Z. Mao, J. Zhou, J. Shen, X. Hu, C. Han, Collagen/chitosan porous scaffolds with improved biostability for skin tissue engineering, Biomaterials 24(26) (2003) 4833-4841.
[62] A.D. Metcalfe, M.W.J. Ferguson, Bioengineering skin using mechanisms of regeneration and repair, 2007, pp. 5100-5113.
[63] K.A. Blackwood, R. McKean, I. Canton, C.O. Freeman, K.L. Franklin, D. Cole, I. Brook, P. Farthing, S. Rimmer, J.W. Haycock, A.J. Ryan, S. MacNeil, Development of biodegradable electrospun scaffolds for dermal replacement, Biomaterials 29(21) (2008) 3091-3104.
[64] R. Jayakumar, M. Prabaharan, P.T. Sudheesh Kumar, S.V. Nair, H. Tamura, Biomaterials based on chitin and chitosan in wound dressing applications, 2011, pp. 322-337.

[65] V. Jayarama Reddy, S. Radhakrishnan, R. Ravichandran, S. Mukherjee, R. Balamurugan, S. Sundarrajan, S. Ramakrishna, Nanofibrous structured biomimetic strategies for skin tissue regeneration, 2013, pp. 1-16.
[66] J.N. Mansbridge, Tissue-engineered skin substitutes in regenerative medicine, 2009, pp. 563-567.
[67] Y.Z. Zhang, J. Venugopal, Z.M. Huang, C.T. Lim, S. Ramakrishna, Characterization of the surface biocompatibility of the electrospun PCL-Collagen nanofibers using fibroblasts, Biomacromolecules 6(5) (2005) 2583-2589.
[68] G.D. Winter, EFFECT OF AIR EXPOSURE AND OCCLUSION ON EXPERIMENTAL HUMAN SKIN WOUNDS, Nature 200 (1963) 378-9.
[69] C.D. Hinman, H. Maibach, EFFECT OF AIR EXPOSURE AND OCCLUSION ON EXPERIMENTAL HUMAN SKIN WOUNDS, Nature 200 (1963) 377-8.
[70] S. Dhivya, V.V. Padma, E. Santhini, Wound dressings - a review, Biomedicine (Taipei) 5(4) (2015) 22.
[71] P. Zahedi, I. Rezaeian, S.-O. Ranaei-Siadat, S.-H. Jafari, P. Supaphol, A review on wound dressings with an emphasis on electrospun nanofibrous polymeric bandages, Polymers for Advanced Technologies 21(2) (2009) 77-95.
[72] R. Barbucci, S. Lamponi, A. Magnani, F.M. Piras, A. Rossi, E. Weber, Role of the Hyal-Cu (II) complex on bovine aortic and lymphatic endothelial cells behavior on microstructured surfaces, Biomacromolecules 6(1) (2005) 212-219.
[73] G. Borkow, J. Gabbay, R.C. Zatcoff, Could chronic wounds not heal due to too low local copper levels?, Medical Hypotheses 70(3) (2008) 610-613.
[74] C. Gérard, L.J. Bordeleau, J. Barralet, C.J. Doillon, The stimulation of angiogenesis and collagen deposition by copper, Biomaterials 31(5) (2010) 824-831.
[75] S. Zhao, H. Wang, Y. Zhang, W. Huang, M.N. Rahaman, Z. Liu, D. Wang, C. Zhang, Copper-doped borosilicate bioactive glass scaffolds with improved angiogenic and osteogenic capacity for repairing osseous defects, Acta Biomaterialia 14 (2015) 185-196.
[76] G. Borkow, J. Gabbay, A. Lyakhovitsky, M. Huszar, Improvement of facial skin characteristics using copper oxide containing pillowcases: A double-blind, placebo-controlled, parallel, randomized study, International Journal of Cosmetic Science 31(6) (2009) 437-443.
[77] R.W. Gorter, M. Butorac, E.P. Cobian, Examination of the cutaneous absorption of copper after the use of copper-containing ointments, American Journal of Therapeutics 11(6) (2004) 453-458.
[78] N. Philips, H. Hwang, S. Chauhan, D. Leonardi, S. Gonzalez, Stimulation of Cell Proliferation and Expression of Matrixmetalloproteinase-1 and Interluekin-8 Genes in Dermal Fibroblasts by Copper, Connective Tissue Research 51(3) (2010) 224-229.
[79] J. Li, D. Zhai, F. Lv, Q. Yu, H. Ma, J. Yin, Z. Yi, M. Liu, J. Chang, C. Wu, Preparation of copper-containing bioactive glass/eggshell membrane nanocomposites for improving angiogenesis, antibacterial activity and wound healing, Acta Biomaterialia 36 (2016) 254-266.
[80] M. Shi, Z. Chen, S. Farnaghi, T. Friis, X. Mao, Y. Xiao, C. Wu, Copper-doped mesoporous silica nanospheres, a promising immunomodulatory agent for inducing osteogenesis, Acta Biomaterialia 30 (2016) 334-344.
[81] S. Zhao, L. Li, H. Wang, Y. Zhang, X. Cheng, N. Zhou, M.N. Rahaman, Z. Liu, W. Huang, C. Zhang, Wound dressings composed of copper-doped borate bioactive glass microfibers stimulate angiogenesis and heal full-thickness skin defects in a rodent model, Biomaterials 53 (2015) 379-391.
[82] V. Aspinall, The Complete Textbook of Veterinary Nursing, Saunders/Elsevier2011.
[83] T.A. Söderberg, Trace Elements in Normal and Impaired Wound Healing, Springer Berlin Heidelberg1995, pp. 183-199.
[84] D. Keilin, T. Mann, Carbonic anhydrase. Purification and nature of the enzyme, The Biochemical journal 34(June) (1940) 1163-1176.
[85] B.L. O'Dell, Zinc Plays Both Structural and Catalytic Roles in Metalloproteins, 1992, pp. 48-50.
[86] B.L. Vallee, K.H. Falchuk, The biochemical basis of zinc physiology, 1993.

[87] B.L. O'Dell, Role of zinc in plasma membrane function, The Journal of nutrition 130 (2000) 1432S-6S.
[88] C.A. Pasternak, G.M. Alder, C.L. Bashford, Y.E. Korchev, C. Pederzolli, T.K. Rostovtseva, Membrane damage: common mechanisms of induction and prevention, FEMS Microbiology Letters 105(1-3) (1992) 83-92.
[89] A.B.G. Lansdown, Metallothioneins: Potential therapeutic aids for wound healing in the skin, 2002, pp. 130-132.
[90] L. Ravanti, V.M. Kähäri, Matrix metalloproteinases in wound repair (review), 2000, pp. 391-407.
[91] J.K. Barral, N.K. Bangerter, B.S. Hu, D.G. Nishimura, In vivo high-resolution magnetic resonance skin imaging at 1.5 T and 3 T, Magnetic Resonance in Medicine 63(3) (2010) 790-795.
[92] B. Dasgeb, J. Kainerstorfer, D. Mehregan, A. Van Vreede, A. Gandjbakhche, An introduction to primary skin imaging, International Journal of Dermatology 52(11) (2013) 1319-1330.
[93] M. Hassan, R.F. Little, A. Vogel, K. Aleman, K. Wyvill, R. Yarchoan, A.H. Gandjbakhche, Quantitative assessment of tumor vasculature and response to therapy in Kaposi's sarcoma using functional noninvasive imaging, Technology in Cancer Research and Treatment 3(5) (2004) 451-457.
[94] A. Vogel, V.V. Chernomordik, J.D. Riley, M. Hassan, F. Amyot, B. Dasgeb, S.G. Demos, R. Pursley, R.F. Little, R. Yarchoan, Y. Tao, A.H. Gandjbakhche, Using noninvasive multispectral imaging to quantitatively assess tissue vasculature, Journal of Biomedical Optics 12(5) (2007) 051604-051604.
[95] E. Craythorne, F. Al-Niami, Skin cancer, Medicine 45(7) (2017) 431-434.
[96] P.J. Nelemans, H. Groenendal, L.A. Kiemeney, F.H. Rampen, D.J. Ruiter, A.L. Verbeek, Effect of intermittent exposure to sunlight on melanoma risk among indoor workers and sun-sensitive individuals, Environ Health Perspect 101(3) (1993) 252-5.
[97] J.P. McCool, A.I. Reeder, E.M. Robinson, K.J. Petrie, D.F. Gorman, Outdoor workers' perceptions of the risks of excess sun-exposure, J Occup Health 51(5) (2009) 404-11.
[98] H.E. Hanwell, R. Vieth, D.E. Cole, A. Scillitani, S. Modoni, V. Frusciante, G. Ritrovato, I. Chiodini, S. Minisola, V. Carnevale, Sun exposure questionnaire predicts circulating 25-hydroxyvitamin D concentrations in Caucasian hospital workers in southern Italy, J Steroid Biochem Mol Biol 121(1-2) (2010) 334-7.
[99] B.J. Hall, Sauer's manual of skin diseases, 10th ed. ed., Wolters Kluwer/Lippincott Williams & Wilkins Health, Philadelphia, 2010.
[100] H. Morsy, S. Kamp, L. Thrane, N. Behrendt, B. Saunder, H. Zayan, E.A. Elmagid, G.B.E. Jemec, Optical coherence tomography imaging of psoriasis vulgaris: Correlation with histology and disease severity, Archives of Dermatological Research 302(2) (2010) 105-111.
[101] M. Mogensen, H.A. Morsy, B.M. Nurnberg, G.B.E. Jemec, Optical coherence tomography imaging of bullous diseases, Journal of the European Academy of Dermatology and Venereology 22(12) (2008) 1458-1464.
[102] V.R. Korde, G.T. Bonnema, W. Xu, C. Krishnamurthy, J. Ranger-Moore, K. Saboda, L.D. Slayton, S.J. Salasche, J.A. Warneke, D.S. Alberts, J.K. Barton, Using optical coherence tomography to evaluate skin sun damage and precancer, Lasers in Surgery and Medicine 39(9) (2007) 687-695.
[103] K. Sahu, Y. Verma, M. Sharma, K.D. Rao, P.K. Gupta, Non-invasive assessment of healing of bacteria infected and uninfected wounds using optical coherence tomography, Skin Research and Technology 16(4) (2010) 428-437.
[104] A. Bossen, R. Lehmann, C. Meier, Internal fingerprint identification with optical coherence tomography, IEEE Photonics Technology Letters 22(7) (2010) 507-509.
[105] K. Wårdell, A. Jakobsson, G.E. Nilsson, Laser Doppler Perfusion Imaging by Dynamic Light Scattering, IEEE Transactions on Biomedical Engineering 40(4) (1993) 309-316.
[106] E. Rosato, C. Rossi, I. Molinaro, A. Giovannetti, S. Pisarri, F. Salsano, Laser Doppler perfusion imaging in systemic sclerosis impaired response to cold stimulation involves digits and hand dorsum, Rheumatology 50(9) (2011) 1654-1658.

[107] I. Kuzmina, I. Diebele, D. Jakovels, J. Spigulis, L. Valeine, J. Kapostinsh, A. Berzina, Towards noncontact skin melanoma selection by multispectral imaging analysis, Journal of Biomedical Optics 16(6) (2011) 060502-060502.
[108] D.S. Gareau, Y.G. Patel, Y. Li, I. Aranda, A.C. Halpern, K.S. Nehal, M. Rajadhyaksha, Confocal mosaicing microscopy in skin excisions: A demonstration of rapid surgical pathology, Journal of Microscopy 233(1) (2009) 149-159.
[109] S. Nori, F. Rius-Díaz, J. Cuevas, M. Goldgeier, P. Jaen, A. Torres, S. González, Sensitivity and specificity of reflectance-mode confocal microscopy for in vivo diagnosis of basal cell carcinoma: A multicenter study, Journal of the American Academy of Dermatology 51(6) (2004) 923-930.
[110] E.L. Psaty, A.C. Halpern, Current and emerging technologies in melanoma diagnosis: the state of the art, Clinics in Dermatology 27(1) (2009) 35-45.
[111] M.P. André, I. Akiyama, M. Andre, W. Arnold, J. Bamber, V. Burov, N. Chubachi, K. Erikson, H. Ermert, M. Fink, W.S. Gan, B. Granz, J. Greenleaf, J. Hu, J.P. Jones, P. Khuri-Yakub, P. Laugier, H. Lee, S. Lees, V.M. Levin, R. Maev, L. Masotti, A. Nowicki, W. O'Brien, M. Prasad, P. Rafter, D. Rouseff, J. Thijssen, B. Tittmann, P. Tortoli, A. Steen, R. Waag, P. Wells, M. Vogt, R. Scharenberg, G. Moussa, M. Sand, K. Hoffmann, P. Altmeyer, H. Ermert, A New High Frequency Ultrasound Skin Imaging System: Imaging Properties and Clinical in Vivo Results, 2007, pp. 137-144.
[112] D.H. Turnbull, B.G. Starkoski, K.A. Harasiewicz, J.L. Semple, L. From, A.K. Gupta, D.N. Sauder, F.S. Foster, A 40-100 MHz B-scan ultrasound backscatter microscope for skin imaging, Ultrasound in Medicine and Biology 21(1) (1995) 79-88.
[113] X. Wortsman, J. Wortsman, Clinical usefulness of variable-frequency ultrasound in localized lesions of the skin, Journal of the American Academy of Dermatology 62(2) (2010) 247-256.
[114] F. Lacarrubba, B. Nardone, M.L. Musumeci, G. Micali, Ultrasound evaluation of clobetasol propionate 0.05% foam application in psoriatic and healthy skin: A pilot study, Dermatologic Therapy 22(SUPPL. 1) (2009).
[115] X. Fu, W. Zeng, A.C. Ramírez-Pérez, G. Lisak, 3-D and electrically conducting functional skin mapping for biomedical applications, Chemical Communications 54(8) (2018) 980-983.
[116] R.M. Sapstead, N. Corden, A.R. Hillman, Latent fingerprint enhancement via conducting electrochromic copolymer films of pyrrole and 3,4-ethylenedioxythiophene on stainless steel, Electrochimica Acta 162 (2015) 119-128.
[117] S. Abadie, C. Jardet, J. Colombelli, B. Chaput, A. David, J.L. Grolleau, P. Bedos, V. Lobjois, P. Descargues, J. Rouquette, 3D imaging of cleared human skin biopsies using light-sheet microscopy: A new way to visualize in-depth skin structure, Skin Res Technol 24(2) (2018) 294-303.
[118] M.T. Clementoni, R. Lavagno, M. Catenacci, R. Kantor, G. Mariotto, I. Shvets, 3D in vivo optical skin imaging for intense pulsed light and fractional ablative resurfacing of photodamaged skin, Facial Plast Surg Clin North Am 19(4) (2011) 737-57, x.
[119] H. Zafar, J. Enfield, M.L. O'Connell, B. Ramsay, M. Lynch, M.J. Leahy, Assessment of psoriatic plaque in vivo with correlation mapping optical coherence tomography, Skin Res Technol 20(2) (2014) 141-6.
[120] E.Z. Zhang, B. Povazay, J. Laufer, A. Alex, B. Hofer, B. Pedley, C. Glittenberg, B. Treeby, B. Cox, P. Beard, W. Drexler, Multimodal photoacoustic and optical coherence tomography scanner using an all optical detection scheme for 3D morphological skin imaging, Biomedical Optics Express 2(8) (2011) 2202-2215.
[121] H. Wannous, S. Treuillet, Y. Lucas, B. Albouy, Mapping Classification Results on 3D model: a Solution for Measuring the Real Areas Covered by Skin Wound Tissues, 2008 3rd International Conference on Information and Communication Technologies: From Theory to Applications, 2008, pp. 1-6.
[122] A.F.M. Hani, N.M. Eltegani, S.H. Hussein, A. Jamil, P. Gill, Assessment of Ulcer Wounds Size Using 3D Skin Surface Imaging, in: H. Badioze Zaman, P. Robinson, M. Petrou, P. Olivier, H. Schröder, T.K. Shih (Eds.) Visual Informatics: Bridging Research and Practice, Springer Berlin Heidelberg, Berlin, Heidelberg, 2009, pp. 243-253.

[123] L. Petit, D. Zugaj, V. Bettoli, B. Dreno, S. Kang, J. Tan, V. Torres, A.M. Layton, P. Martel, Validation of 3D skin imaging for objective repeatable quantification of severity of atrophic acne scarring, Skin Res Technol 24(4) (2018) 542-550.
[124] M. Alpern, S. Thompson, M.S. Lee, Spectral Transmittance of Visible Light by the Living Human Eye*, Journal of the Optical Society of America 55(6) (1965) 723-727.
[125] E. LUDVIGH, E.F. McCARTHY, ABSORPTION OF VISIBLE LIGHT BY THE REFRACTIVE MEDIA OF THE HUMAN EYE, Archives of Ophthalmology 20(1) (1938) 37-51.
[126] I.J. Bigio, J.R. Mourant, Ultraviolet and visible spectroscopies for tissue diagnostics: Fluorescence spectroscopy and elastic-scattering spectroscopy, Physics in Medicine and Biology 42(5) (1997) 803-814.
[127] R. Jolivot, Y. Benezeth, F. Marzani, Skin parameter map retrieval from a dedicated multispectral imaging system applied to dermatology/cosmetology, International Journal of Biomedical Imaging 2013 (2013).
[128] M. Gattrell, N. Gupta, A. Co, Electrochemical reduction of CO2 to hydrocarbons to store renewable electrical energy and upgrade biogas, Energy Conversion and Management 48(4) (2007) 1255-1265.
[129] M. Moncrieff, S. Otton, E. Claridge, P. Hall, Spectrophotometric intracutaneous analysis: A new technique for imaging pigmented skin lesions, British Journal of Dermatology 146(3) (2002) 448-457.
[130] D. Yudovsky, A. Nouvong, L. Pilon, Hyperspectral imaging in diabetic foot wound care, Journal of diabetes science and technology 4(5) (2010) 1099-113.
[131] U. Zschieschang, T. Yamamoto, K. Takimiya, H. Kuwabara, M. Ikeda, T. Sekitani, T. Someya, H. Klauk, Organic electronics on banknotes, Advanced Materials 23(5) (2011) 654-658.
[132] Z. Zhang, R. Roy, F.J. Dugre, D. Tessier, H. L Dao, In vitro biocompatibility study of electrically conductive polypyrrole-coated polyester fabrics, Journal of Biomedical Materials Research 57(1) (2001) 63-71.
[133] X. Fu, J.K. Wang, A.C. Ramírez-Pérez, C. Choong, G. Lisak, Flexible conducting polymer-based cellulose substrates for on-skin applications, Materials Science and Engineering: C 108 (2020) 110392.
[134] M. Talikowska, X. Fu, G. Lisak, Application of conducting polymers to wound care and skin tissue engineering: A review, Biosens Bioelectron 135 (2019) 50-63.
[135] R. Balint, N.J. Cassidy, S.H. Cartmell, Conductive polymers: Towards a smart biomaterial for tissue engineering, Acta Biomaterialia 10(6) (2014) 2341-2353.
[136] M. Li, J. Chen, M. Shi, H. Zhang, P.X. Ma, B. Guo, Electroactive anti-oxidant polyurethane elastomers with shape memory property as non-adherent wound dressing to enhance wound healing, Chemical Engineering Journal 375 (2019) 121999.
[137] Y. Liang, X. Zhao, T. Hu, B. Chen, Z. Yin, P.X. Ma, B. Guo, Adhesive Hemostatic Conducting Injectable Composite Hydrogels with Sustained Drug Release and Photothermal Antibacterial Activity to Promote Full-Thickness Skin Regeneration During Wound Healing, Small 15(12) (2019) e1900046.
[138] J. Qu, X. Zhao, Y. Liang, Y. Xu, P.X. Ma, B. Guo, Degradable conductive injectable hydrogels as novel antibacterial, anti-oxidant wound dressings for wound healing, Chemical Engineering Journal 362 (2019) 548-560.
[139] J. Qu, X. Zhao, Y. Liang, T. Zhang, P.X. Ma, B. Guo, Antibacterial adhesive injectable hydrogels with rapid self-healing, extensibility and compressibility as wound dressing for joints skin wound healing, Biomaterials 183 (2018) 185-199.
[140] X. Zhao, B. Guo, H. Wu, Y. Liang, P.X. Ma, Injectable antibacterial conductive nanocomposite cryogels with rapid shape recovery for noncompressible hemorrhage and wound healing, Nature Communications 9(1) (2018).
[141] M.R. Gizdavic-Nikolaidis, J.R. Bennett, S. Swift, A.J. Easteal, M. Ambrose, Broad spectrum antimicrobial activity of functionalized polyanilines, Acta Biomaterialia 7(12) (2011) 4204-4209.
[142] E. Nazarzadeh Zare, M. Mansour Lakouraj, M. Mohseni, Biodegradable polypyrrole/dextrin conductive nanocomposite: Synthesis, characterization, antioxidant and antibacterial activity, Synthetic Metals 187 (2014) 9-16.

[143] L.J. Bessa, P. Fazii, M. Di Giulio, L. Cellini, Bacterial isolates from infected wounds and their antibiotic susceptibility pattern: some remarks about wound infection, International Wound Journal 12(1) (2013) 47-52.
[144] S. Zhou, M. Wang, X. Chen, F. Xu, Facile Template Synthesis of Microfibrillated Cellulose/Polypyrrole/Silver Nanoparticles Hybrid Aerogels with Electrical Conductive and Pressure Responsive Properties, ACS Sustainable Chemistry & Engineering 3(12) (2015) 3346-3354.
[145] R. Gharibi, H. Yeganeh, H. Gholami, Z.M. Hassan, Aniline tetramer embedded polyurethane/siloxane membranes and their corresponding nanosilver composites as intelligent wound dressing materials, RSC Advances 4(107) (2014) 62046-62060.
[146] N.A. Chowdhury, A.M. Al-Jumaily, Regenerated cellulose/polypyrrole/silver nanoparticles/ionic liquid composite films for potential wound healing applications, Wound Medicine 14 (2016) 16-18.
[147] N. Maráková, P. Humpolíček, V. Kašpárková, Z. Capáková, L. Martinková, P. Bober, M. Trchová, J. Stejskal, Antimicrobial activity and cytotoxicity of cotton fabric coated with conducting polymers, polyaniline or polypyrrole, and with deposited silver nanoparticles, Applied Surface Science 396 (2017) 169-176.
[148] L.J. Wilkinson, R. White, J.K. Chipman, Silver and nanoparticles of silver in wound dressings: A review of efficacy and safety, 2011.
[149] J.R. Morones, J.L. Elechiguerra, A. Camacho, K. Holt, J.B. Kouri, J.T. Ramirez, M.J. Yacaman, The bactericidal effect of silver nanoparticles, Nanotechnology 16(10) (2005) 2346-53.
[150] J. Kaveeta Pergas, R.G.S.V. Prasad, J. Venkata Srinivas, R.S.L. Aparna, A.R. Phani, Antibacterial Activity of Nanostructured Polyaniline Combined With Mupirocin, Nano Biomedicine & Engineering 4(3) (2012) 144-149.
[151] R.R. Isseroff, S.E. Dahle, Electrical Stimulation Therapy and Wound Healing: Where Are We Now?, Advances in wound care 1(6) (2012) 238-243.
[152] R. Balint, N.J. Cassidy, S.H. Cartmell, Electrical stimulation: a novel tool for tissue engineering, Tissue Eng Part B Rev 19(1) (2013) 48-57.
[153] I.S. Foulds, A.T. Barker, Human skin battery potentials and their possible role in wound healing, British Journal of Dermatology 109(5) (1983) 515-522.
[154] M. Zhao, B. Song, J. Pu, T. Wada, B. Reid, G. Tai, F. Wang, A. Guo, P. Walczysko, Y. Gu, T. Sasaki, A. Suzuki, J.V. Forrester, H.R. Bourne, P.N. Devreotes, C.D. McCaig, J.M. Penninger, Electrical signals control wound healing through phosphatidylinositol-3-OH kinase-gamma and PTEN, Nature 442(7101) (2006) 457-60.
[155] P. E Houghton, Electrical stimulation therapy to promote healing of chronic wounds: a review of reviews, 2017.
[156] M. Hepel, F. Mahdavi, Application of the Electrochemical Quartz Crystal Microbalance for Electrochemically Controlled Binding and Release of Chlorpromazine from Conductive Polymer Matrix, Microchemical Journal 56(1) (1997) 54-64.
[157] L.L. Miller, X.Q. Zhou, Poly(N-methylpyrrolylium) poly(styrenesulfonate) - a conductive, electrically switchable cation exchanger that cathodically binds and anodically releases dopamine, Macromolecules 20(7) (1987) 1594-1597.
[158] T.M. Nguyen, S. Lee, S.B. Lee, Conductive polymer nanotube patch for fast and controlled ex vivo transdermal drug delivery, Nanomedicine (Lond) 9(15) (2014) 2263-72.
[159] N. Paradee, A. Sirivat, Electrically Controlled Release of Benzoic Acid from Poly(3,4-ethylenedioxythiophene)/Alginate Matrix: Effect of Conductive Poly(3,4-ethylenedioxythiophene) Morphology, The Journal of Physical Chemistry B 118(31) (2014) 9263-9271.
[160] S. Niamlang, N. Paradee, A. Sirivat, Hybrid transdermal drug delivery patch made from poly(p-phenylene vinylene)/natural rubber latex and controlled by an electric field, Polymer International 67(6) (2018) 747-754.
[161] C.J. Pérez-Martínez, S.D. Morales Chávez, T. del Castillo-Castro, T.E. Lara Ceniceros, M.M. Castillo-Ortega, D.E. Rodríguez-Félix, J.C. Gálvez Ruiz, Electroconductive nanocomposite hydrogel for pulsatile drug release, Reactive and Functional Polymers 100 (2016) 12-17.

[162] S. Oktay, N. Alemdar, Electrically controlled release of 5-fluorouracil from conductive gelatin methacryloyl-based hydrogels, Journal of Applied Polymer Science 136(1) (2018) 46914.
[163] P. Chansai, A. Sirivat, S. Niamlang, D. Chotpattananont, K. Viravaidya-Pasuwat, Controlled transdermal iontophoresis of sulfosalicylic acid from polypyrrole/poly(acrylic acid) hydrogel, International Journal of Pharmaceutics 381(1) (2009) 25-33.
[164] G.A. Justin, S. Zhu, T.R. Nicholson, 3rd, J. Maskrod, J. Mbugua, M. Chase, J.H. Jung, R.M. Mercado, On-demand controlled release of anti-inflammatory and analgesic drugs from conducting polymer films to aid in wound healing, Conf Proc IEEE Eng Med Biol Soc 2012 (2012) 1206-9.
[165] A.C.L. Campos, A. Borges-branco, A.K. Groth, Wound healing, Arquivos brasileiros de cirurgia digestiva 20(1) (2007) 51-58.
[166] K.C. Dee, D.A. Puleo, R. Bizios, Wound Healing, 2003, pp. 127-147.
[167] M.C. Regan, A. Barbul, The Cellular Biology of Wound Healing, 1994, pp. 3-17.
[168] D. Williamson, K. Harding, Wound healing, 2004, pp. 4-7.
[169] A. O'Loughlin, M. Kulkarni, E.E. Vaughan, M. Creane, A. Liew, P. Dockery, A. Pandit, T. O'Brien, Autologous circulating angiogenic cells treated with osteopontin and delivered via a collagen scaffold enhance wound healing in the alloxan-induced diabetic rabbit ear ulcer model, Stem Cell Res Ther 4(6) (2013) 158.
[170] E.E. Vaughan, A. Liew, K. Mashayekhi, P. Dockery, J. McDermott, B. Kealy, A. Flynn, A. Duffy, C. Coleman, A. O'Regan, F.P. Barry, T. O'Brien, Pretreatment of endothelial progenitor cells with osteopontin enhances cell therapy for peripheral vascular disease, Cell Transplant 21(6) (2012) 1095-107.
[171] T. Ehashi, T. Takemura, N. Hanagata, T. Minowa, H. Kobayashi, K. Ishihara, T. Yamaoka, Comprehensive genetic analysis of early host body reactions to the bioactive and bio-inert porous scaffolds, PLoS ONE 9(1) (2014).
[172] G. Jin, M.P. Prabhakaran, S. Ramakrishna, Photosensitive and biomimetic core-shell nanofibrous scaffolds as wound dressing, Photochemistry and Photobiology 90(3) (2014) 673-681.
[173] V. Vachhrajani, P. Khakhkhar, Introduction, Science of Wound Healing and Dressing Materials, Springer Singapore, Singapore, 2020, pp. 1-10.
[174] M.R. dos Santos, J.J. Alcaraz-Espinoza, M.M. da Costa, H.P. de Oliveira, Usnic acid-loaded polyaniline/polyurethane foam wound dressing: preparation and bactericidal activity, Materials Science and Engineering: C 89 (2018) 33-40.
[175] R. Gharibi, H. Yeganeh, A. Rezapour-Lactoee, Z.M. Hassan, Stimulation of Wound Healing by Electroactive, Antibacterial, and Antioxidant Polyurethane/Siloxane Dressing Membranes: In Vitro and in Vivo Evaluations, ACS Applied Materials & Interfaces 7(43) (2015) 24296-24311.
[176] P. Moutsatsou, K. Coopman, S. Georgiadou, Biocompatibility Assessment of Conducting PANI/Chitosan Nanofibers for Wound Healing Applications, 2017.
[177] M. Karim, A. Al-Ahmari, M. Dar, O. Aijaz, M.L. Mollah, P.M. Ajayan, J. Yeum, K.-S. Kim, Conducting and Biopolymer Based Electrospun Nanofiber Membranes for Wound Healing Applications, 2016.
[178] M. Gizdavic-Nikolaidis, S. Ray, J.R. Bennett, A.J. Easteal, R.P. Cooney, Electrospun Functionalized Polyaniline Copolymer-Based Nanofibers with Potential Application in Tissue Engineering, Macromolecular Bioscience 10(12) (2010) 1424-1431.
[179] E. Hirata, M. Uo, H. Takita, T. Akasaka, F. Watari, A. Yokoyama, Multiwalled carbon nanotube-coating of 3D collagen scaffolds for bone tissue engineering, Carbon 49(10) (2011) 3284-3291.
[180] A. Abarrategi, M.C. Gutiérrez, C. Moreno-Vicente, M.J. Hortigüela, V. Ramos, J.L. López-Lacomba, M.L. Ferrer, F. del Monte, Multiwall carbon nanotube scaffolds for tissue engineering purposes, Biomaterials 29(1) (2008) 94-102.
[181] G. Jia, H. Wang, L. Yan, X. Wang, R. Pei, T. Yan, Y. Zhao, X. Guo, Cytotoxicity of Carbon Nanomaterials: Single-Wall Nanotube, Multi-Wall Nanotube, and Fullerene, Environmental Science & Technology 39(5) (2005) 1378-1383.

[182] F.A.G. da Silva, C.M.S. de Araújo, J.J. Alcaraz-Espinoza, H.P. de Oliveira, Toward flexible and antibacterial piezoresistive porous devices for wound dressing and motion detectors, Journal of Polymer Science Part B: Polymer Physics 56(14) (2018) 1063-1072.
[183] X. Zhao, H. Wu, B. Guo, R. Dong, Y. Qiu, P.X. Ma, Antibacterial anti-oxidant electroactive injectable hydrogel as self-healing wound dressing with hemostasis and adhesiveness for cutaneous wound healing, Biomaterials 122 (2017) 34-47.
[184] G.W. Dombi, K. Purohit, L.M. Martin, S.C. Yang, Collagen gel formation in the presence of a carbon nanobrush, J Mater Sci Mater Med 26(1) (2015) 5356.
[185] M.K. Satapathy, B. Nyambat, C.W. Chiang, C.H. Chen, P.C. Wong, P.H. Ho, P.R. Jheng, T. Burnouf, C.L. Tseng, E.Y. Chuang, A Gelatin Hydrogel-Containing Nano-Organic PEI(-)Ppy with a Photothermal Responsive Effect for Tissue Engineering Applications, Molecules 23(6) (2018).
[186] H. Maleki, L. Durães, C.A. García-González, P. del Gaudio, A. Portugal, M. Mahmoudi, Synthesis and biomedical applications of aerogels: Possibilities and challenges, Advances in Colloid and Interface Science 236 (2016) 1-27.
[187] P. James Lingane, D.G. Peters, Chronopotentiometry, C R C Critical Reviews in Analytical Chemistry 1(4) (1971) 587-634.
[188] N. Elgrishi, K.J. Rountree, B.D. McCarthy, E.S. Rountree, T.T. Eisenhart, J.L. Dempsey, A Practical Beginner's Guide to Cyclic Voltammetry, Journal of Chemical Education 95(2) (2018) 197-206.
[189] J.K. Wang, B. Luo, V. Guneta, L. Li, S.E.M. Foo, Y. Dai, T.T.Y. Tan, N.S. Tan, C. Choong, M.T.C. Wong, Supercritical carbon dioxide extracted extracellular matrix material from adipose tissue, Materials Science and Engineering C 75 (2017) 349-358.
[190] J.K. Wang, G.M. Xiong, B. Luo, C.C. Choo, S. Yuan, N.S. Tan, C. Choong, Surface modification of PVDF using non-mammalian sources of collagen for enhancement of endothelial cell functionality, Journal of Materials Science: Materials in Medicine 27(3) (2016) 1-15.
[191] T.W. Chung, D.Z. Liu, S.Y. Wang, S.S. Wang, Enhancement of the growth of human endothelial cells by surface roughness at nanometer scale, Biomaterials 24(25) (2003) 4655-4661.
[192] M. Abd Mutalib, M.A. Rahman, M.H.D. Othman, A.F. Ismail, J. Jaafar, Chapter 9 - Scanning Electron Microscopy (SEM) and Energy-Dispersive X-Ray (EDX) Spectroscopy, Elsevier B.V2017.
[193] C. Das, S. Bose, Characterization Techniques, 1 ed., Routledge2017.
[194] W.R. Bowen, Atomic force microscopy in process engineering introduction to AFM for improved processes and products, 1st ed. ed., Elsevier/BH, Amsterdam ;, 2009.
[195] H.-R. Fuh, Y.-P. Liu, Y.-K. Wang, First principle research of possible HM-AFM in double perovskites A.sub.2MoOsO.sub.6 and A.sub.2TcReO.sub.6 (A = Si, Ge, Sn, and Pb) with group IVA elements set on the A-site position.(Report), Solid State Sciences 19 (2013) 94.
[196] T. Yoshizawa, Handbook of optical metrology : principles and applications, (2015).
[197] J.R. Ferraro, Introductory Raman spectroscopy, 2nd ed. ed., Academic Press, Amsterdam ;, 2003.
[198] V. Falanga, K. Faria, T. Bollenbach, Chapter 77 - Bioengineered Skin Constructs, in: R. Lanza, R. Langer, J. Vacanti (Eds.), Principles of Tissue Engineering (Fourth Edition), Academic Press, Boston, 2014, pp. 1619-1643.
[199] A. de Leon, R.C. Advincula, Chapter 11 - Conducting Polymers with Superhydrophobic Effects as Anticorrosion Coating, in: A. Tiwari, J. Rawlins, L.H. Hihara (Eds.), Intelligent Coatings for Corrosion Control, Butterworth-Heinemann, Boston, 2015, pp. 409-430.
[200] H. Groult, C.M. Julien, A. Bahloul, S. Leclerc, E. Briot, A.-G. Porras-Gutierrez, A. Mauger, Chapter 11 - Electrodeposition of Polypyrrole on CFx Powders Used as Cathode in Primary Lithium Battery, in: T. Nakajima, H. Groult (Eds.), Advanced Fluoride-Based Materials for Energy Conversion, Elsevier2015, pp. 237-260.
[201] J.H. Kaufman, K.K. Kanazawa, G.B. Street, Gravimetric Electrochemical Voltage Spectroscopy: In Situ Mass Measurements during Electrochemical Doping of the Conducting Polymer Polypyrrole, Physical Review Letters 53(26) (1984) 2461-2464.
[202] P. Kleesz, R. Darlenski, J.W. Fluhr, Full-body skin mapping for six biophysical parameters: baseline values at 16 anatomical sites in 125 human subjects, Skin Pharmacol Physiol 25(1) (2012) 25-33.

[203] C.V. Wa, H.I. Maibach, Mapping the human face: biophysical properties, Skin Res Technol 16(1) (2010) 38-54.
[204] S. Sun, M. Gilbertson, B.W. Anthony, 6-DOF probe tracking via skin mapping for freehand 3D ultrasound, 2013 IEEE 10th International Symposium on Biomedical Imaging, 2013, pp. 780-783.
[205] M. Toma, G. Loget, R.M. Corn, Fabrication of broadband antireflective plasmonic gold nanocone arrays on flexible polymer films, Nano Lett 13(12) (2013) 6164-9.
[206] C.-K. Cho, W.-J. Hwang, K. Eun, S.-H. Choa, S.-I. Na, H.-K. Kim, Mechanical flexibility of transparent PEDOT:PSS electrodes prepared by gravure printing for flexible organic solar cells, Solar Energy Materials and Solar Cells 95(12) (2011) 3269-3275.
[207] G. Latessa, F. Brunetti, A. Reale, G. Saggio, A. Di Carlo, Piezoresistive behaviour of flexible PEDOT:PSS based sensors, Sensors and Actuators B: Chemical 139(2) (2009) 304-309.
[208] A.L. Beresford, A.R. Hillman, Letters to Analytical Chemistry Electrochromic Enhancement of Latent Fingerprints on Stainless Steel Surfaces, Analytical chemistry 82(2) (2010) 483-486.
[209] A. Lisowska-Oleksiak, A.P. Nowak, M. Wilamowska, M. Sikora, W. Szczerba, C. Kapusta, Ex situ XANES, XPS and Raman studies of poly(3,4-ethylenedioxythiophene) modified by iron hexacyanoferrate, Synthetic Metals 160(11) (2010) 1234-1240.
[210] G. Inzelt, Classification of Electrochemically Active Polymers, in: G. Inzelt (Ed.), Conducting Polymers: A New Era in Electrochemistry, Springer Berlin Heidelberg, Berlin, Heidelberg, 2008, pp. 7-65.
[211] J. Huang, P.F. Miller, J.C. de Mello, A.J. de Mello, D.D.C. Bradley, Influence of thermal treatment on the conductivity and morphology of PEDOT/PSS films, Synthetic Metals 139(3) (2003) 569-572.
[212] R.D. Ead, R.A. Fairbank, W.J. Cunliffe, Sebum excretion rate, surface lipid composition and constitutional eczema, Clin Exp Dermatol 2(4) (1977) 361-4.
[213] E.W. Powell, G.W. Beveridge, Sebum excretion and sebum composition in adolescent men with and without acne vulgaris, Br J Dermatol 82(3) (1970) 243-9.
[214] S. Kim, B. Sanyoto, W.T. Park, S. Kim, S. Mandal, J.C. Lim, Y.Y. Noh, J.H. Kim, Purification of PEDOT:PSS by Ultrafiltration for Highly Conductive Transparent Electrode of All-Printed Organic Devices, Adv Mater 28(46) (2016) 10149-10154.
[215] Y. Kim, A.M. Ballantyne, J. Nelson, D.D.C. Bradley, Effects of thickness and thermal annealing of the PEDOT:PSS layer on the performance of polymer solar cells, Organic Electronics 10(1) (2009) 205-209.
[216] H. Yan, H. Okuzaki, Effect of solvent on PEDOT/PSS nanometer-scaled thin films: XPS and STEM/AFM studies, Synthetic Metals 159(21) (2009) 2225-2228.
[217] F.B. Dias, L. Plomp, J.B.J. Veldhuis, Trends in polymer electrolytes for secondary lithium batteries, Journal of Power Sources 88(2) (2000) 169-191.
[218] D. Blanc, P. Agache, Sebum Excretion. Methods of measurement and influence of physical factors, Int J Cosmet Sci 2(5) (1980) 243-50.
[219] E.O. Butcher, A. Coonin, The physical properties of human sebum, J Invest Dermatol 12(4) (1949) 249-54.
[220] A. Crisp, E. de Juan, Jr., J. Tiedeman, Effect of Silicone Oil Viscosity on Emulsification, Archives of Ophthalmology 105(4) (1987) 546-550.
[221] A.S. Tascini, M.G. Noro, R.J. Chen, J.M. Seddon, F. Bresme, Understanding the interactions between sebum triglycerides and water: a molecular dynamics simulation study, Physical Chemistry Chemical Physics 20(3) (2018) 1848-1860.
[222] M. Wagner, G. Lisak, A. Ivaska, J. Bobacka, Durable PEDOT:PSS films obtained from modified water-based inks for electrochemical sensors, Sensors and Actuators, B: Chemical 181 (2013) 694-701.
[223] J. Zhang, Z. Liu, Q. Kong, C. Zhang, S. Pang, L. Yue, X. Wang, J. Yao, G. Cui, Renewable and superior thermal-resistant cellulose-based composite nonwoven as lithium-ion battery separator, ACS Applied Materials and Interfaces 5(1) (2013) 128-134.

[224] P. Kalakonda, M.A. Aldhahri, M.S. Abdel-Wahab, A. Tamayol, K.M. Moghaddam, F. Ben Rached, A. Pain, A. Khademhosseini, A. Memic, S. Chaieb, Microfibrous silver-coated polymeric scaffolds with tunable mechanical properties, RSC Advances 7(55) (2017) 34331-34338.
[225] M. Dietrich, J. Heinze, G. Heywang, F. Jonas, Electrochemical and spectroscopic characterization of polyalkylenedioxythiophenes, Journal of Electroanalytical Chemistry 369(1-2) (1994) 87-92.
[226] R. Kiebooms, A. Aleshin, K. Hutchison, F. Wudl, Thermal and Electromagnetic Behavior of Doped Poly(3,4-ethylenedioxythiophene) Films, The Journal of Physical Chemistry B 101(51) (1997) 11037-11039.
[227] S.A. Sapp, G.A. Sotzing, J.L. Reddinger, J.R. Reynolds, Rapid switching solid state electrochromic devices based on complementary conducting polymer films, Advanced Materials 8(10) (1996) 808-811.
[228] L. Bacakova, E. Filova, M. Parizek, T. Ruml, V. Svorcik, Modulation of cell adhesion, proliferation and differentiation on materials designed for body implants, 2011, pp. 739-767.
[229] C. Wu, M. Chen, T. Zheng, X. Yang, Effect of surface roughness on the initial response of MC3T3-E1 cells cultured on polished titanium alloy, Bio-Medical Materials and Engineering 26 (2015) S155-S164.
[230] V. Brunetti, G. Maiorano, L. Rizzello, B. Sorce, S. Sabella, R. Cingolani, P.P. Pompa, Neurons sense nanoscale roughness with nanometer sensitivity, Proceedings of the National Academy of Sciences 107(14) (2010) 6264-6269.
[231] H.-I. Chang, Y. Wang, Cell Responses to Surface and Architecture of Tissue Engineering Scaffolds, 2011.
[232] R. Dong, X. Zhao, B. Guo, P.X. Ma, Biocompatible Elastic Conductive Films Significantly Enhanced Myogenic Differentiation of Myoblast for Skeletal Muscle Regeneration, Biomacromolecules 18(9) (2017) 2808-2819.
[233] S.H. Ku, S.H. Lee, C.B. Park, Synergic effects of nanofiber alignment and electroactivity on myoblast differentiation, Biomaterials 33(26) (2012) 6098-6104.
[234] Y. Liu, J. Hu, X. Zhuang, P. Zhang, X. Chen, Y. Wei, X. Wang, Preparation and Characterization of Biodegradable and Electroactive Polymer Blend Materials Based on mPEG/Tetraaniline and PLLA, Macromolecular Bioscience 11(6) (2011) 806-813.
[235] L.F. Brown, K.T. Yeo, B. Berse, T.K. Yeo, D.R. Senger, H.F. Dvorak, L. van de Water, Expression of vascular permeability factor (vascular endothelial growth factor) by epidermal keratinocytes during wound healing, J Exp Med 176(5) (1992) 1375-9.
[236] T.P. Sullivan, W.H. Eaglstein, S.C. Davis, P. Mertz, The pig as a model for human wound healing, Wound Repair Regen 9(2) (2001) 66-76.
[237] S. Werner, R. Grose, Regulation of wound healing by growth factors and cytokines, Physiol Rev 83(3) (2003) 835-70.
[238] A.T. Trott, Chapter 4 - Wound Healing and Cosmetic Outcome, in: A.T. Trott (Ed.), Wounds and Lacerations (Fourth Edition), W.B. Saunders, Philadelphia, 2012, pp. 15-26.
[239] A.A. Chaudhari, K. Vig, D.R. Baganizi, R. Sahu, S. Dixit, V. Dennis, S.R. Singh, S.R. Pillai, Future Prospects for Scaffolding Methods and Biomaterials in Skin Tissue Engineering: A Review, Int J Mol Sci 17(12) (2016).
[240] A.C.d.O. Gonzalez, T.F. Costa, Z.d.A. Andrade, A.R.A.P. Medrado, Wound healing - A literature review, Anais brasileiros de dermatologia 91(5) (2016) 614-620.
[241] R.M. Ayling, CHAPTER 10 - Clinical biochemistry of nutrition, in: W.J. Marshall, M. Lapsley, A.P. Day, R.M. Ayling (Eds.), Clinical Biochemistry: Metabolic and Clinical Aspects (Third Edition), Churchill Livingstone2014, pp. 180-199.
[242] E.M. Butt, R.E. Nusbaum, T.C. Gilmour, S.L. Didio, S. Mariano, Trace Metal Levels in Human Serum and Blood, Archives of Environmental Health: An International Journal 8(1) (1964) 52-57.
[243] A. Gopal, V. Kant, A. Gopalakrishnan, S.K. Tandan, D. Kumar, Chitosan-based copper nanocomposite accelerates healing in excision wound model in rats, European Journal of Pharmacology 731(1) (2014) 8-19.

[244] A. Michopoulou, P. Rousselle, How do epidermal matrix metalloproteinases support re-epithelialization during skin healing?, European Journal of Dermatology 25(1) (2015) 33-42.
[245] R. Visse, H. Nagase, Matrix Metalloproteinases and Tissue Inhibitors of Metalloproteinases, Circulation Research 92(8) (2003) 827-839.
[246] H. Diener, K. Herberger, M. Augustin, E.S. Debus, Chronical wound management, Phlebologie 40(6) (2011) 303-+.
[247] D. Jaklic, K. Zupancic, A. Lapanje, D. Smrke, M. Cimerman, Z. Parac, Z. Arnez, N. Gunde-Cimerman, INTRODUCTION OF CHRONICAL WOUNDS HEALING WITH LUCILIA SERICATA LARVAE IN SLOVENIA, Zdravniski Vestnik-Slovenian Medical Journal 77(3) (2008) 199-206.
[248] S. Chernousova, M. Epple, Silver as Antibacterial Agent: Ion, Nanoparticle, and Metal, Angewandte Chemie-International Edition 52(6) (2013) 1636-1653.
[249] A.R. Im, J.Y. Kim, H.S. Kim, S. Cho, Y. Park, Y.S. Kim, Wound healing and antibacterial activities of chondroitin sulfate- and acharan sulfate-reduced silver nanoparticles, Nanotechnology 24(39) (2013) 395102.
[250] V.K. Sharma, R.A. Yngard, Y. Lin, Silver nanoparticles: Green synthesis and their antimicrobial activities, Advances in Colloid and Interface Science 145(1-2) (2009) 83-96.
[251] Y. Wang, X. Zhang, Y. Bai, W. Li, X. Li, X. Xing, C. Wang, L. Gao, M. Yogi, M.K. Swamy, K. Dupadahalli, G.R. Rudramurthy, B. Purushotham, K.C. Rohit, J. Fu, Anticancer and Antibacterial Activities of Silver Nanoparticles (AgNPs) Synthesized from Cucumis melo L, J Nanosci Nanotechnol 20(7) (2020) 4143-4151.
[252] A. Knauer, J.M. Koehler, Screening of nanoparticle properties in microfluidic syntheses, Nanotechnology Reviews 3(1) (2014) 5-26.
[253] C. Marambio-Jones, E.M.V. Hoek, A review of the antibacterial effects of silver nanomaterials and potential implications for human health and the environment, Journal of Nanoparticle Research 12(5) (2010) 1531-1551.
[254] Sigma-Aldrich, aniline, MSDS, Sigmaaldrich, 2016.
[255] Sigma-Aldrich, pyrrole, MSDS, Sigmaaldrich, Sigmaaldrich, 2016.
[256] Sigma-Aldrich, 3,4-Ethylenedioxythiophene, MSDS, 2016.